Intelligent Global Maximum Power Point Tracking Strategies Based on Shading Perception for Photovoltaic Systems

Thesis submitted in accordance with the requirements of the University of Liverpool for the degree of Doctor in Philosophy by

Ziqiang Bi

September 2021

Abstract

When a Photovoltaic (PV) system is partially shaded in the environment, the current-voltage (I-V) and power-voltage (P-V) curves exhibit multiple stairs/peaks and the locus of Maximum Power Point (MPP) varies over a wide range. Such Partial Shading Conditions (PSC) bring challenges to the Maximum Power Point Tracking (MPPT) systems. This thesis presents some novel shading information to characterize the complex PSC and MPPT techniques based on the shading perception.

Shading information is the mathematical indicator to express the shading patterns. The existing shading information, such as shading rate and shading strength, has the limitations that they can only characterize the PSC with two irradiation levels. To improve the application range of the shading information, the shading matrix and shading vector are proposed in this thesis. The identification and detection methods for the proposed shading information are also included. Results from simulations and experiments have shown the effectiveness and accuracy of the proposed shading detection methods.

Under PSC, the power characteristics of the PV systems are too complicated that there exist multiple MPPs. The traditional MPPT techniques may be trapped in the Local MPPs (LMPPs) instead of the Global MPP (GMPP). In this thesis, some novel methods are proposed to estimate the GMPP location from the detected shading information. The proposed MPPT techniques based on the shading perception are capable of tracking the GMPP fast and accurately. Simulations and experiments are conducted to validate the performance of the proposed MPPT methods with the comparison with some well-known MPPT methods.

Acknowledgements

First and foremost, I wish to express my deepest thanks and gratitude to my supervisors Prof. Ka Lok Man, Prof. Jeremy S. Smith, and Prof. Yong Yue, who had provided unreserved and invaluable professional guidance for my research during the past five years. I appreciate their patience in our weekly/monthly meetings. Also, I would like to thank Dr. Jieming Ma, who shared a large number of experiences on conducting researches with me. Without their support and help, I might have failed to settle in the field of research.

I would like to express my appreciation to the examiners, Prof. Hirotaka Koizumi from the Tokyo University of Science and Dr. Fei Xue, for their insightful comments and suggestions. I also wish to thank my Independent Progress Assessment Panel (IPAP) members, Dr. Dawei Liu and Dr. Waleed Al-Nuaimy, for reviewing my annual report. Their questions and efforts during our annual meetings contributed to the successful progress of my research on this thesis.

I would also like to thank all the staff members at the Xi'an Jiaotong-Liverpool University (XJTLU) and the University of Liverpool (UoL). Many thanks to my colleagues for their useful discussions, suggestions, and help. They are Dr. Yuechun Wang, Yuxuan Zhao, Dr. Fangyu Wu, Qi Chen, Jing Qian, Xianbin Hong, Xuan Zhao, Kangshi Wang, Dr. Hang Dong, Dr. Jie Zhang, Dr. Wei Wang, Dr. Xiaohui Zhu, Dr. David Afolabi, Dr. Vijayakumar Nanjappan, Dr. Yizhang Xia, Dr. Shiyang Yan, and Dr. Dacheng Jiang.

Finally, I would like to take this opportunity to express my great gratitude to my parents for their support and encouragement. Furthermore, I would like to acknowledge the financial support from XJTLU and UoL.

Contents

List of Figures

List of Tables

Chapter 1

Introduction

This chapter first presents the background and motivation of the thesis, followed by the introduction of the thesis's aims and objectives. Afterward, the main contributions are highlighted along with a list of publications. Finally, the outline of the thesis is given at the end of this chapter.

1.1 Background and Motivation

Nowadays, due to the worldwide environmental concerns about global warming, the demand for renewable energy resources is increasing year by year. Solar energy is one of the most popular renewable energy resources since it is silent and an environmental-friendly power-generating process. Photovoltaic (PV) is the technology for converting solar energy to electricity using semiconducting materials [1]. PV has grown to be an important renewable energy source because of its environmental friendliness. In practical PV applications, the occurrence of Partial Shading Conditions (PSC), raised from passing clouds, nearby trees, or buildings, is quite common and causes power loss, hotspots, and threatens the reliability of the PV system [2]. Therefore, it is of importance to prevent hotspot damage and optimize the output power for a partially shaded PV array.

Bypassing shaded cells through bypass diodes has been proven to be an effective strategy in protecting against hotspot damage [3]. However, early studies have shown that the current-voltage (I-V) and power-voltage (P-V) curves of a partially shaded PV array exhibit various shapes and the locus of Maximum Power Point (MPP) varies over a wide range under PSC [4]. Figure 1.1 shows the P-V characteristic curves of a PV system under

Uniform Irradiation Conditions (UIC) and PSC. Only one peak exists in the P-V characteristics under UIC. However, there are multiple peaks on the P-V characteristic curve under PSC, where the one with the largest power is called the Global Maximum Power Point (GMPP), the rest are called the Local Maximum Power Point (LMPP). Tracking the GMPP is one of the most economical ways of optimizing the output power for a PV array.

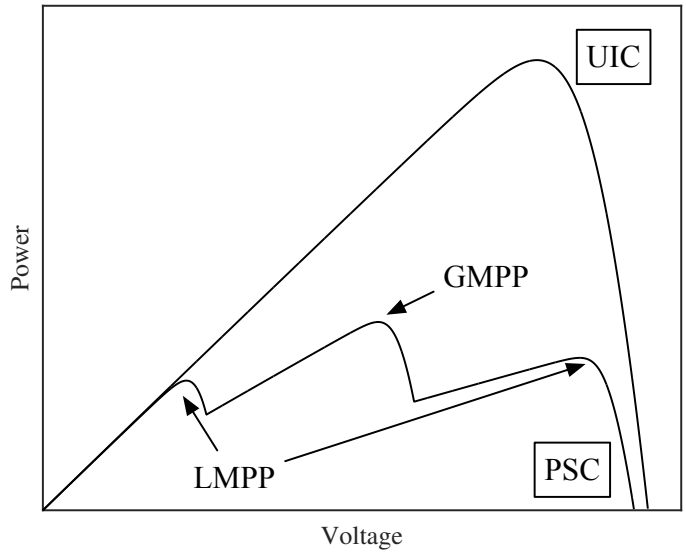

Figure 1.1: P-V characteristics of a PV system under UIC and PSC.

The traditional Maximum Power Point Tracking (MPPT) methods, such as Perturb & Observe (P&O) [5], and Incremental Conductance (IncCond) [6], are capable of tracking the MPP under the rapidly changing atmospheric conditions but they would fail under PSC where exists multiple peaks in the P-V characteristic. Recently, many optimization algorithms such as Particle Swarm Optimization (PSO) and Genetic Algorithms (GA) have been applied to optimize the PV output power [7, 8]. These optimized methods usually require significant computing power and in some cases may be trapped in LMPPs rather than the GMPP. The DC-DC converters are usually used to enable the PV string to operate at the MPP by varying the load [7, 9, 10].

To aid the MPPT methods to locate the GMPP, the identification of the PSC is necessary. Some standard shading information factors have been proposed in recent years including shading rate and shading strength, to characterize the shading. The shading

rate χ is the percentage of the number of shaded PV modules in the PV string [11]. The shading strength or shading factor ρ is defined as the ratio of the solar irradiance on shaded modules to that on insolated modules [12]. However, the definition of the existing shading information is only applied to simple shading conditions with two solar irradiation levels. Therefore, the existing shading information cannot characterize the complex shading scenarios with more than two irradiation levels. Furthermore, early studies have shown that the location of MPP under PSC is related to the shading conditions [11]. Thus, the MPPT technique based on the detection of the PSC is a new research direction for PV systems.

1.2 Aims and Objectives

The main aim of the thesis is the construction of the environmental perception model for the estimation of the shading information and the locus of MPP which would be further utilized to enhance the efficiency of the MPPT methods. The objectives of the thesis are given as follows:

1. **Shading detection method based on the switching control strategy**

   The traditional shading detection methods require a large number of voltage and current sensors which increases the capital cost of the PV system. The switching control strategy is proposed in the shading detection system to reduce the number of utilized sensors. The utilized sensors/PV modules ratio would be reduced compared with the traditional methods.

2. **Environmental perception model for estimating shading information**

   The shading information has a large impact on the location of the MPP. However, directly using physical irradiance measurement instruments (e.g. pyranometers and pyrheliometers) to detect the shading information is too expensive. This thesis uses the environmental perception model to estimate the value of the shading information. The shading rate and the shading strength are estimated by the string voltage characteristics, and the shaded and insolated string current, respectively. These methods decrease the cost as they avoid using physical irradiance measurement instruments.

3. **Maximum power point tracking based on the environmental perception**

   The environmental perception MPP estimation model directly estimates the voltage at MPP under partial shading conditions. This can ensure that the estimated MPP

location is near the practical global MPP, reducing the possibility of being trapped in the local MPPs. The estimated MPP is used as the initial value of traditional MPPT methods (e.g. P&O), which not only keeps the simple advantage of traditional methods, but also allows the environmental perception model to guide the tracking step in real-time.

1.3 Contributions

The main focus of the thesis is to maximize the output power of the PV systems based on the shading detection results. To address the research objectives in Section 1.2, this thesis contributes to the following:

1. In Chapter 3, an automatic shading detection system is proposed to estimate the shading rate by using voltage sensors. The main features of the proposed method are the utilization of a reduced number of sensors, a simple switching control strategy, and a high detection rate. The feasibility and effectiveness of the proposed shading detecting system are validated by means of a rich set of hardware experiments.

2. In Chapter 4, a shading matrix is proposed to describe the shading rate and shading strength information. The proposed shading matrix would provide MPPT controllers with the essential environmental information to improve the GMPP tracking performance. Furthermore, a Modified Tabu Search (MTS)-based identification method is proposed to estimate the shading matrix. The modified method involves a preselection process of updating the Tabu list to optimize the searching efficiency. The accuracy and efficiency of the proposed analytical estimation expression are verified through simulations and experiments.

3. In Section 5.2, a novel $0.8V_{OC}$-model-based Global Maximum Power Point Tracking (GMPPT) method based on the shading rate detection method is proposed. The mathematical relationship between the shading rate and GMPP location is presented and the GMPP can be estimated by the shading detection results. Simulation results prove the tracking efficiency of the proposed method.

4. In Section 5.3, a shading vector is proposed to characterize the complex PSC. The shading vector improves the performance of the traditional shading information and

is capable of describing complex shading conditions. Based on the electrical characteristics of the PV string, a shading detection circuit is proposed to estimate the shading vector.

5. Section 5.3 also introduces an enhanced GMPPT method based on the detection of the shading vector is proposed. The proposed GMPPT method estimates the $0.8V_{OC}$ region with the GMPP directly from the measured shading vector by the k-Nearest Neighbors (k-NN) approach and saves the time cost in the comparison process used in the conventional method. Simulation and experimental results demonstrate that the proposed method is capable of tracking the GMPP efficiently and accurately under various shading patterns.

These contributions have led to a number of peer-reviewed publications, which are split into journal papers and conference papers:

Journal Papers

1. Ziqiang Bi, Jieming Ma, Ka Lok Man, Jeremy S. Smith, Yong Yue, Huiqing Wen, "An Enhanced $0.8V_{OC}$-Model-Based Global Maximum Power Point Tracking Method for Photovoltaic Systems," IEEE Transactions on Industry Applications, vol. 56, no. 6, pp. 6825-6834, 2020.

2. Ziqiang Bi, Jieming Ma, Kangshi Wang, Ka Lok Man, Jeremy S. Smith, Yong Yue, "Identification of Partial Shading Conditions for Photovoltaic Strings," IEEE Access, vol. 8, pp. 75491-75502, 2020.

3. Jieming Ma, Haochuan Jiang, Kaizhu Huang, Ziqiang Bi, Ka Lok Man, "Novel Field-Support Vector Regression-Based Soft Sensor for Accurate Estimation of Solar Irradiance," IEEE Transactions on Circuits and Systems I: Regular Papers, vol. 64, no. 12, pp. 3183-3191, 2017.

Conference Papers

1. Ziqiang Bi, Jieming Ma, Ka Lok Man, Yong Yue, Jeremy S. Smith, "A Novel Global Maximum Power Point Tracking Technique based on Shading Detection for Photovoltaic Strings," International SoC Design Conference (ISOCC), pp. 165-166, 2020.

2. Ziqiang Bi, Jieming Ma, Ka Lok Man, Yong Yue, Jeremy S. Smith, "A Novel Global Maximum Power Point Tracking Method based on Shading Detection," International SoC Design Conference (ISOCC), pp. 188-189, 2019.

3. Ziqiang Bi, Jieming Ma, Ka Lok Man, Jeremy S. Smith, Yong Yue, Huiqing Wen, "Global MPPT Method for Photovoltaic Systems Operating under Partial Shading Conditions using the $0.8V_{OC}$ Model," IEEE International Conference on Environment and Electrical Engineering and IEEE Industrial and Commercial Power Systems Europe (EEEIC/I&CPS Europe), 2019.

4. Jieming Ma, Ziqiang Bi, Ka Lok Man, Hai-Ning Liang, Jeremy S. Smith, "Predicting the Global Maximum Power Point Locus using Shading Information," IEEE International Conference on Environment and Electrical Engineering and IEEE Industrial and Commercial Power Systems Europe (EEEIC/I&CPS Europe), 2019.

5. Jieming Ma, Ziqiang Bi, Ka Lok Man, Yong Yue, Jeremy S. Smith, "Automatic Shading Detection System for Photovoltaic Strings," International SoC Design Conference (ISOCC), pp. 176-177, 2018.

6. Jieming Ma, Ziqiang Bi, Ka Lok Man, Huan Dai, Zhengtian Wu, "Identification of Partial Shading in Photovoltaic Arrays using Optimal Sensor Placement Schemes," 7th International Conference on Renewable Energy Research and Applications (ICRERA), pp. 458-462, 2018.

1.4 Thesis Outline

The thesis is organized as follows:

In Chapter 2, the related work is introduced. The electrical characteristics of a PV string are modeled in Section 2.1. The traditional shading information and some state-of-art MPPT methods are presented in Sections 2.3 and 2.4.

Chapter 3 presents an automatic shading perception system. The main features of the proposed method are the utilization of a reduced number of sensors, a simple switching control strategy, and a high detection rate. The feasibility and effectiveness of the proposed shading detecting system are verified through hardware experiments.

In Chapter 4, the shading matrix is introduced to describe the PSC, which would provide MPPT controllers with the essential environmental information to improve the

GMPP tracking performance. An MTS-based identification method is proposed to estimate the shading matrix. The accuracy and efficiency of the proposed analytical estimation expression are verified through simulations and experiments.

Chapter 5 introduces the proposed GMPPT techniques based on the shading perception. The methodologies for each GMPPT method are illustrated. Simulations and experimental results validate the proposed techniques.

Chapter 6 summarizes the thesis and discusses the future directions of this research.

Chapter 2

Literature Review

In this chapter, the main purpose is to give a literature review on the topic of the thesis. Some related work is also introduced in this chapter. Therefore, this chapter first introduces the most popular Photovoltaic (PV) modeling methods to characterize the PV electrical characteristics. Afterward, some shading detection systems and traditional shading information are presented. The literature review for the Maximum Power Point Tracking (MPPT) techniques is conducted toward the end of this chapter.

2.1 Electrical Characteristics of Photovoltaic Strings

2.1.1 Single-diode Electrical Equivalent Circuit

Some typical electrical characteristics of PV modules can be found on PV manufacturers' datasheets. These characteristical values usually include the short-circuit current, the open-circuit voltage, the current at Maximum Power Point (MPP), the voltage at MPP, and the power at MPP. However, these values are obtained at the Standard Test Conditions (STC), which is at the solar irradiance of 1000 W/m^2, the temperature of 25 °C, and 1.5 air mass spectral distributions. In order to acquire the PV characteristics under varied environmental scenarios, a number of equivalent circuit models have been proposed. Equivalent circuit models define the current-voltage (I-V) characteristic curve of a PV cell, module, or array as a function for a given environmental setup. The single-diode model is one of the most popular and simplest PV equivalent circuit models [13]. A equivalent circuit for the single-diode model is shown in Figure 2.1. The circuit includes a diode in

parallel with a current source, a shunt resistor, and a series resistor. The two resistive elements account for the power losses. The model characteristic equation can be obtained as shown in Equation (2.1) from a current balance for the currents through the resistors, diode, and current source.

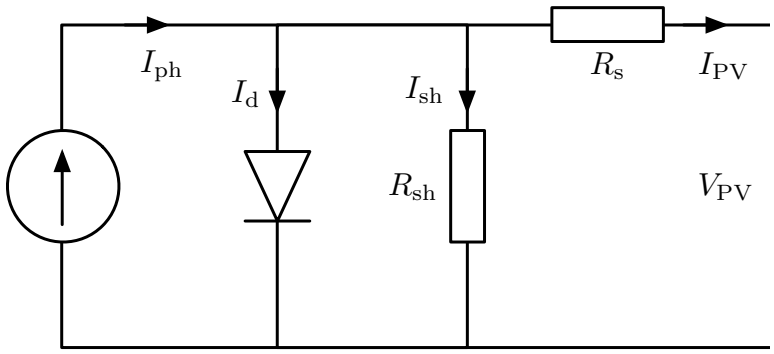

Figure 2.1: Single-diode electrical equivalent circuit for a PV cell.

$$I_{PV} = I_{ph} - I_d - I_{sh}, \tag{2.1}$$

where I_{PV} is the current of the PV cell. I_{ph} is the light-generated photocurrent. I_d and I_{sh} are the current through the diode and shunt resistor, respectively.

I_d can be calculated based on the Shockley diode equation, as given in Equation (2.2).

$$I_d = I_{sat}\{\exp[\frac{q(V_{PV} + I_{PV}R_s)}{nkT}] - 1\}, \tag{2.2}$$

where I_{sat} is the reverse saturation current. R_s is the series resistance. n is the ideality factor of the diode. q is the electron charge. k is the Boltzmann's constant, and T is the temperature in Kelvin.

The shunt current I_{sh} can be expressed by Equation (2.3).

$$I_{sh} = \frac{V_{PV} + I_{PV}R_s}{R_{sh}}, \tag{2.3}$$

where R_{sh} is the shunt resistance.

Therefore, Equation (2.1) can be extended as Equation (2.4).

$$I_{\mathrm{sh}} = I_{\mathrm{ph}} - I_{\mathrm{sat}}\{\exp[\frac{q(V_{\mathrm{PV}} + I_{\mathrm{PV}}R_{\mathrm{s}})}{nkT}] - 1\} - \frac{V_{\mathrm{PV}} + I_{\mathrm{PV}}R_{\mathrm{s}}}{R_{\mathrm{sh}}}. \tag{2.4}$$

2.1.2 Modeling for Photovoltaic String under Uniform Irradiation Conditions

The I-V characteristics of a PV string under Uniform Irradiation Conditions (UIC) can be expressed by the single-diode model as shown in Equation (2.5) [14–16].

$$I_{\mathrm{S}} = I_{\mathrm{ph}} - I_{\mathrm{sat}}\{\exp[\frac{q(V_{\mathrm{S}} + I_{\mathrm{S}}R_{\mathrm{s}})}{nkTN_{\mathrm{S}}}] - 1\} - \frac{V_{\mathrm{S}} + I_{\mathrm{S}}R_{\mathrm{s}}}{R_{\mathrm{sh}}}, \tag{2.5}$$

where I_{S} and V_{S} are the current and voltage of the PV string, respectively. $N_{\mathrm{S}} = N_{\mathrm{String}} \times N_{\mathrm{Series}}$ (N_{String} is the number of modules in the PV string and N_{Series} is the number of series cells in the PV module). As the shunt resistance R_{sh} is relatively large in the majority of the PV modules, the terms related to R_{sh} can be omitted [17] and Equation (2.5) can be further simplified to Equation (2.6).

$$I_{\mathrm{S}} = I_{\mathrm{ph}} - I_{\mathrm{sat}}\big\{\exp[\frac{q(V_{\mathrm{S}} + I_{\mathrm{S}}R_{\mathrm{s}})}{nkTN_{\mathrm{S}}}] - 1\big\}. \tag{2.6}$$

Thus, based on Equation (2.6), the current slope with respect to the voltage $dI_{\mathrm{S}}/dV_{\mathrm{S}}$ can be calculated by Equation (2.7).

$$\frac{dI_{\mathrm{S}}}{dV_{\mathrm{S}}} = -I_{\mathrm{sat}}\frac{q}{nkTN_{\mathrm{S}}}(1 + \frac{dI_{\mathrm{S}}}{dV_{\mathrm{S}}}R_{\mathrm{s}})\exp[\frac{q(V_{\mathrm{S}} + I_{\mathrm{S}}R_{\mathrm{s}})}{nkTN_{\mathrm{S}}}]. \tag{2.7}$$

By solving Equation (2.7), the value of $dI_{\mathrm{S}}/dV_{\mathrm{S}}$ can be obtained as given in Equation (2.8).

$$\frac{dI_{\mathrm{S}}}{dV_{\mathrm{S}}} = -1/\big\{\frac{nkTN_{\mathrm{S}}}{qI_{\mathrm{sat}}\exp[q(V_{\mathrm{S}} + I_{\mathrm{S}}R_{\mathrm{s}})/(nkTN_{\mathrm{S}})]} + R_{\mathrm{s}}\big\}. \tag{2.8}$$

Figure 2.2 shows the I-V and P-V characteristics of a PV string under UIC with varied solar irradiances. The MPPs are marked with the red circles on the I-V curves. As can be found from Figure 2.2, the slope of the I-V curve before the MPP is relatively flat and the

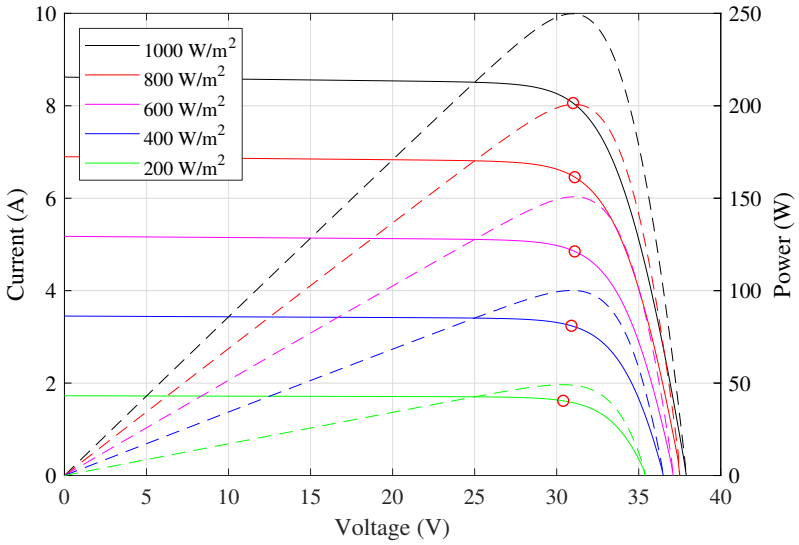

Figure 2.2: Electrical characteristics of a PV string under UIC.

slope after the MPP is high. Therefore, the slope at the MPP could be used as a reference slope D_{ref} to distinguish the points with low slopes and points with high slopes. D_{ref} can be expressed by Equation (2.9).

$$\begin{aligned} D_{\text{ref}} &= \frac{dI_{\text{MPP}}}{dV_{\text{MPP}}} \\ &= -1/\Big\{\frac{nkTN_{\text{S}}}{qI_{\text{sat}}\exp[q(V_{\text{MPP}}+I_{\text{MPP}}R_{\text{s}})/(nkTN_{\text{S}})]}+R_{\text{s}}\Big\}, \end{aligned} \tag{2.9}$$

where V_{MPP} and I_{MPP} are respectively the voltage and current at the MPP.

2.2 Partial Shading Detection

Partial shading in PV systems usually brings power losses. To avoid the reduction in the efficiency and potential problems, the shading detection system is required for identifying the partially shaded PV systems.

In recent years, many shading detection methods have been proposed to detect or distinguish partial shading in PV systems from UIC. A diagnosis method based on characteristics deviation analyses was presented in [18]. It indicates that the Partial Shading

Conditions (PSC) can be distinguished by observing the stairs in I-V characteristic curves. This method cannot detect the PSC automatically since manual observations are required. In [19], an Artificial Neural Network (ANN) is used to detect the faults under normal and partially shaded conditions. The ANN-based fault diagnosis method is capable of distinguishing the PSC from UIC automatically by inputting the solar radiation, temperature, and measured output power. Zhao et al. proposed a novel PV array fault diagnosis method based on Fuzzy C-Mean (FCM) and fuzzy membership algorithms in [20]. It uses clustering to analyze different PV faults under both UIC and PSC. By comparing with the K-means, the running time of the FCM algorithm is longer, but the accuracy is higher. In [21], a fault diagnostic technique for PV systems based on measured I-V characteristics was proposed. The partial shading faults can be distinguished by a multi-class Adaptive Boosting (AdaBoost) from some other PV faults such as the short-circuit and abnormal aging. Principal Component Analysis (PCA) was applied to identify the shading in PV systems using the features from I-V characteristic curves in [22]. This method only uses the PV current and voltage, which avoids additional hardware and costs.

However, these shading detection systems can only detect the existence of PSC. The detailed shading conditions cannot be identified. Thus, in Section 2.3, the shading information is introduced which gives a quantitative analysis to PSC.

2.3 Traditional Shading Information

In order to analyze PSC, the shading information has been proposed in the recent ten years [23]. The shading information is the mathematical indicator to quantitatively evaluate the PSC. Typically, the shading information refers to the shading rate and shading strength [11]. The shading rate represents the percentage of the shaded PV modules in the PV string [11]. The shading strength reflects the ratio of the solar irradiance of the PV modules in the PV string [12]. Different combinations of the shading rate and shading strength will result in varied PV characteristics. Early studies have shown that these two shading factors directly influence the locus of the Global Maximum Power Point (GMPP) [24, 25]. Many shading information detection methods have been proposed. An automatic shading detection method by using voltage sensors and a switch matrix was proposed in [26]. The detection system has the ability to estimate the shading rate effectively. An ANN is used in [12] to detect the shading information including both the shading rate and shading strength but this method uses separate ANN models to predict different shading

information. In [11], a shading detection method was proposed to predict the shading rate by a sorting algorithm. After determining the shading rate, the shading strength is estimated by Multi-output Support Vector Regression (M-SVR). However, this detection method uses expensive solar irradiance sensors and also carries heavy computational burdens. Some researches have shown that the values of the shading information are related to the location of the turning point in the I-V curves [27, 28]. The number of shaded modules is estimated through the voltage at the turning point in [29]. The shading rate can be further estimated by this identification method. Lei et al. interpreted the PV characteristics under PSC via an analytical model [30]. The shading strength variation is shown to be well-correlated to the height of the current steps (turning points) in the I-V characteristics. In [28], the Discrete Wavelet Transform (DWT) is used to interpret the traced I-V curve of the PV system and locate the turning points. However, the definitions of the aforementioned shading information are based on a strong assumption that the PSC only has two irradiation levels.

Two typical shading information, the shading rate and shading strength, are investigated in this section. According to [11], the definitions for both the shading rate and shading strength are based on a strong assumption. That is the PV string is supposed to be subjected to two different solar irradiation levels. The PV modules that receive the higher irradiance are called insolated modules, and those receiving the lower irradiance are called shaded modules. The shading rate χ is expressed by Equation (2.10), which is the ratio of the number of shaded PV modules to the total number of modules in the PV string.

$$\chi = \frac{N_{\text{Shaded}}}{N_{\text{String}}}, \tag{2.10}$$

where N_{Shaded} is the number of shaded PV modules and N_{String} is the number of modules in the PV string. The shading rate is a factor to reflect the shading ratio of a PV string. The shading strength is denoted as ρ. The definition of the shading strength is given in Equation (2.11).

$$\rho = \frac{G_{\text{Shaded}}}{G_{\text{Insolated}}}, \tag{2.11}$$

where G_{Shaded} is the solar irradiance of the shaded PV module and $G_{\text{Insolated}}$ is the normal irradiance that the unshaded PV modules receive. The value of the shading strength

indicates the solar irradiation situation for a partial shading scenario.

Take the PV string in Figure 2.3 as an example, the PV string comprises four PV modules where two PV modules are shaded. Thus, the number of shaded PV modules N_{Shaded} is 2, and the number of modules in the PV string N_{String} is 4. The insolated PV modules get the solar irradiance of 1000 W/m^2 and the shaded modules receive the irradiance of 600 W/m^2. Under such PSC, the solar irradiance of the shaded PV module G_{Shaded} is equal to 600 W/m^2. The insolated irradiance $G_{\text{Insolated}}$ is 1000 W/m^2. Finally, the shading rate and shading strength under the shading scenario in Figure 2.3 can be calculated in Equation (2.12).

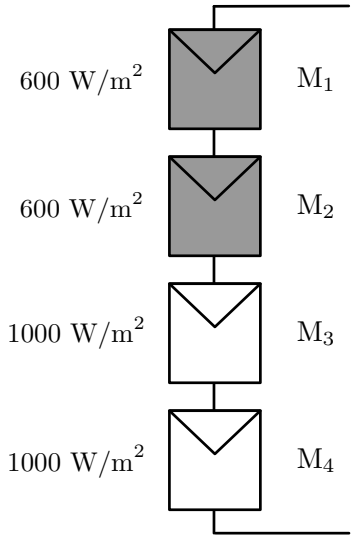

Figure 2.3: An example of partial shading conditions.

$$\begin{aligned} \chi &= \frac{N_{\text{Shaded}}}{N_{\text{String}}} = \frac{2}{4} = 0.5, \\ \rho &= \frac{G_{\text{Shaded}}}{G_{\text{Insolated}}} = \frac{600}{1000} = 0.6. \end{aligned} \tag{2.12}$$

The shading rate is usually used to indicate the shading ratio of the PV string under PSC. The shading strength reflects the solar irradiation conditions for the shaded PV modules. The combination of the shading rate and the shading strength is capable of expressing the number and the received irradiation condition of the shaded PV modules in

the PV strings. Unfortunately, these two types of shading information are limited to the PSC with two irradiation levels according to their definitions. Thus, the previous shading information is not compatible with the PSC with more than two irradiation levels. In the thesis, to address the complicated shading information, two kinds of novel shading information will be proposed, namely shading matrix and shading vector. The introduction of the shading matrix and the shading vector will solve the disadvantages of the traditional shading information and support the characterization for PSC with more than two irradiation levels.

2.4 Maximum Power Point Tracking Techniques

The electrical characteristics of PV systems have been discussed in Section 2.1. The I-V and power-voltage (P-V) characteristics of a PV module is shown in Figure 2.4. At the open-circuit voltage V_{OC} and the short-circuit current I_{SC} points, the power generated is zero. The maximum power P_{MPP} is generated at a point where the product of module current and voltage reaches the maximum. And this point is called the Maximum Power Point (MPP). MPPT technique is used to improve the efficiency of the PV module by tracking such MPP.

There are different kinds of techniques for tracking the MPP. Some of the most popular techniques are Perturb and Observe (P&O) [5, 31], Incremental Conductance (IncCond) [32], Fractional Open-Circuit Voltage (FOCV) [33], and Fractional Short-Circuit Current (FSCC) [34–36]. P&O and IncCond are two typical search-based MPPT techniques. Such search-based MPPT methods perturb the system operating point and observe whether the power increases. The increase in the power means that the perturbation direction is correct, and vice versa. The FOCV and FSCC are two fundamental fraction-based MPPT methods. This kind of method usually estimates the location of the MPP by the product of a fixed or adaptive fractional value and the open-circuit voltage or short-circuit current. These MPPT techniques are popular for their simplicities. They normally work well for the PV systems under UIC. However, when applying these techniques in the PSC, they may not track the GMPP in most shading scenarios. The direct influence of the PSC is the reduction of the generated power from the PV array [37]. Besides, the I-V and P-V characteristics of the PV systems under PSC exhibit multiple stairs and peaks [38]. Only one GMPP and several Local Maximum Power Points (LMPPs) occur at the P-V characteristic curves under PSC. Thus, under such situations, the above search-based

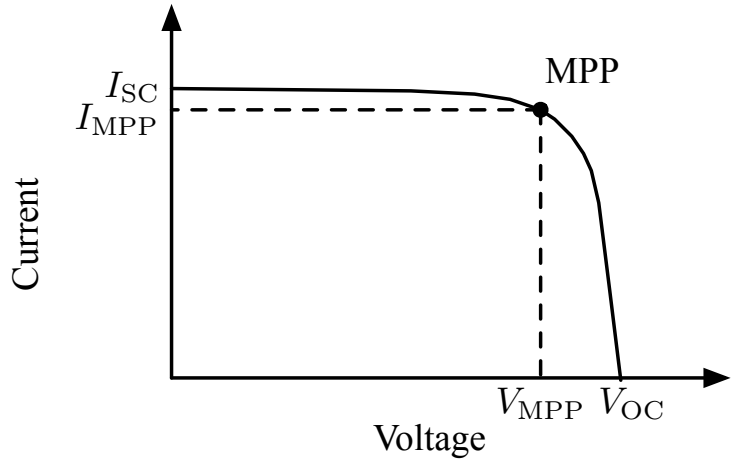

(a)

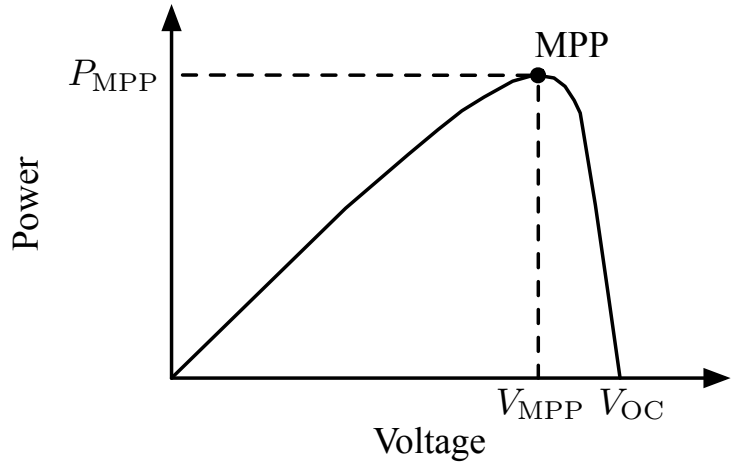

(b)

Figure 2.4: PV characteristics of a PV module: (a) current-voltage; (b) power-voltage.

MPPT methods are not capable of distinguishing the GMPP and the LMPPs. The wrong selection of the initial search point may result in the LMPP instead of the GMPP [39]. Therefore, the capability of searching for the GMPP is critical for a GMPPT system. To address this issue, a number of Global Maximum Power Point Tracking (GMPPT) methods have been proposed in recent years. Early studies have shown that according to the features, there are mainly three categories for the GMPPT methods [40, 41]:

1. Soft computing methods: The soft computing methods are the applications of the Artificial Intelligence (AI) (such as ANN [42–44], Particle Swarm Optimization (PSO) [45, 46], and Fuzzy Logic Control (FLC) [47–50]) into the MPPT techniques. Since PSC can be considered as an optimization problem, these methods can provide good performance under different shading patterns. However, these methods usually require significant computation processing and are difficult to implement.

2. Segmental search methods: The segmental search methods contain Dividing Rectangle (DIRECT) method [51] and the Fibonacci method [52]. This category of methods takes advantage of simplicity and rapid tracking speed since they are based on some solid mathematical theories. However, these approaches may be trapped into one of the LMPPs but not the GMPP under some special shading patterns.

3. Two-stage methods: According to its name, the two-stage methods contain two steps. An approximate position at the GMPP is determined in the first stage, and then the traditional search-based MPPT methods are applied to find the exact GMPP from the determined location in the second stage. A number of two-stage MPPT methods have been proposed during the last ten years [53–55]. The main difference between these methods is the determination method at the first stage. Thus, the main challenge is how to locate the GMPP in the first stage in a fast and efficient way.

At the end of this section, some MPPT methods used in the comparison studies of this thesis are illustrated with detailed methodologies.

2.4.1 Incremental Conductance Method

The derivative of power to voltage is given in Equation (2.13).

$$\frac{dP(k)}{dV(k)} = \frac{d(V(k) \times I(k))}{dV(k)} = I(k) + V(k) \times \frac{dI(k)}{dV(k)}, \tag{2.13}$$

where $P(k)$, $V(k)$, and $I(k)$ are the power, voltage, and current of the PV system at time k respectively.

According to the P-V characteristics in Figure 2.4(b), the value of $dP(k)/dV(k)$ is positive at the left slope to the MPP, zero at the MPP, and negative at the right slope to the MPP. Therefore, the corresponding relations is formulated in Equation (2.14).

$$\frac{dP(k)}{dV(k)} = \begin{cases} I(k) + V(k) \times \dfrac{dI(k)}{dV(k)} > 0, & V(k) < V_{\mathrm{MPP}}, \\ I(k) + V(k) \times \dfrac{dI(k)}{dV(k)} = 0, & V(k) = V_{\mathrm{MPP}}, \\ I(k) + V(k) \times \dfrac{dI(k)}{dV(k)} < 0, & V(k) > V_{\mathrm{MPP}}, \end{cases} \tag{2.14}$$

where V_{MPP} is the voltage at MPP. Equation (2.14) can be further revised as Equation (2.15).

$$\begin{cases} \dfrac{dI(k)}{dV(k)} > -\dfrac{I(k)}{V(k)}, & V(k) < V_{\mathrm{MPP}}, \\ \dfrac{dI(k)}{dV(k)} = -\dfrac{I(k)}{V(k)}, & V(k) = V_{\mathrm{MPP}}, \\ \dfrac{dI(k)}{dV(k)} < -\dfrac{I(k)}{V(k)}, & V(k) > V_{\mathrm{MPP}}. \end{cases} \tag{2.15}$$

Based on Equation (2.15), the position of the current operating point $V(k)$ can be obtained by comparing the value of $dI(k)/dV(k)$ and $-I(k)/V(k)$. When $dI(k)/dV(k) = -I(k)/V(k)$, the MPP is reached; when $dI(k)/dV(k) > -I(k)/V(k)$, the current operating point is to the left of the MPP; when $dI(k)/dV(k) < -I(k)/V(k)$, the current operating point is to the right of the MPP. The detailed flowchart to show the procedure of the IncCond MPPT method is shown in Figure 2.5. V_{Step} is the voltage step.

To avoid the situation that $dV(k) = 0$, where $dI(k)/dV(k)$ has no meaning, the IncCond method first check if $dV(k)$ is zero. When $dV(k) = 0$, the next determination of the next voltage locus $dV(k+1)$ depends on the value of $dI(k)$. When $dV(k)$ is not zero, then compare the values of $dI(k)/dV(k)$ and $-I(k)/V(k)$. Based on the rules in Equation (2.15), the IncCond updates the next voltage $dV(k+1)$. Finally, the PV system reaches the MPP by updating the operating point under such a procedure.

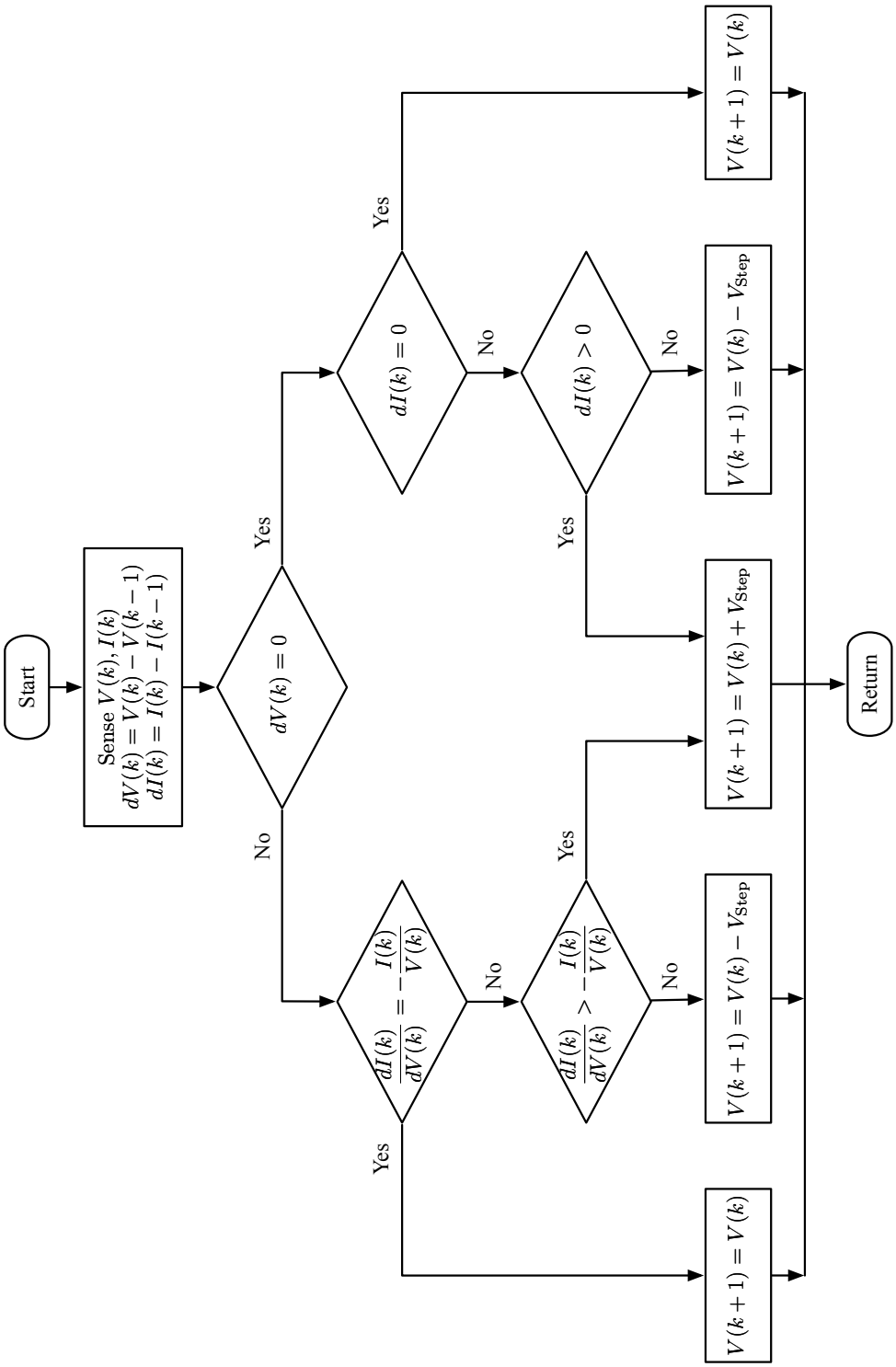

Figure 2.5: Flowchart of the incremental conductance MPPT method.

2.4.2 Full Scanning Method

The Full Scanning (FS) technique was proposed by Koutroulis and Blaabjerg [54] in 2012. This is a straightforward method that blindly scans the whole voltage range to search the GMPP. This method takes advantage of its simplicity, but a few power loss points are involved in the scanning area (e.g. short-circuit point and open-circuit point). Besides, the tracking performance is highly dependent on the scanning step. With a smaller scanning step, the system can track the precise GMPP, but the scanning procedure is longer. With a larger scanning step, the scanning speed is faster but the system may overlook the GMPP.

2.4.3 $0.8V_{OC}$-Model-Based Method

The $0.8V_{OC}$ model originated from the work in [56] and [57] has shown that all the peaks in the P-V characteristic curve occur at the integer multiples of 80% of the open-circuit voltage ($0.8V_{OC}$). Compared with the FS technique in [54], only the vicinities of the $0.8V_{OC}$ are scanned, and as a result, the scanning time is significantly reduced. A comparative study was conducted in [58] between the conventional P&O technique, the FS technique, and a $0.8V_{OC}$-model-based method. The comparative results showed that under some shading patterns, the P&O technique is trapped at the LMPPs. The full scanning method tracks the GMPP accurately, but the convergence time is significant. The GMPP is not guaranteed to be tracked by the $0.8V_{OC}$-model-based method, but compared with the full scanning technique, the tracking speed is largely improved [58].

In recent years, a number of $0.8V_{OC}$-model-based MPPT methods have been proposed [39, 55, 59–64]. In [59], a new hybrid GMPPT algorithm containing an improved $0.8V_{OC}$-model-based approach, with a smart power scanning procedure, was proposed. The tracking efficiency has been improved by up to 11.29% compared with the technique which monitors voltage and current variations. Limited and adaptive scanning approaches have been proposed to improve the $0.8V_{OC}$ model [39, 61, 62]. The scanning ranges of the duty cycle for each $0.8V_{OC}$ region are generated from the PV parameters. By scanning the generated duty cycle ranges, this approach avoids the voltage tuning process and makes the system simple. However, some regions are scanned repeatedly since overlaps exist between two adjacent scanning ranges. A modified IncCond method based on the idea of the $0.8V_{OC}$ model was proposed in [55]. A novel duty cycle computation method for tuning the operating voltage was introduced to improve the scanning speed. The Search-Skip-Judge Global MPPT (SSJ-GMPPT) method in [63] modifies the comparing procedure of the

original $0.8V_{OC}$ model to avoid some unnecessary scanning processes under some specific shading scenarios. The Rapid Global MPPT (R-GMPPT) method in [63] introduces the current sensing circuit for estimating the approximate GMPP. Therefore, the tracking time of the R-GMPPT is significantly reduced by more than 90% compared to the traditional global search method [63]. To obtain the peak power at each multiple of the $0.8V_{OC}$ region, Aquib et al. [64] proposed an intelligent technique to compute the reference voltage value for the traditional P&O method. The GMPP is determined afterward by comparing each peak power. The $0.8V_{OC}$ model is capable of determining the GMPP under most shading patterns. However, one of the critical disadvantages of the aforementioned $0.8V_{OC}$-model-based approaches is that the tracking performance of the $0.8V_{OC}$ model is highly dependent on the length of the PV string [25]. More computation time is required on iteratively scanning the $0.8V_{OC}$ vicinities for the longer PV strings.

Figure 2.6 shows the P-V curves under varied shading patterns for a PV string with three modules. The peaks in the P-V curves are distributed into three individual regions marked by peak regions 1-3. Different colors in the P-V curves are used to distinguish that the GMPP appears at different peak regions. For example, the GMPP exists at the peak region 3 for the blue P-V curves. Therefore, under various shading conditions, the GMPP may appear at any peak region.

For a single PV module, the MPP appears at the vicinity of $0.8\times V_{OC,M}$, where $V_{OC,M}$ is the open-circuit voltage of a single PV module. For a PV string, based on the $0.8V_{OC}$ model, the peak regions of the P-V curve are approximately at the multiples of $0.8\times V_{OC,M}$ and the GMPP is the peak region with the largest power.

The $0.8V_{OC}$-model-based MPPT method is a typical two-stage GMPPT method. At the first stage, the $0.8V_{OC}$ model determines the $0.8V_{OC}$ region with the largest power as the GMPP region by iteratively measuring and comparing the power at each $0.8V_{OC}$ region. At the second stage, the conventional MPPT technique (such as P&O and IncCond) is used to track the accurate GMPP. However, such measuring and comparing process takes a long time to get the GMPP region, especially for long PV strings. The efficiency of the $0.8V_{OC}$-model-based MPPT method can be improved by solving this problem.

2.4.4 Particle-Swarm-Optimization-Based Methods

In recent years, many metaheuristic optimization algorithms have been applied to address the MPPT problems under partial shading conditions [65–70]. According to the intrinsic

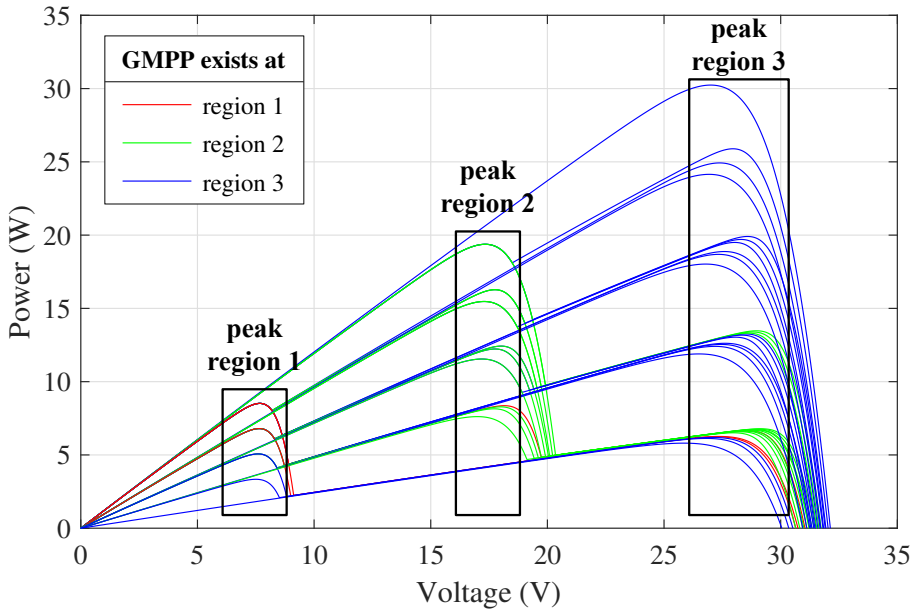

Figure 2.6: P-V curves of a PV string with three series modules owning three peak regions.

properties of the optimization algorithms, these methods have the following two drawbacks. First, due to random sampling, the optimization-algorithm-based methods may get different prediction/tracking errors in each run. Moreover, the optimization algorithms cannot guarantee that the global optimum can be obtained every time [71]. Sometimes these optimization-algorithm-based methods will be trapped in the local MPPs.

PSO is one of the most popular optimization algorithms. A number of studies have been conducted to utilize the PSO algorithm to solve the MPPT problems [7, 45, 46, 72–76]. The PSO-based MPPT methods can be considered as an adaptive version of P&O method [45]. In P&O, the duty cycle $d(k)$ is updated as shown in Equation (2.16).

$$d(k+1) = \begin{cases} d(k) + \phi, & \text{if } P(k+1) \geq P(k), \\ d(k) - \phi, & \text{if } P(k+1) < P(k), \end{cases} \tag{2.16}$$

where ϕ is the step of duty cycle.

PSO algorithm keeps a swarm of particles and each particle represents a candidate solution. The position of each particle is influenced by its best solution as well as the global best solution obtained by the other particles in the entire population. Based on the idea of the PSO algorithm, Equation (2.16) can be written as Equation (2.17).

$$d(k+1,i) = d(k,i) + \phi(k+1,i), \tag{2.17}$$

where $d(k,i)$ is the duty cycle (position) of the ith particle. $\phi(k,i)$ is the velocity component of the ith particle, which can be considered as an adaptive step size of duty cycle. And $\phi(k,i)$ is updated according to Equation (2.18).

$$\phi(k+1,i) = \omega\phi(k,i) + c_1 r_1[P_{\text{Best},i} - d(k,i)] + c_2 r_2[G_{\text{Best}} - d(k,i)], \tag{2.18}$$

where ω is the inertia weight. c_1 and c_2 are the acceleration coefficients. r_1 and r_2 are two random number between 0 and 1. $P_{\text{Best},i}$ is the personal best position of partial i. G_{Best} is the global best position of partials in the entire population. The value of $\phi(k,i)$ is the perturbation in the duty cycle, which is determined by the $P_{\text{Best},i}$ and G_{Best}. If the current duty cycle is far from these two best values, the resulting perturbation is large, and vice versa. With a proper selection of the updating parameters (i.e., ω, c_1, and c_2), a suitable PSO-based MPPT method could be easily designed.

2.5 Summary

In this chapter, some related work has been introduced as supplementary materials to the following chapters. By analyzing the electrical characteristics for the PV strings in Section 2.1, the equation for a reference slope is constructed for the identification methods in Chapter 4. Some shading detection methods in the literature are presented in Section 2.2. The traditional shading information is formulated in Section 2.3, which is the fundamental information for the rest of this thesis. Section 2.4 summarizes the background of the MPPT techniques. Some GMPPT methods used in the comparison studies in the thesis are also illustrated, including IncCond, FS, $0.8V_{OC}$-model-based, and PSO-based methods.

Chapter 3

Automatic Shading Detection System

Partial shading is one of the main factors that affect the output power of series-parallel PV strings. However, physical irradiance measurement instruments are rarely used in commercial PV systems due to their high cost. This chapter proposes an automatic shading detection system for estimating the shading rate by using voltage sensors. The main features of the proposed method are the utilization of a reduced number of sensors, a simple switching control strategy, and a high detection rate. The feasibility and effectiveness of the proposed shading detecting system are verified through hardware experiments.

The contents of this chapter have been published in the following paper:

- Jieming Ma, Ziqiang Bi, Ka Lok Man, Yong Yue, Jeremy S. Smith, "Automatic Shading Detection System for Photovoltaic Strings," International SoC Design Conference (ISOCC), pp. 176-177, 2018.

3.1 Introduction

Even in near-ideal solar locations, partial shade from passing clouds, neighboring buildings, trees or dust is inevitable in PV strings. Early studies have shown that partial shade can dramatically cut an entire solar string's output [77]. Bypass diodes serve as a protection mechanism that allows the PV module to continue producing power under PSC [78]. Experiments demonstrate that the P-V characteristic curves of PV strings obtain multiple

peaks under PSC [79]. Therefore, knowing the PSC information is important for MPPT control and system maintenance.

Zheng et al. [80] demonstrated that the number of local maximum power points depends on the bypass diode configurations and string topology under PSC. The occurrence of partial shade is usually identified by a sudden significant change in output power. However, it is hard to distinguish the PSC from the rapidly changing atmospheric conditions. Ma et al. [81] proposed a partial shading detection method by the relations between the module voltage and the string voltage, but the system cost is high. Silvestre et al. [82] proposed reference thresholds for detecting PSC based on the errors between simulated and measured capture losses. Although many shading detection methods have been proposed in recent years, not many of them can estimate the shading rate [11] of the partially shaded PV systems.

In this chapter, an automatic shading detection system has been proposed, which is the first detection system to estimate the shading rate of PV strings. The main features of the detection system are not only the high detection rate, but also the utilization of the reduced number of sensors and the simple control strategy.

3.2 Shading Detection Strategy

This section describes the methodology for the proposed shading detection system. The voltage measurement system with switching controlling is introduced to detect the shading and estimate the shading rate χ. The resetting strategy is proposed to ensure a continuous detection.

3.2.1 Voltage Measurement System

Figure 3.1 is an example of the voltage characteristics of a PV string under PSC. A PV string with three modules is shown in Figure 3.1(a). Figure 3.1(b) is the output voltage versus the duty cycle of the DC-DC converter for each PV module. In such shading scenario, M_3 is bypassed by the bypass diode as it is shaded. As a result, M_3 does not output any voltage. For the rest of the PV string, the voltages of M_1 and M_2 are the same which are half of the string voltage. Based on the above observations, the voltages for all the insolated PV modules in the PV string are distributed evenly. When each PV module with the same model operates at the same irradiation and temperature conditions,

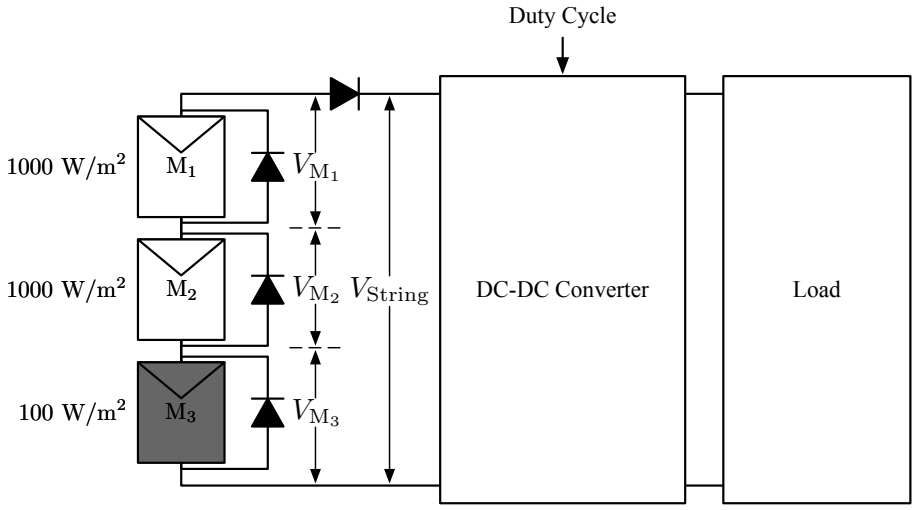

(a)

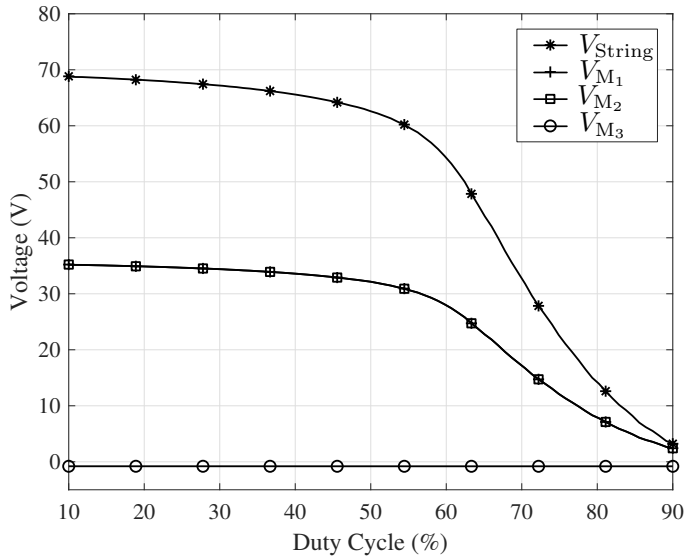

(b)

Figure 3.1: An example for the voltage characteristics of a PV string: (a) the diagram for the PV string; (b) the voltage versus duty cycle for each module.

the resistance characteristic should be identical. Based on the voltage divider rule, the voltage across each PV module should be the same. According to these characteristics, the number of insolated PV modules in this PV string can be calculated by Equation (3.1).

$$N_{\text{Insolated}} = \frac{V_{\text{String}}}{V_{\text{M}_1}} = \frac{V_{\text{String}}}{V_{\text{M}_2}}, \tag{3.1}$$

where $N_{\text{Insolated}}$ is the number of insolated PV modules. V_{String} is the string voltage. V_{M_1} and V_{M_2} are the voltages for M_1 and M_2, respectively.

When $V_{\text{Insolated}}$ denotes the voltage for one insolated PV module, Equation (3.1) can be generalized to Equation (3.2).

$$N_{\text{Insolated}} = \frac{V_{\text{String}}}{V_{\text{Insolated}}}. \tag{3.2}$$

Based on the definition of the shading rate in Equation (2.10), the shading rate χ can be calculated by Equation (3.3).

$$\chi = 1 - \frac{N_{\text{Insolated}}}{N_{\text{String}}}. \tag{3.3}$$

Finally, the shading rate χ (the proportion of shaded modules in the PV string), can be estimated as soon as one unshaded module voltage is measured. Thus, the proposed shading detection system estimates the shading rate by measuring the module voltages. Figure 3.2 shows the block diagram of the proposed shading rate estimation system for a PV string with N_{String} modules. Only two voltage sensors are utilized in the voltage measurement system. One is used to measure the string voltage V_{String} and the other one is used to measure the module voltage $V_{\text{Insolated}}$. A switch module is used to enable the voltage sensor to read the voltage for different sub-strings. Although the voltage sensor measuring the string voltage can be removed by adding one more path in the switch module, more operations are required to measure the string voltage. And in most cases, no action is needed for the switch module when the first PV module is insolated. Thus, a specialized voltage sensor for measuring the string voltage is used to improve the detection efficiency.

3.2.2 Switching Control Strategy

When the string current is larger than the short-circuit of the shaded PV modules, the current bypasses the shaded modules. The voltage across the bypass diodes is around

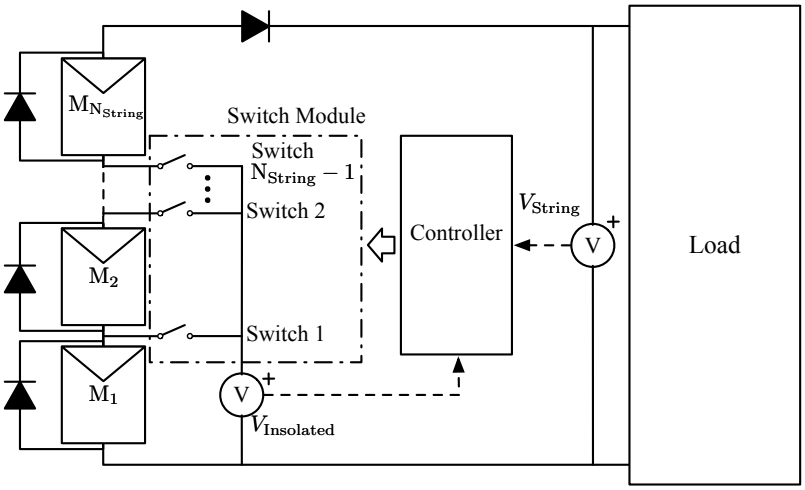

Figure 3.2: Block diagram of the shading rate detection circuit.

0.7 V. Thus, in this detection system, a module is considered as a shaded module if the measured sub voltage is less than the threshold voltage V_{Th} (V_{Th} is set to 1 V based on the error observation from the simulation). Since the bypassed shaded modules generate the reversed voltage, the string voltage V_{String} is nearly the summation of the voltage of the insolated modules. Assume $V_{\mathrm{Insolated}}$ is the voltage of an insolated module, the number of insolated modules can be calculated by the ratio between V_{String} and $V_{\mathrm{Insolated}}$ as the voltages for the PV module are evenly distributed.

Thus, the shading rate can be estimated by measuring the voltage of an insolated PV module $V_{\mathrm{Insolated}}$. The pseudocode of the controlling algorithm, for the switch module, to measure the voltage of the first insolated module in the PV string is shown in Algorithm 3.1. The flowchart of the procedure to get the final shading rate value is given in Figure 3.3. Let i be the switch index ($0 < i < N_{\mathrm{String}}$). If a shaded module is detected ($V_{\mathrm{Insolated}} < V_{\mathrm{Th}}$), switch i will be opened and switch $i + 1$ will be closed. As soon as the system gets the voltage of an insolated module $V_{\mathrm{Insolated}}$, the number of the insolated PV modules $N_{\mathrm{Insolated}}$ can be expressed as Equation (3.4).

$$N_{\mathrm{Insolated}} = \mathrm{round}(\frac{V_{\mathrm{String}}}{V_{\mathrm{Insolated}}}). \tag{3.4}$$

By substituting the value of $N_{\mathrm{Insolated}}$ into Equation (3.3), the estimation value of the shading rate is obtained.

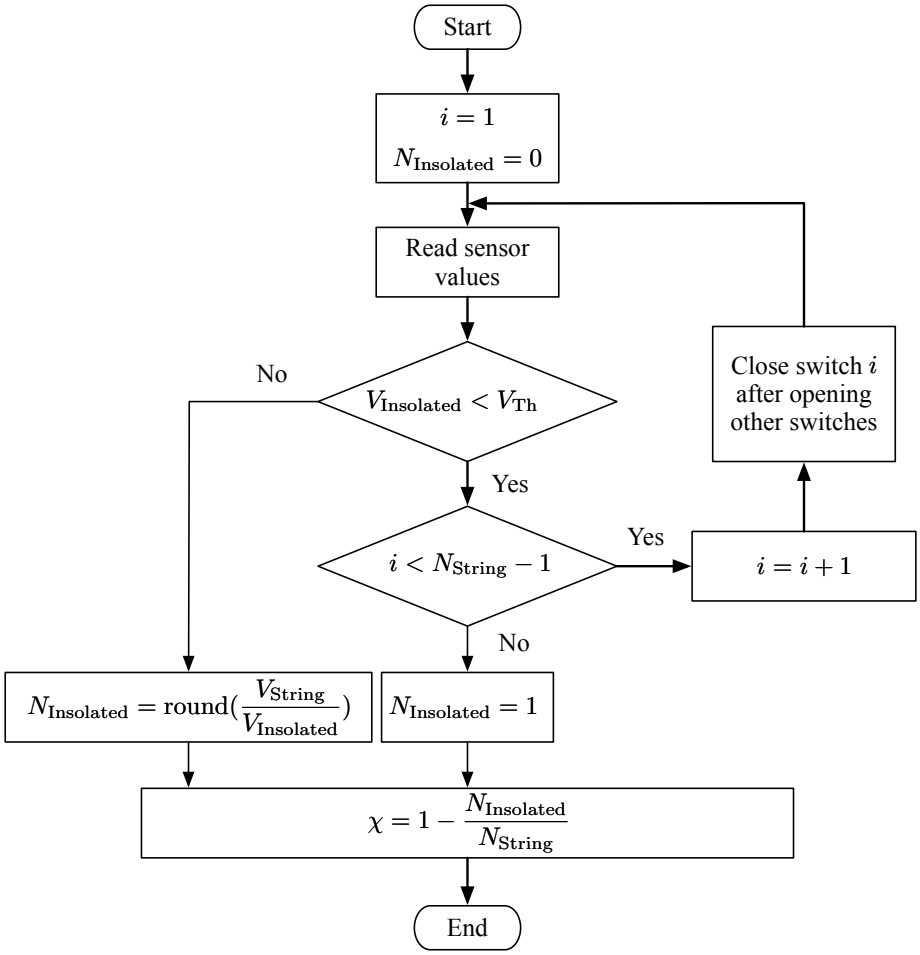

Figure 3.3: Flowchart of the shading detection algorithm.

3.2.3 Resetting Strategy

The PSC may not be fixed for a continuous operating shading rate estimating system. The estimating system needs to be reset when the bypassed shaded module becomes insolated again. Two new parameters V_{Std} and β have been proposed to detect the anomaly. V_{Std} is initialized to V_{String} and it will be updated to $V_{\text{Insolated}}$ every time when the system successfully obtains the $N_{\text{Insolated}}$. β is a ratio value and set to 1.5 in this method. Thus, $V_{\text{Insolated}} > \beta V_{\text{Std}}$ indicates that there exists more than one insolated PV module among the measured modules and the detection system will be set to the initial state as shown in Algorithm 3.2. The flowchart to obtain the value of the shading rate is shown in Figure 3.4.

Algorithm 3.1 Switching control strategy.

Input: the switch index i, the threshold voltage V_{Th}
Output: the number of the insolated PV modules $N_{\mathrm{Insolated}}$

```
i ← 1; N_Insolated ← 0
while !N_Insolated do
    Read sensor values
    if V_Insolated < V_Th then
        if i < N_String − 1 then
            i ← i + 1
        else
            N_Insolated ← 1
        end if
    else
        N_Insolated ← round(V_String/V_Insolated)
    end if
    Close switch i after opening other switches
end while
```

Algorithm 3.2 Switching control and resetting strategy.

```
i ← 1; β ← 1.5
V_Std ← V_String; N_Insolated ← 0
while true do
    Read sensor values
    if V_Insolated < V_Th then
        if i < N_String − 1 then
            i ← i + 1
        else
            N_Insolated ← 1
            V_Std ← (V_String − V_Insolated)
        end if
    else if V_Insolated > βV_Std then
        i ← 1
    else
        N_Insolated ← round(V_String/V_Insolated)
        V_Std ← V_Insolated
    end if
    Close switch i after opening other switches
end while
```

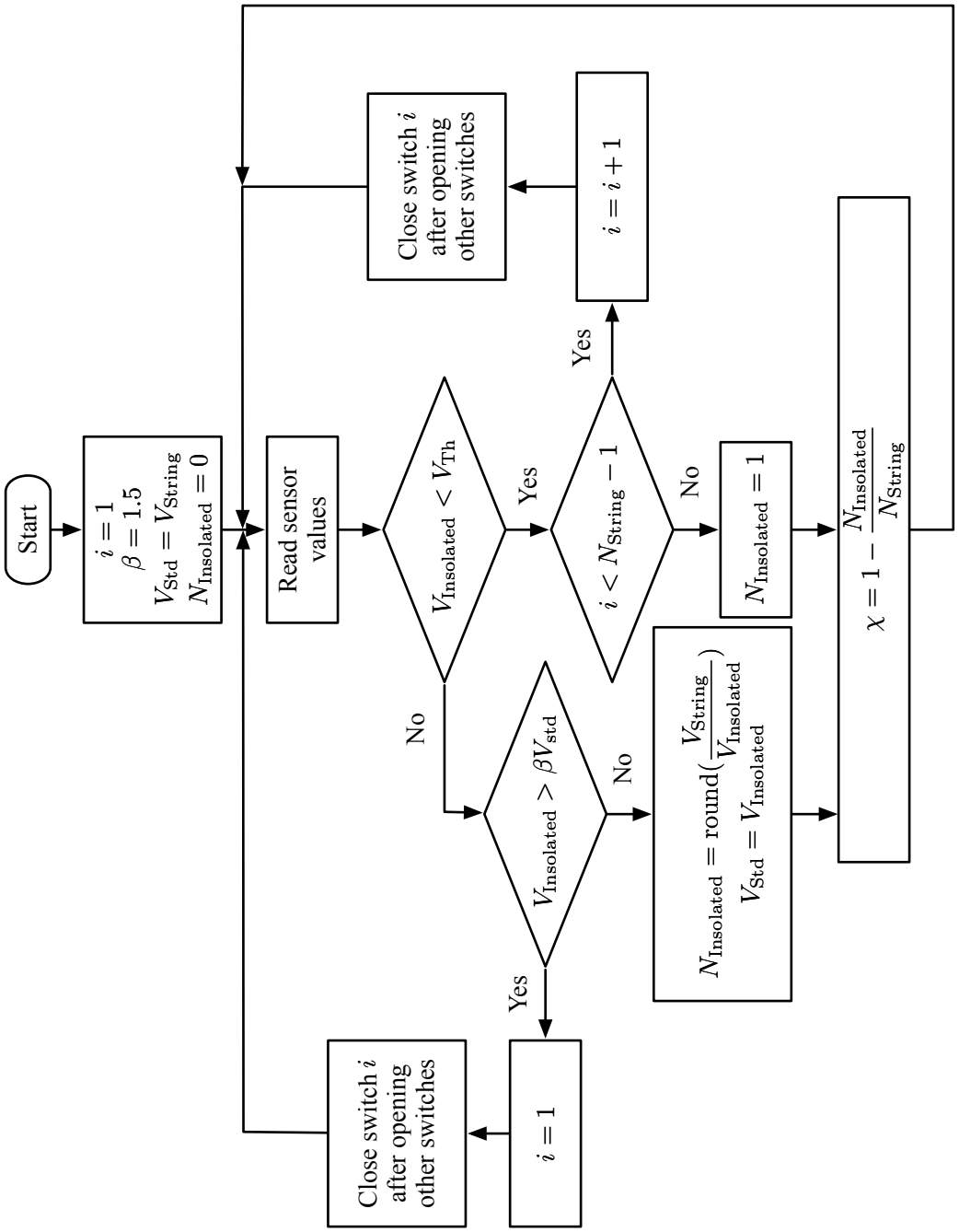

Figure 3.4: Flowchart of the shading detection algorithm with resetting strategy.

3.3 Experimental Validation

Both instantaneous and dynamic experiments were conducted in order to validate the feasibility of the above two algorithms in Section 3.2. Section 3.3.1 introduces the experimental setup and environment. The experimental results are shown in Sections 3.3.2 and 3.3.3.

3.3.1 Experimental Setup

The overview of the experimental setup is shown in Figure 3.5. The experimental detection system consists of four 10 W PV modules (I_{SC} = 1.23 A,V_{OC} = 10.71 V), a DC electronic load (ITECH IT8512A+), an oscilloscope (GWINSTEK GDS-2202A), a voltage sensor module, a relay module, and a central controller (UDOO NEO FULL). Experiments were conducted to evaluate the feasibility of the proposed method.

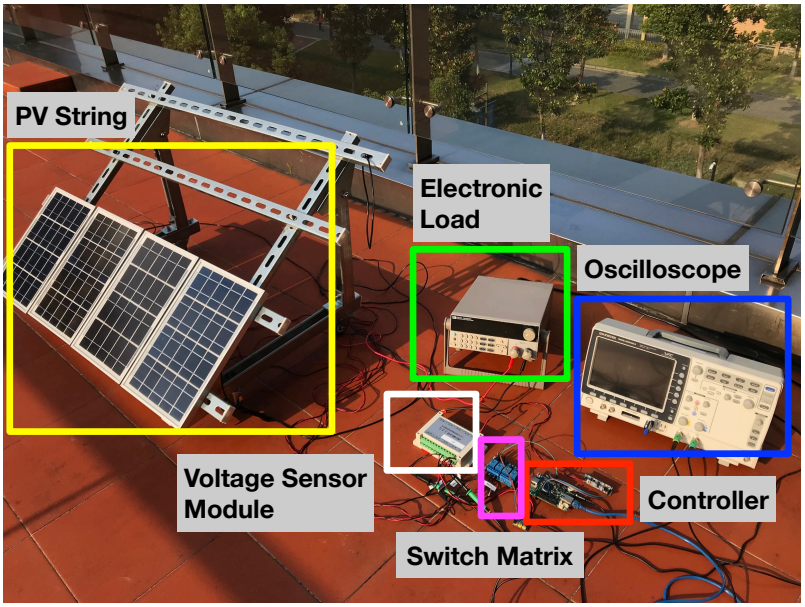

Figure 3.5: Experimental setup of the validation system.

The experiment was conducted in Xi'an Jiaotong-Liverpool University, Suzhou, China (latitude 31.2745°N, longitude 120.7383°E roughly). It was a sunny day at around 16:20, 9 August 2018. The ambient temperature during the experiment was around 31 °C. The insolated PV modules received about 600 W/m^2 and shaded modules received 55 W/m^2. The DC electronic load was set to constant resistance mode.

3.3.2 Instantaneous Results

Table 3.1 shows the instantaneous experimental results under different shading patterns. The complete PV module (all the PV cells in the module) was manually shaded by the double-layer cardboard. For the shading pattern in the table, '1' represents the shaded modules and '0' represents the insolated modules. The correctness of the proposed detection system was 100% among 15 shading patterns as shown in Table 3.1. The maximum number of the shaded PV modules is 3 as the situation that all the modules in the string are shaded that is not included in this work.

Table 3.1: Experimental results under different shading patterns.

Shading Pattern (M1-M4)	V_{String} (V)	$V_{\text{Insolated}}$ (V)	Switch Index i	$V_{\text{String}}/V_{\text{Insolated}}$	$N_{\text{Insolated}}$
0000	42.44	10.54	1	4.0265	4
0001	31.83	10.56	1	3.0142	3
0010	31.60	10.54	1	2.9981	3
0011	21.65	10.87	1	1.9917	2
0100	32.47	10.82	1	3.0009	3
0101	22.20	10.96	1	2.0255	2
0110	22.03	10.94	1	2.0137	2
0111	10.98	10.92	1	1.0054	1
1000	31.97	10.54	2	3.0332	3
1001	21.49	10.75	2	1.9990	2
1010	21.07	10.56	2	1.9952	2
1011	10.62	10.56	2	1.0056	1
1100	20.95	10.33	3	2.0281	2
1101	10.49	10.42	3	1.0067	1
1110	10.43	0.22	3	/	1

3.3.3 Dynamic Results

Figure 3.6 shows the time-sequence results of the experiment to test the robustness of the proposed detection method under a rapidly changing partial shading condition. The values of $V_{\text{Insolated}}$ and V_{String} are respectively shown by yellow and cyan curves on the oscilloscope. The bottom red wave is the calculated $N_{\text{Insolated}}$. Four different PSC were manually set in the experiment. In T1, all modules were insolated and $N_{\text{Insolated}} = 4$. In T2, T4, and T6, it could be observed that $N_{\text{Insolated}}$ was correctly estimated. Due to the voltage measuring interval (the voltages were measured every 3 seconds in this experiment), the right switches could not be closed in T3 and T5, which led to wrong estimates. As soon as the controller got the new voltages, the $N_{\text{Insolated}}$ could be predicted and the χ could be calculated by Equation (3.3).

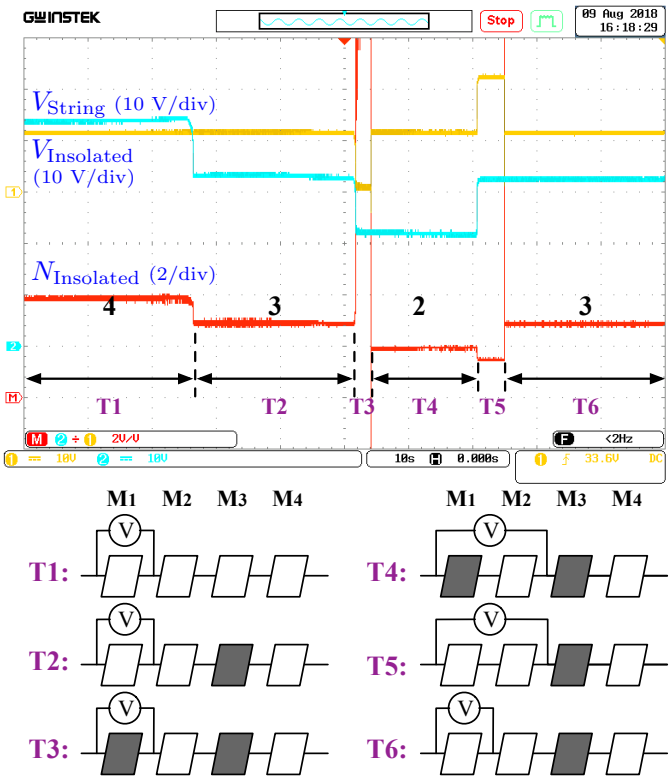

Figure 3.6: Time-sequence experimental results.

3.4 Summary

This chapter has presented a novel automatic shading detection system for PV strings, which is the first detection system to detect the shading rate information. The shading is detected by using a voltage measurement system with the proposed switching control strategy. The value of the shading rate can be estimated through the voltage distribution relation among the PV modules. A resetting strategy is proposed to make sure that the estimation method is capable for long-term running tasks. Instantaneous and dynamic experiments have been conducted with a 4-module PV string. Experimental results have shown that the system has the ability to estimate the shading rate effectively. When more modules are connected in a PV string, the efficiency of the proposed detection system is not affected too much. In most cases, the system will obtain the result in one step when the first PV module in the PV string is not shaded.

Chapter 4

Identification of Partial Shading Conditions

Under Partial Shading Conditions (PSC), the power-voltage (P-V) characteristic curve of Photovoltaic (PV) strings exhibits multiple peaks. Such mismatching phenomenon brings challenges in controlling the output power. To analyze the electrical characteristics of PV strings in complex environments, a quantitative analysis method is required to characterize the PSC. This chapter introduces the shading matrix to describe the shading rate and shading strength information. The proposed shading matrix would provide Maximum Power Point Tracking (MPPT) controllers with the essential environmental information to improve the Global Maximum Power Point (GMPP) tracking performance. A Modified Tabu Search (MTS) based identification method is proposed to estimate the shading matrix. The proposed modified method involves a preselection process of updating the Tabu list to optimize the searching efficiency. The accuracy and efficiency of the proposed analytical estimation expression are validated through simulations and experiments. By comparing with Binary Search (BS), Golden-section Search (GS), and Tabu Search (TS) algorithms, the proposed MTS algorithm can be applied to perceive the shading information at least 18.75% faster.

The contents of this chapter have been published in the following paper:

- Ziqiang Bi, Jieming Ma, Kangshi Wang, Ka Lok Man, Jeremy S. Smith, Yong Yue, "Identification of Partial Shading Conditions for Photovoltaic Strings," IEEE Access, vol. 8, pp. 75491-75502, 2020.

4.1 Introduction

In PV systems, PV modules are usually connected in series or parallel to form a PV string or array in order to generate sufficient power. The series-connected PV string is the prior configuration of PV modules in terms of the lowest mismatch power losses due to the non-uniform irradiance [83]. When the PV modules in a PV string receive non-uniform solar irradiations, the string is considered to operate under PSC. The shaded PV modules would be easily damaged under PSC without any protection due to the "hotspot" effect [84]. As a result, bypass diodes are normally connected to the PV modules [85]. However, with the existence of the bypass diodes, the current-voltage (I-V) characteristic curves exhibit multiple stairs with turning points [27, 28, 86]. Correspondingly, the P-V characteristic curves of the PV string exhibit multiple peaks [38] under PSC. That brings difficulties in controlling and optimizing the output string power. A quantitative analysis of PSC would provide necessary information for the power management systems.

Although the traditional shading information introduced in the Section 2.3 is a mathematical method to characterize the PSC, the existing shading information are limited to express simple shading scenarios, which have only two solar irradiation levels. In order to cover the complicated PSC, this chapter proposes a comprehensive shading identification approach. The shading matrix is introduced to quantitatively analyze the PSC with multiple irradiation levels. An MTS-based identification method is proposed to estimate the shading matrix from the located turning points. The proposed method would provide MPPT controllers with the essential environmental information to improve the GMPP tracking performance.

The rest of the chapter is organized as follows: Section 4.2 introduces the shading matrix for PSC. The methodologies of the identification method for the shading matrix are shown in Section 4.3. The simulation and experimental results are demonstrated in Section 4.4 to verify the accuracy and efficiency of the proposed identification method. Section 4.5 summarizes this chapter.

4.2 Shading Matrix

Figure 4.1 shows the I-V characteristics of a PV string with three modules. The PV string operates under the PSC with three individual irradiation levels. Two turning points are exhibited on the I-V curve, which are marked with red circles. For a PV string with N_{String}

modules, the I-V curve is divided into N_{String} adjacent intervals with the same length. The boundaries of the intervals are at the integer multiples of $V_{\text{OC,String}}/N_{\text{String}}$ and marked by the blue vertical dashed lines in Figure 4.1. Each interval has at most one turning point. Assume that one turning point at V_{TP} is located in the mth interval, then the range of V_{TP} can be obtained as given in Equation (4.1).

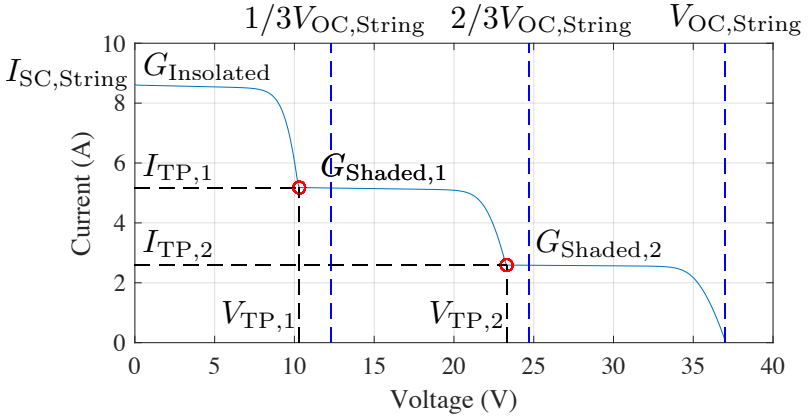

Figure 4.1: I-V characteristics of a PV string under PSC.

$$(m-1)\frac{V_{\text{OC,String}}}{N_{\text{String}}} < V_{\text{TP}} < m\frac{V_{\text{OC,String}}}{N_{\text{String}}}, \tag{4.1}$$

where $V_{\text{OC,String}}$ is the open-circuit voltage of the PV string. Multiplied by $N_{\text{String}}/V_{\text{OC,String}}$ on all sides of Equation (4.1), it can be rewritten as in Equation (4.2).

$$m-1 < \frac{N_{\text{String}}}{V_{\text{OC,String}}}V_{\text{TP}} < m. \tag{4.2}$$

m can be rounded upward to the nearest integer as shown in Equation (4.3).

$$m = \text{ceil}(\frac{N_{\text{String}}}{V_{\text{OC,String}}}V_{\text{TP}}), \tag{4.3}$$

where $ceil(\cdot)$ is a function that rounds the number to the nearest following integer. The boundary voltage of the interval where the turning points are located can be calculated from the voltage at the turning points.

The shading matrix is the combination of the shading rate and shading strength information. The shading matrix M_{S} is expressed by Equation (4.4).

$$M_{\mathrm{S}} = \begin{bmatrix} \rho_1 & \chi_1 \\ \rho_2 & \chi_2 \\ \vdots & \vdots \\ \rho_{\mathrm{M}-1} & \chi_{\mathrm{M}-1} \end{bmatrix}, \tag{4.4}$$

where M is the number of the irradiation levels; ρ_i and χ_i are respectively the ith shading strength information and the corresponding shading rate information as shown in Equation (4.5) and Equation (4.6).

$$\rho_i = \frac{G_{\mathrm{Shaded},i}}{G_{\mathrm{Insolated}}}, \tag{4.5}$$

where $G_{\mathrm{Shaded},i}$ is the ith shaded irradiance and $G_{\mathrm{Insolated}}$ is the solar irradiance of the insolated PV modules.

$$\chi_i = \frac{N_{\mathrm{Shaded},i}}{N_{\mathrm{String}}}, \tag{4.6}$$

where $N_{\mathrm{Shaded},i}$ is the number of shaded modules under the ith shaded irradiance.

For a PV string with M irradiation levels, the dimension of the corresponding shading matrix is $(\mathrm{M}-1)\times 2$. Each turning point in the I-V characteristic curve represents a row of the shading matrix. Each row of the shading matrix is a pair of shading rate and strength information. These $\mathrm{M}-1$ pairs of shading information form the shading matrix.

For example, a PV string with four modules under PSC is shown in Figure 4.2. The solar irradiances for the four PV modules are 400, 400, 600, and 1000 W/m^2 respectively. Hence, there are three irradiation levels for such PSC, and $\mathrm{M}=3$. In accordance with the above definition for the shading matrix, the shading matrix for the PSC in Figure 4.2 is a three-by-two matrix. And for each row, the shading rate and shading strength information can be obtained by the irradiance values. Finally, the shading matrix to characterize such PSC is given in Equation (4.7).

$$M_{\mathrm{S}} = \begin{bmatrix} 0.4 & 0.5 \\ 0.6 & 0.25 \end{bmatrix}. \tag{4.7}$$

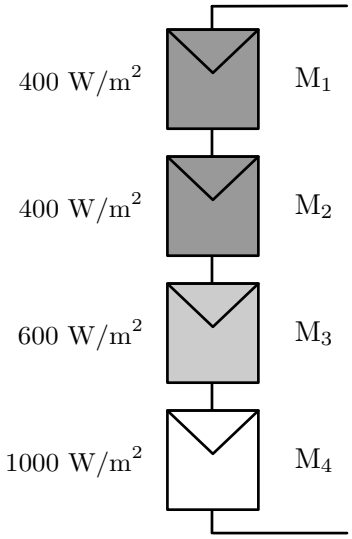

Figure 4.2: An example of PSC for obtaining the shading matrix.

4.3 Identification of Shading Matrix

The proposed shading matrix identification method is composed of two stages. In the first stage, the searching method based on an MTS algorithm is used to locate the position of the turning points. In the second stage, the analytical expressions are adopted to estimate the value of the shading matrix.

4.3.1 Locating Turning Points by a Modified Tabu Search Algorithm

Turning points are the crucial operating points in the I-V characteristic curves of a PV string. The mismatches among the PV cells in the PV string under PSC will result in the existence of the turning points, whose locations reflect the values of the shading information.

The TS algorithm is a metaheuristic search method employing local search methods used for global mathematical optimization [87, 88]. Inspired by the idea of Tabu lists in the TS algorithm, a modified TS-based method is proposed to search for the turning points in the I-V curve. The proposed method preselects the Tabu lists based on the I-V characteristics to optimize the searching efficiency.

In the preselection process, the Tabu list records the intervals that do not contain turning points. With the establishment of the Tabu list, the proposed identification system

only searches the intervals containing turning points and skips the unnecessary intervals, accelerating the searching process. The intervals that may contain the turning points are called candidate intervals. A candidate list is introduced to record the candidate intervals. The Tabu list and candidate list are two opposite lists. These two lists are updated iteratively according to a judging criterion until the termination condition is satisfied.

The pseudocode of the MTS-based searching method is given in Algorithm 4.1. It consists of two main procedures including the preselection stage and the judging stage.

4.3.1.1 Preselection Stage

At the beginning, $V_{\mathrm{OC,String}}$ and $I_{\mathrm{SC,String}}$ are mearsured. The I-V curve is divided into several intervals with an interval length of $V_{\mathrm{OC,String}}/N_{\mathrm{String}}$ according to the finding that each $V_{\mathrm{OC,String}}/N_{\mathrm{String}}$ interval contains at most one turning point.

Figure 4.3(a) is a typical example of an I-V characteristics curve from a PV string with three modules under PSC. The I-V curve is divided into three intervals. With the observation that the turning points cannot exist in the last $V_{\mathrm{OC,String}}/N_{\mathrm{String}}$ interval, the last $V_{\mathrm{OC,String}}/N_{\mathrm{String}}$ interval is recorded in the Tabu list. The intervals in the Tabu list are marked by a shadow as shown in Figure 4.3(a).

For the remaining intervals in the candidates, an initial selection rule will be applied. As shown in Figures 4.3(b) and 4.3(c), for each initial candidate interval, the current difference across the whole interval ΔI is measured and compared with a reference value ΔI_{ref}. If $\Delta I > \Delta I_{\mathrm{ref}}$, as shown in Figure 4.3(b), then the current interval is considered as a candidate interval. Otherwise, as shown in Figure 4.3(c), the interval is listed in the Tabu list.

The determination of the reference current difference ΔI_{ref} is calculated as follows. The current difference between the boundaries of the $V_{\mathrm{OC,String}}/N_{\mathrm{String}}$ interval ΔI can be considered as the difference of two short-circuit currents as shown in Equation (4.8) assuming that the temperature does not change during the two current sampling processes.

$$\Delta I = \Delta I_{\mathrm{SC}}. \tag{4.8}$$

Since the short-circuit current I_{SC} can be modeled by Equation (4.9) [15], Equation (4.8) can be extended to Equation (4.10)

$$I_{\mathrm{SC}} = (I_{\mathrm{SC,STC}} + K_{\mathrm{I}}\Delta T)\frac{G}{G_{\mathrm{STC}}}, \tag{4.9}$$

Algorithm 4.1 The turning point searching method based on an MTS algorithm

Input: the terminated smallest interval length L_{T}, the reference slope D_{ref} by Equation (2.9), the reference current difference ΔI_{ref} by Equation (4.11)

Output: the location of the turning points

%% Preselection Stage

Measure $I_{\mathrm{SC,String}}$ and $V_{\mathrm{OC,String}}$.

Divide the I-V characteristic curve into N_{String} adjacent $V_{\mathrm{OC,String}}/N_{\mathrm{String}}$ intervals from 0 to $V_{\mathrm{OC,String}}$.

Tabu list $\leftarrow$ the last $V_{\mathrm{OC,String}}/N_{\mathrm{String}}$ interval.

for *interval* in the rest $V_{\mathrm{OC,String}}/N_{\mathrm{String}}$ intervals **do**

    Measure the current difference between the interval boundaries ΔI.

    if $\Delta I \leq \Delta I_{\mathrm{ref}}$ **then**

        Tabu list $\leftarrow$ *interval*.

    else

        candidate list $\leftarrow$ *interval*.

    end if

end for

%% Judging Stage

for *candidate interval* in ***candidate list*** **do**

    Obtain the reference current I_{ref} by Equation (4.12).

    while the length of *candidate interval* is greater than L_{T} **do**

        Randomly sample a new point in *interval*.

        if $D_{\mathrm{new}} > D_{\mathrm{ref}}$ && $I_{\mathrm{new}} < I_{\mathrm{ref}}$ **then**

            Tabu list $\leftarrow$ the interval right of the new point.

        else

            Tabu list $\leftarrow$ the interval left of the new point.

        end if

        Reduce the *candidate interval* by ***Tabu list***.

    end while

    Record the V_{TP} in the *candidate interval* as the right boundary. Measure the current at the turning point.

end for

where $I_{\mathrm{SC,STC}}$ is the reference short-circuit current at Standard Test Conditions (STC, 25 °C and 1000 W/m^2); K_{I} is the short-circuit current temperature co-efficient; $\Delta T = T - T_{\mathrm{STC}}$ is the temperature difference between the actual temperature and the reference temperature at STC; G is the actual solar irradiance and G_{STC} is the reference irradiance

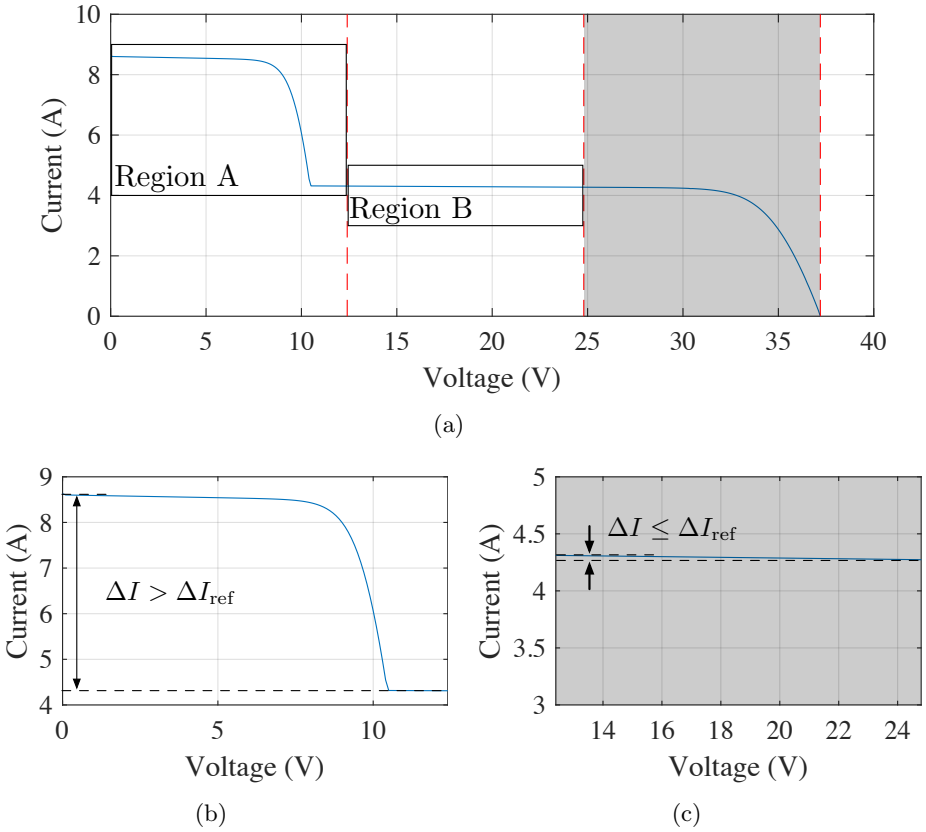

Figure 4.3: Initial selection rule for the Tabu List: (a) overall I-V curve; (b) region A; (c) region B.

at STC. $I_{\text{SC,STC}}$ and K_{I} can be found in the datasheet of the PV modules.

$$\Delta I = \Delta I_{\text{SC}} = [I_{\text{SC,STC}} + K_{\text{I}}(T - T_{\text{STC}})]\frac{\Delta G}{G_{\text{STC}}}. \tag{4.10}$$

Therefore, ΔI_{ref} can be expressed by Equation (4.11).

$$\Delta I_{\text{ref}} = [I_{\text{SC,STC}} + K_{\text{I}}(T - T_{\text{STC}})]\frac{\Delta G_{\text{tolerance}}}{G_{\text{STC}}}, \tag{4.11}$$

where $\Delta G_{\text{tolerance}}$ is the tolerated solar irradiance, which means that below this reference value, two irradiation levels are considered as the same level. In this research, the $\Delta G_{\text{tolerance}}$ is set to 50 W/m^2, which allows that the system could have a tolerance of 5%. Hence, $\Delta I_{\text{ref}} = 0.05 \times [I_{\text{SC,STC}} + K_{\text{I}}(T - 298.15)]$. For a more accurate identification result,

this tolerance parameter could be set to a lower value.

4.3.1.2 Judging Stage

In the preselection stage, the intervals containing the turning points are selected. Afterward, for each candidate interval, new sampling points are iteratively and randomly selected to reduce the intervals. A judging criterion is introduced to update the Tabu list and the candidate list. Figure 4.4 shows the judging criterion for three major cases. For each $V_{\mathrm{OC,String}}/N_{\mathrm{String}}$ interval in the candidate list, a reference current I_{ref} is defined as the mean value of two boundary currents and can be expressed by Equation (4.12). I_{ref} is represented as the red horizontal dashed lines in Figures 4.4(a) and 4.4(b).

$$I_{\mathrm{ref}} = \frac{1}{2}(I_{\mathrm{lb}} + I_{\mathrm{rb}}), \tag{4.12}$$

where I_{lb} and I_{rb} are respectively current at the left and right boundaries of the initial candidate interval.

A reference slope D_{ref} is set by Equation (2.9) in Chapter 2 to distinguish if the newly sampled point is in the flat region or steep region. Totally there are three cases, as follows, for the position of the newly sampled point.

When the slope of the newly sampled point D_{new} is larger than D_{ref}, the new point is sampled on the flat region. As shown in Figures 4.4(a) and 4.4(b), there are two different cases. The current of the newly sampled point is measured as I_{new}. If $I_{\mathrm{new}} > I_{\mathrm{ref}}$ as shown in Figure 4.4(a), the new point is on the higher flat region, and the turning point is to the right of the point as a result, the interval left of the point is added to the Tabu list. Otherwise, the right interval is added to the Tabu list as shown in Figure 4.4(b).

When $D_{\mathrm{new}} \leq D_{\mathrm{ref}}$ as shown in Figure 4.4(c), the new point is located on the steep slope. The position of the turning point is to the right of the current point. Therefore, the Tabu list is updated by adding the interval left of the point.

This judging rule is used to reduce each candidate interval until the termination condition is satisfied. The termination condition is that the length of the interval is not larger than the selected threshold L_{T}. The value of the L_{T} will affect the accuracy of the searched turning points. A smaller L_{T} can find the turning points more accurately but the searching time is longer and vice versa. Usually, the value of L_{T} could be set to 0.1 V.

When the termination condition is satisfied, the voltage at the right boundary of the reduced candidate interval is used as the voltage of the turning point in this interval. The

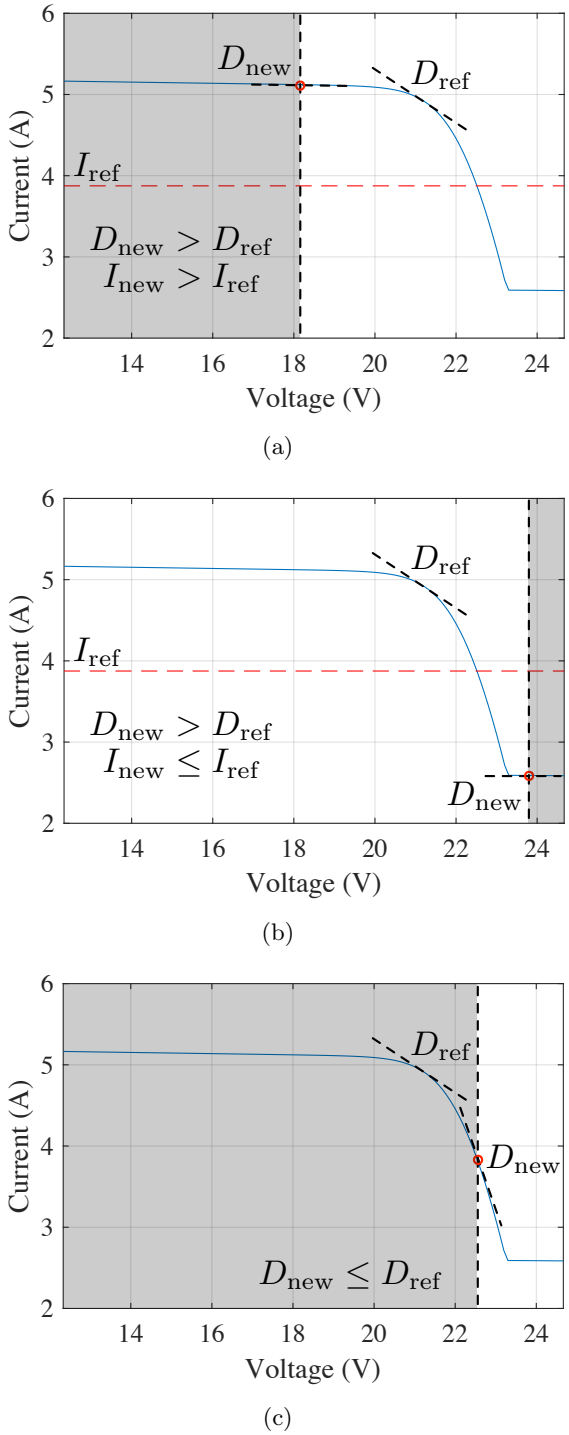

Figure 4.4: The judging criterion for three different cases: (a) case 1: $D_{\text{new}} > D_{\text{ref}}$, $I_{\text{new}} > I_{\text{ref}}$; (b) case 2: $D_{\text{new}} > D_{\text{ref}}$, $I_{\text{new}} \leq I_{\text{ref}}$; (c) case 3: $D_{\text{new}} \leq D_{\text{ref}}$.

current at the turning point can be obtained when the voltage is known.

4.3.2 Analytical Expressions for Shading Matrix

In order to have an easier analysis of the relationship between the shading matrix and the positions of the turning points, the situation with only two solar irradiation levels (one turning point) is investigated. Figure 4.5 depicts the relationships between the shading information and the position of the turning point under various shading patterns. As can be seen from Figures 4.5(b) and 4.5(d), the value of the shading rate information is linearly proportional to the voltage at the turning point while the shading strength information has a linear relation with the current at the turning point. With these findings, the shading matrix under the PSC with multiple irradiation levels can be estimated by the located turning points.

4.3.2.1 Estimating the Shading Rate Information

As shown in Equation (4.13), the operating voltage V_{PV} of the PV string equals the sum of the voltages from the insolated modules and the voltages from the shaded modules [29].

$$V_{\mathrm{PV}} = (N_{\mathrm{String}} - N_{\mathrm{Shaded}})V_{\mathrm{Insolated}} + N_{\mathrm{Shaded}}V_{\mathrm{Shaded}}, \tag{4.13}$$

where N_{Shaded} is the number of shaded modules; $V_{\mathrm{Insolated}}$ and V_{Shaded} are respectively the voltage of the insolated modules and shaded modules.

When operating at the ith turning point $V_{\mathrm{TP},i}$, the shaded modules are at the reverse breakdown point because of the bypass diodes. In [29], the voltage of the insolated modules is assumed to be the $V_{\mathrm{OC,Module}}$, which is the open-circuit voltage of the individual PV module. Let N_i denote the number of the shaded modules with the irradiation not higher than $G_{\mathrm{Shaded},i}$, Equation (4.13) at the ith turning point $V_{\mathrm{TP},i}$ is rewritten as Equation (4.14).

$$V_{\mathrm{TP},i} = (N_{\mathrm{String}} - N_i) \times V_{\mathrm{OC,Module}} + N_i \times (-V_{\mathrm{BD}}), \tag{4.14}$$

where $-V_{\mathrm{BD}}$ is the breakdown voltage of the shaded modules. However, the value of $V_{\mathrm{Insolated}}$ is closer to $V_{\mathrm{TP},i}/N_{\mathrm{Insolated}}$, which is smaller than $V_{\mathrm{OC,Module}}$. The gap between $V_{\mathrm{TP},i}/N_{\mathrm{Insolated}}$ and $V_{\mathrm{OC,Module}}$ cannot be omitted under some shading patterns. As a result, a fractional factor α_i is proposed in this research to improve the accuracy of the model. The new model is as shown in Equation (4.15).

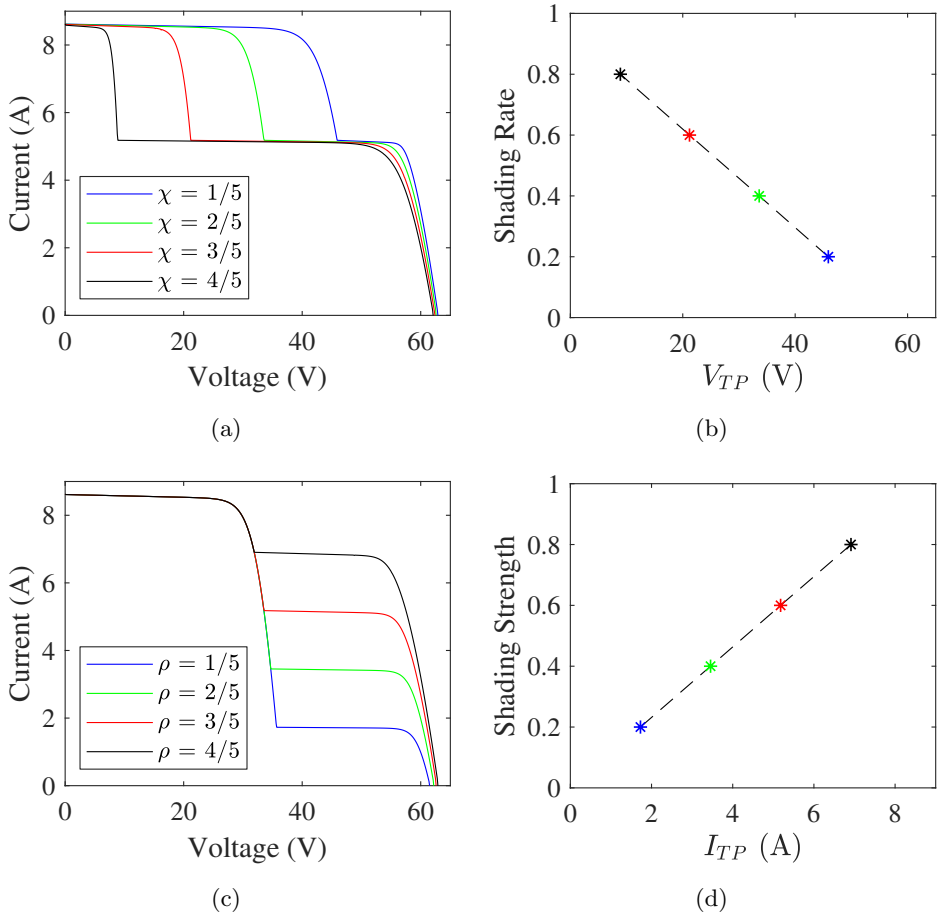

Figure 4.5: Relationships between the shading information and the position of the turning point for a PV string with five PV modules. (a) I-V curves with different shading rate information; (b) the relationship between the shading rate information and the voltage at the turning point V_{TP}; (c) I-V curves with different shading strength information; (d) the relationship between the shading strength information and the current at the turning point I_{TP}.

$$V_{\mathrm{TP},i} = (N_{\mathrm{String}} - N_i) \times \alpha_i V_{\mathrm{OC,Module}} + N_i \times (-V_{\mathrm{BD}}). \tag{4.15}$$

In Equation (4.15), the breakdown voltage V_{BD} is much smaller than the voltage at turning point $V_{\mathrm{TP},i}$. Thus, the value of α_i can be approximately calculated by letting $V_{\mathrm{BD}} = 0$ and the expression of α_i is given in Equation (4.16).

$$\alpha_i = V_{\mathrm{TP},i} \big/ \big[(N_{\mathrm{String}} - N_i) \times V_{\mathrm{OC,Module}} \big]. \tag{4.16}$$

The denominator of Equation (4.16) is also the first integer multiples of $V_{\mathrm{OC,String}}/N_{\mathrm{String}}$ right to the current ith turning point. According to Equation (4.1) and Equation (4.3), Equation (4.16) can be rewritten as in Equation (4.17).

$$\alpha_i = V_{\mathrm{TP},i} \Bigg/ \left[\frac{V_{\mathrm{OC,String}}}{N_{\mathrm{String}}} \mathrm{ceil}\left(\frac{N_{\mathrm{String}}}{V_{\mathrm{OC,String}}} V_{\mathrm{TP},i} \right) \right]. \tag{4.17}$$

Thus, Equation (4.18) represents the number of shaded modules with their irradiation not higher than $G_{\mathrm{Shaded},i}$.

$$N_i = \frac{\alpha_i V_{\mathrm{OC,String}} - V_{\mathrm{TP},i}}{\alpha_i V_{\mathrm{OC,Module}} + V_{\mathrm{BD}}}. \tag{4.18}$$

For a PV string with M irradiation levels, the index i in N_i is from 1 to M $-$ 1. For simplicity, let $N_{\mathrm{M}} = 0$, then the number of shaded modules with the ith shaded irradiance $N_{\mathrm{Shaded},i}$ can be expressed as in Equation (4.19).

$$N_{\mathrm{Shaded},i} = N_i - N_{i+1}. \tag{4.19}$$

Finally, by substituting Equation (4.19) into Equation (4.6), the shading rate information can be estimated by Equation (4.20).

$$\chi_i = \frac{N_i - N_{i+1}}{N_{\mathrm{String}}}. \tag{4.20}$$

4.3.2.2 Estimating the Shading Strength Information

The I-V curve of a PV string under PSC is merged by I-V curves of individual PV modules across the voltage from the higher irradiance to the lower irradiance [40]. Therefore, the current at the ith turning point, denoted as $I_{\mathrm{TP},i}$, approximately equals to the ith shaded short-circuit current $I_{\mathrm{SC,Shaded},i}$ as shown in Equation (4.21).

$$I_{\mathrm{TP},i} \approx I_{\mathrm{SC,Shaded},i}. \tag{4.21}$$

By substituting Equation (4.9) into Equation (4.21), $I_{\mathrm{TP},i}$ can be expressed by Equation (4.22).

$$I_{\mathrm{TP},i} = (I_{\mathrm{SC,STC}} + K_{\mathrm{I}}\Delta T)\frac{G_{\mathrm{Shaded},i}}{G_{\mathrm{STC}}}. \tag{4.22}$$

Similarly, the string short-circuit current $I_{\mathrm{SC,String}}$ is the short-circuit current of the insolated modules $I_{\mathrm{SC,Insolated}}$ as expressed in Equation (4.23).

$$I_{\mathrm{SC,String}} = I_{\mathrm{SC,Insolated}} = (I_{\mathrm{SC,STC}} + K_{\mathrm{I}}\Delta T)\frac{G_{\mathrm{Insolated}}}{G_{\mathrm{STC}}}. \tag{4.23}$$

By substituting Equation (4.22) and Equation (4.23) into Equation (4.5), the shading strength information ρ_i can be estimated by Equation (4.24).

$$\rho_i = \frac{I_{\mathrm{TP},i}}{I_{\mathrm{SC,String}}}. \tag{4.24}$$

After the turning points are located by the searching method, the shading rate information and the shading strength information in the shading matrix can be respectively estimated by Equation (4.20) and Equation (4.24).

4.4 Results and Discussions

The proposed shading identification method was validated using simulations in MATLAB/Simulink and experiments with the PV emulator. The specifications of the PV module under STC used in both the simulations and experiments are given in Table 4.1.

Table 4.1: Specifications of the PV module used in this research under standard test conditions.

Parameters	**Variable**	**Value**
Short-circuit current	I_{SC}	1.22 A
Open-circuit voltage	V_{OC}	10.71 V
Current at MPP	I_{MPP}	1.12 A
Voltage at MPP	V_{MPP}	9.00 V
Maximum power	P_{MPP}	10.00 W
Temperature co-effcient of I_{SC}	K_{I}	0.062 A/K
Temperature co-effcient of V_{OC}	K_{V}	-0.080 V/K

4.4.1 Simulation Results

The simulations were conducted using MATLAB/Simulink 2018a. To validate the performance of the proposed identification method, the PV strings with a varied number of modules from 3 to 5 were involved in the simulations. The simulations analyzed the following two aspects:

1. The verification of the proposed analytical expressions for the shading matrix by the dataset generated through the simulations.
2. The analyses of the proposed MTS-based method searching for the turning points compared with the basic TS-based method and two other classical searching algorithms: the BS algorithm and the GS algorithm.

A dataset was generated in Simulink to analyze the accuracy of the proposed analytical expressions for the shading matrix. All the possible shading patterns were involved in the dataset over the temperature range from 0 to 50 °C. The shading strength information and shading rate information in the shading matrix were separately evaluated by three mathematical indicators including Root Mean Squared Error (RMSE), Mean Absolute Error (MAE), and R squared (R^2). Since the dimension of the shading matrix varied from different shading patterns, one estimation's results were split into multiple records in the dataset according to the dimension of the shading matrix. Hence, each record of the dataset only contained one shading strength information and one shading rate information.

The estimation results based on the three mathematical indicators were recorded as shown in Table 4.2. The size of the dataset N_{Dataset} is also included. According to the results in Table 4.2, the proposed analytical expression for the shading matrix had a low RMSE value of around 5e-4 when estimating the shading strength information. However, the error of the estimated shading strength information became larger with the increase of the string length N_{String}. The accuracy of the estimated shading rate information was stable and not influenced by N_{String}.

In order to verify the efficiency of the proposed identification method based on the MTS algorithm, the other three searching algorithms including BS, GS, and TS are involved in the comparison study. Figures 4.6, 4.7, and 4.8 show the comparison results of the searching tracks for a PV string with four modules under three different shading patterns from the three searching algorithms. The solar irradiations of the four PV modules for the three selected shading patterns were {500,1000,1000,1000}W/m^2, {500,800,800,1000}W/m^2, and

Table 4.2: Results of the proposed estimation method for the PV strings with different numbers of modules.

$\mathbf{N_{String}}$	$\mathbf{N_{Dataset}}$	**Shading Strength Information**			**Shading Rate Information**		
		RMSE	MAE	R^2	RMSE	MAE	R^2
3	418	3.769e-4	2.826e-4	1.0000	0.0123	0.0116	0.9924
4	1122	3.996e-4	2.931e-4	1.0000	0.0120	0.0108	0.9946
5	1980	8.122e-4	3.638e-4	1.0000	0.0116	0.0101	0.9953

$\{500,800,300,1000\}\mathrm{W/m^2}$ respectively. The temperature was 25 °C. The red horizontal dashed lines represent the position of the turning points. The searching step was set to 1 s for all three algorithms. Before activating the searching algorithms, the operating voltage was 10 V. All the tests started with measuring the V_{OC} at the time of 10 s. All the turning points were searched and the searching process finished when the voltage dropped back to 10 V. The same judging criterion and termination condition ($L_T = 0.1$ V) were used for the three algorithms. As can be seen from the results of the shading patterns A and B, unnecessary searching was observed in the tracks from the identification method based on the BS, GS, and TS algorithms. However, with the assistance of the preselection processing of the Tabu intervals, the proposed MTS-based identification method was capable of skipping those intervals which do not contain the turning point. In the shading pattern C when the number of the turning points reached the maximum, the proposed MTS-based method did not skip any intervals, but still exhibited a fast searching due to its randomness.

Table 4.3 lists the comparative number of searching steps from the different searching algorithms. Because the random processes existed in the TS-based method and the proposed MTS-based method, the results for the two methods were based on the statistics from 100 runs. The searching rate of the BS, GS, and TS algorithms was not affected by the shading pattern, but mainly influenced by the number of series modules N_{String}. However, the performance of the proposed MTS algorithm was largely affected by the shading pattern. With the number of solar irradiation levels increasing, the average searching step of the proposed algorithm became larger. According to the average searching step for different N_{String}, the proposed MTS algorithm saved at least 18.75% of the searching time and was the most efficient one among the four searching algorithms.

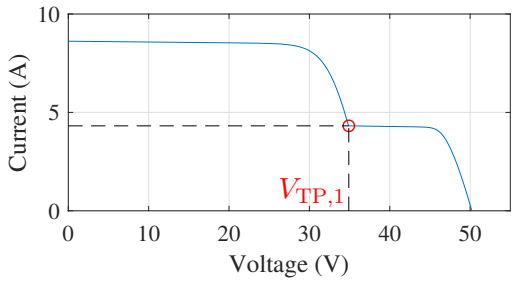

(a)

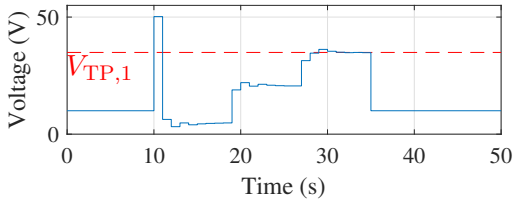

(b)

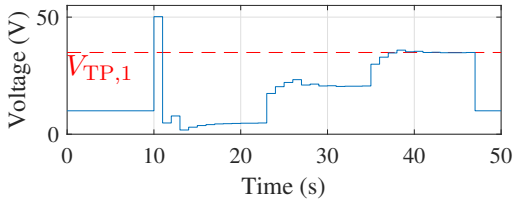

(c)

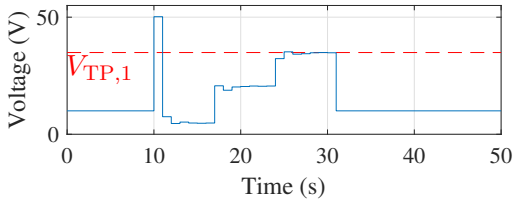

(d)

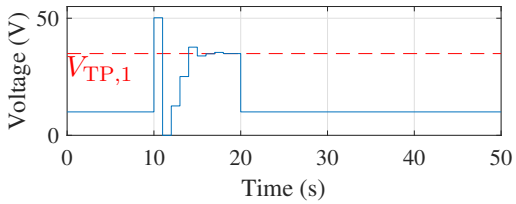

(e)

Figure 4.6: Comparison in the tracking traces from different searching algorithms under shading pattern A ({500,1000,1000,1000}W/m^2, 25°C): (a) I-V characteristics, (b) BS, (c) GS, (d) TS, and (e) MTS.

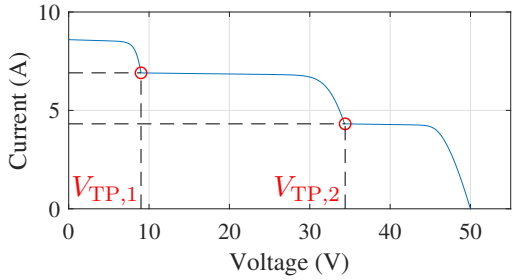

(a)

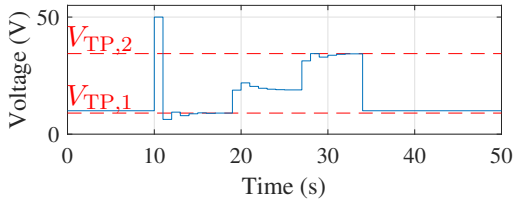

(b)

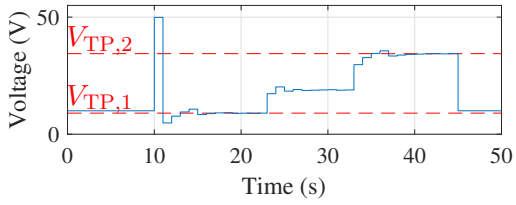

(c)

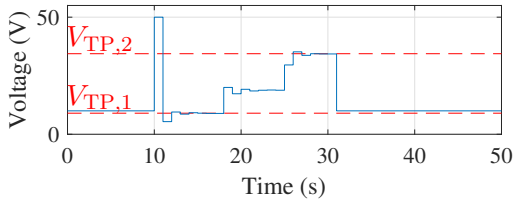

(d)

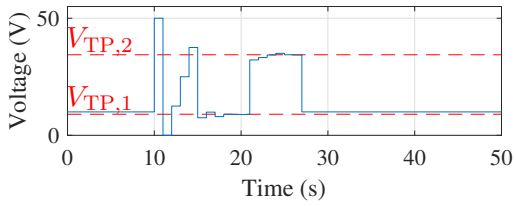

(e)

Figure 4.7: Comparison in the tracking traces from different searching algorithms under shading pattern B ({500,800,800,1000}W/m^2, 25°C): (a) I-V characteristics, (b) BS, (c) GS, (d) TS, and (e) MTS.

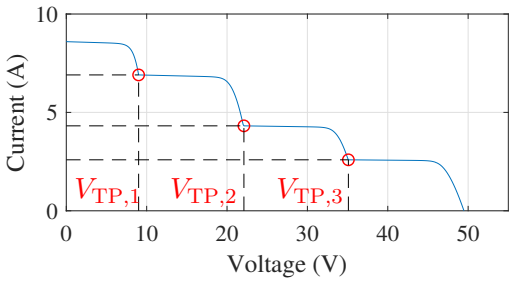

(a)

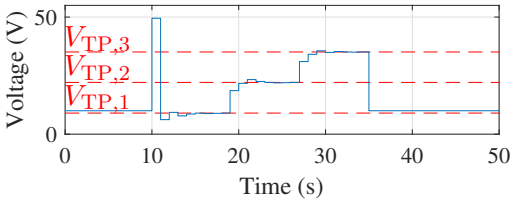

(b)

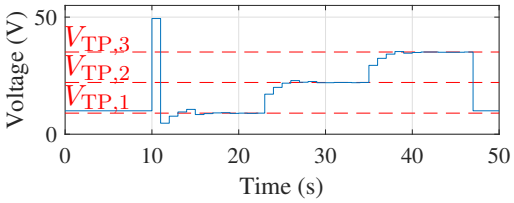

(c)

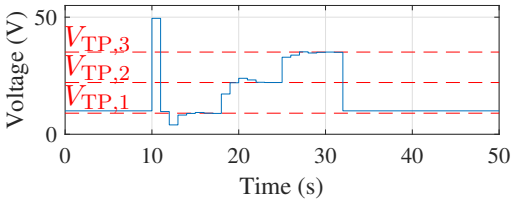

(d)

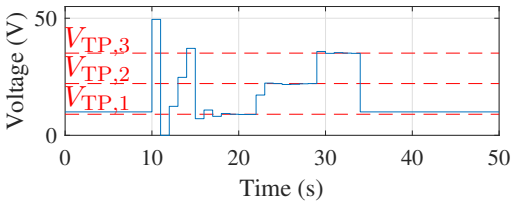

(e)

Figure 4.8: Comparison in the tracking traces from different searching algorithms under shading pattern C ({500,800,300,1000}W/m^2, 25°C): (a) I-V characteristics, (b) BS, (c) GS, (d) TS, and (e) MTS.

Table 4.3: Comparison in searching step numbers for varied string lengths from 3 to 5 by different searching algorithms at the tempature of 25 °C (the results of TS and MTS are based on the statistics of 100 runs).

$\mathbf{N_{String}}$	**Shading Pattern**	**BS**	**GS**	**TS**			**MTS**		
				Min.	Avg.	Max.	Min.	Avg.	Max.
3	{1000,1000,600}W/m^2	16	24	15	18	22	8	11	17
	{800,400,400}W/m^2	16	22	14	17	21	8	11	17
	{1000,300,600}W/m^2	16	22	12	17	21	14	18	23
	Average	16	23	/	17	/	/	13	/
4	{1000,1000,800,800}W/m^2	24	34	23	27	33	9	13	17
	{900,600,600,400}W/m^2	24	34	22	26	31	15	21	29
	{1000,600,200,400}W/m^2	23	36	21	25	30	22	26	32
	Average	24	35	/	26	/	/	17	/
5	{1000,1000,600,600,600}W/m^2	32	46	29	35	43	10	13	19
	{1000,1000,1000,400,800}W/m^2	32	48	28	35	42	16	22	30
	{800,600,400,200,200}W/m^2	31	44	28	36	44	23	31	40
	Average	32	46	/	35	/	/	22	/

4.4.2 Experimental Results

The experiments in this chapter were conducted with the PV emulator (Chroma 62020H-150S) as the shading pattern could be easily configured using this PV emulator. The experimental setup is as shown in Figure 4.9. The computer connected to the PV emulator displays the software panel for the emulator. The programmable load (SOUSIM 300W) works in the constant voltage mode for adjusting the operating voltage of the PV emulator. The controller board (UDOO NEO) executes the identification algorithms and controls the programmable load through serial communication. The oscilloscope (GW Instek GDS-2202A) records the searching traces.

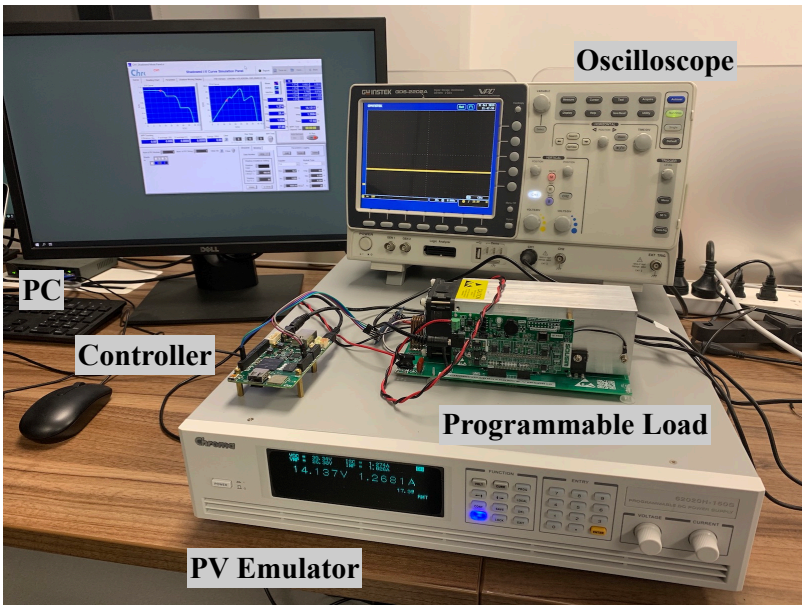

Figure 4.9: Experimental setup.

Figures 4.10, 4.11, and 4.12 show the voltage recorded by the oscilloscope when tracking the turning points under three different shading patterns labeled from 1 to 3 respectively. The solar irradiations for the three shading patterns were {1000,600,400,200}W/m^2 (shading pattern 1), {800,500,1000,1000}W/m^2 (shading pattern 2) and {800,800,400,400}W/m^2 (shading pattern 3). The temperature for the three shading patterns was 25 °C. The PV characteristics curves of each shading pattern are depicted at the top-right corner. The three shading patterns respectively have 3, 2, and 1 turning points. The termination interval length L_{T} was set to 0.2 V in the experiments. According to the specifications of

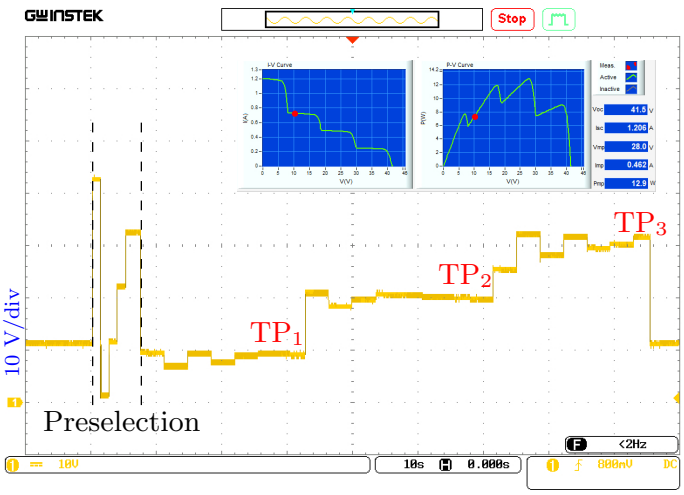

Measured $V_{\mathrm{OC,String}}$: 41.46 V

Measured $I_{\mathrm{SC,String}}$: 1.20 A

Tracked TPs:
(8.07 V, 0.72 A)
(18.54 V, 0.49 A)
(30.02 V, 0.23 A)

Identified M_{S}:

$$\begin{bmatrix} 0.600 & 0.25 \\ 0.408 & 0.25 \\ 0.191 & 0.25 \end{bmatrix}$$

Figure 4.10: The tracked voltage traces recorded by the oscilloscope when searching turning points for a PV string with four modules under shading pattern 1: {1000,600,400,200}W/m^2, 25°C.

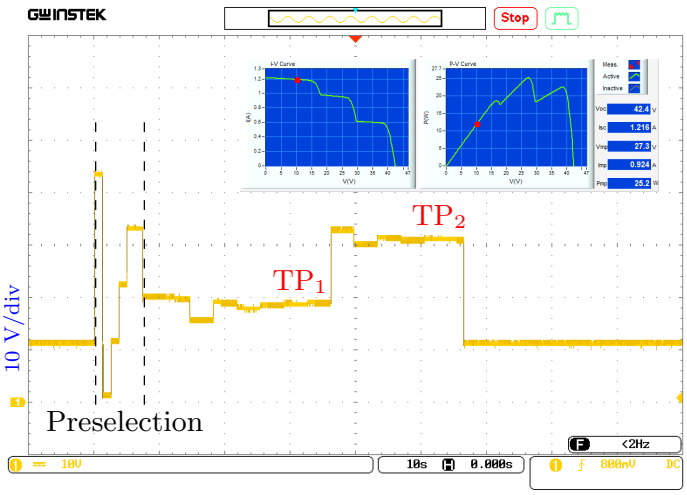

Measured $V_{\mathrm{OC,String}}$: 42.28 V

Measured $I_{\mathrm{SC,String}}$: 1.21 A

Tracked TPs:
(17.79 V, 0.98 A)
(29.55 V, 0.62 A)

Identified M_{S}:

$$\begin{bmatrix} 0.809 & 0.25 \\ 0.512 & 0.25 \end{bmatrix}$$

Figure 4.11: The tracked voltage traces recorded by the oscilloscope when searching turning points for a PV string with four modules under shading pattern 2: {800,500,1000,1000}W/m^2, 25°C.

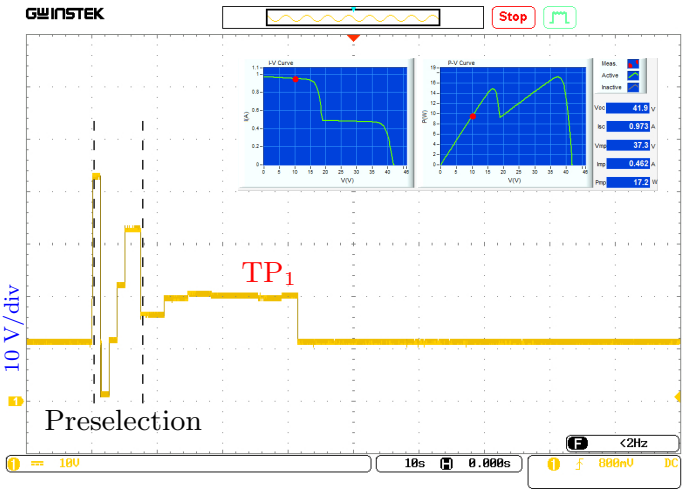

Measured $V_{\mathrm{OC,String}}$:
41.78 V
Measured $I_{\mathrm{SC,String}}$:
0.98 A
Tracked TPs:
(19.02 V, 0.48 A)
Identified M_{S}:
$\begin{bmatrix} 0.489 & 0.50 \end{bmatrix}$

Figure 4.12: The tracked voltage traces recorded by the oscilloscope when searching turning points for a PV string with four modules under shading pattern 3: {800,800,400,400}W/m^2, 25°C.

the PV module, the reference current difference is 0.061 A.

The PV string initially operated at the voltage of 10 V. When starting searching, the identification algorithm obtained the string open-circuit voltage $V_{\mathrm{OC,String}}$ by disabling the programmable load. The current values at each $V_{\mathrm{OC,String}}/N_{\mathrm{String}}$ interval boundaries were measured to determine the initial candidate intervals with the turning points. The measuring step was around 1.5 s at the preselection stage. The searching step was around twice the step in the preselection stage since at each step, two voltage points were measured to acquire the slope information. The turning points were correctly located in all the three situations when the voltage dropped back to 10 V. On average, it took 7 steps to search for each turning point. The mean absolute error for the shading strength information in the identified shading matrix was 0.008. The shading rate information was all correctly identified.

4.5 Summary

In this chapter, a new form of the shading information called the shading matrix has been introduced to quantitatively analyze the complex PSC with multiple solar irradiation lev-

els. A comprehensive shading identification approach based on an MTS algorithm and analytical models has been proposed to estimate the value of the shading matrix. Simulations and experiments have been conducted to verify the efficiency and effectiveness of the proposed identification method. By comparing with the BS, GS, and TS algorithms, the results have shown that the proposed identification method would perceive the shading matrix at least 18.75% faster. In the future work, the shading matrix would be used in the application of the MPPT techniques to optimize the power efficiency of PV systems.

Chapter 5

Maximum Power Point Tracking Methods based on Shading Perception

The traditional $0.8V_{OC}$-model-based Global Maximum Power Point Tracking (GMPPT) method locates the Global Maximum Power Point (GMPP) locus by comparing the power at each local power peak. However, a considerable amount of time is required for iteratively scanning each $0.8V_{OC}$ vicinity. To address this problem, some improved GMPPT methods are proposed in this chapter.

The contents of this chapter have been published in the following papers:

- Ziqiang Bi, Jieming Ma, Ka Lok Man, Jeremy S. Smith, Yong Yue, Huiqing Wen, "An Enhanced $0.8V_{OC}$-Model-Based Global Maximum Power Point Tracking Method for Photovoltaic Systems," IEEE Transactions on Industry Applications, vol. 56, no. 6, pp. 6825-6834, 2020.

- Ziqiang Bi, Jieming Ma, Ka Lok Man, Jeremy S. Smith, Yong Yue, Huiqing Wen, "Global MPPT Method for Photovoltaic Systems Operating under Partial Shading Conditions using the $0.8V_{OC}$ Model," IEEE International Conference on Environment and Electrical Engineering and IEEE Industrial and Commercial Power Systems Europe (EEEIC/I&CPS Europe), 2019.

5.1 Introduction

In Photovoltaic (PV) systems, bypass diodes are used to prevent the hotspot phenomenon, which may permanently damage the PV modules [84]. However, the power-voltage (P-V) characteristic curve of a PV string under Partial Shading Conditions (PSC) exhibits multiple peaks because of the bypass diodes [89]. The conventional Maximum Power Point Tracking (MPPT) methods, such as Perturb and Observation (P&O) [5] and Incremental Conductance (IncCond) [32], search for the peak of the P-V curve from an initial point, as a result, these methods may fail in tracking the GMPP and be trapped at the Local Maximum Power Points (LMPPs) [39, 90]. Hence, the detection of the GMPP is indispensable for a GMPPT system.

To address this issue, a number of GMPPT methods have been proposed in recent years [64, 91–95]. Early studies have shown that according to the features, there are mainly three categories for the GMPPT methods [40, 41]: (a) soft computing methods, (b) segmental search methods, and (c) two-stage methods.

The soft computing methods include Particle Swarm Optimization (PSO) [45, 46], Fuzzy Logic Control (FLC) [47–49], and the Firefly Algorithm (FA) [96]. Since PSC can be considered as an optimization problem, these methods can provide good performance under different shading patterns. However, these methods usually require significant computation processing and are difficult to implement.

The segmental search methods are based on solid mathematical theories and, as a result, the advantages of these methods are their simplicity and rapid tracking speed. Typical examples include the Dividing Rectangle (DIRECT) method [51] and the Fibonacci method [52]. One of the disadvantages of these approaches is that the system may be trapped into one of the LMPPs but not the GMPP under some special shading patterns.

The third category, the two-stage methods, contains two steps. In the first stage, an approximate location for the GMPP is determined and then the conventional MPPT methods such as P&O and IncCond are used to track the exact GMPP in the second stage. Many two-stage MPPT methods have been proposed during the last ten years [53–55]. The main difference between these methods is the determination method in the first stage. Thus, the main challenge is how to locate the GMPP in the first stage in a fast and efficient way.

A full scanning technique was proposed by Koutroulis and Blaabjerg [54] where the P-V curve is fully scanned in order to determine the GMPP. This method takes advantage of

its simplicity, however, the tracking performance is dependent on the value of the scanning step. The tracking speed is too slow with a small scanning step, while it may overlook the GMPP if the step is too large.

The $0.8V_{OC}$-model-based methods [39, 55, 56, 60, 63] are based on the assumption that the peaks of the P-V characteristic curve are at multiples of the $0.8 * V_{OC}$ regions. Compared with the full scanning technique, only the vicinities of the $0.8 * V_{OC}$ regions are scanned. Therefore, these $0.8V_{OC}$-model-based methods reduce the scanning time.

Shading information, such as the shading rate and shading strength, provides mathematical indicators for describing the PSC for PV strings. The shading rate χ expresses the percentage of the shaded PV modules [11] while the shading strength ρ reflects the ratio of received solar irradiance in a PV string [12]. The results in [11] show that the location of the GMPP is related to the value of the shading information. A shading detection method based on the electrical characteristics was proposed in [26] to estimate the shading rate. A GMPP estimation model based on the shading information was proposed in [24]. The voltage at the GMPP is estimated from the shading rate and the shading strength by the Multiple Gaussian Process Regression (M-GPR) method with a Mean Absolute Error (MAE) of 0.381 V under various PSC. In [25], a GMPPT method based on the detection of the shading rate was proposed. The mathematical relationship between the voltage at the GMPP and the shading rate was introduced based on the $0.8V_{OC}$ model. The performance of this method is not affected by the number of modules in the PV string. At the same time, the method saves around 50% of the tracking time compared with the traditional $0.8V_{OC}$-model-based methods for a PV string with three modules. This research has shown that the location of the GMPP can be estimated from the shading information. However, the application area is limited since the existing shading rate and shading strength can only express the PSC with two irradiation levels according to their definitions [11].

In the following sections, some improved GMPPT methods based on shading detection are proposed. Simulations and experimental results validate the performance of the proposed methods.

5.2 An Enhanced 0.8Voc-Model-Based Method using Shading Detection

5.2.1 Related Work

The proposed GMPPT method is based on the $0.8V_{OC}$ model. This section first introduces the $0.8V_{OC}$-model-based MPPT methods. Then, the relationship between the voltage at the GMPP and the shading information is analyzed. Finally, a duty cycle computation method for the DC-DC circuit is presented for faster tuning of the operating point.

5.2.1.1 $0.8V_{OC}$-Model-Based Method

For simplicity, in this research, it is supposed that the solar irradiance for the PV string is separated into two levels under PSC. The modules that receive the higher irradiance $G_{\text{insolated}}$ are called insolated modules, while those receiving the lower irradiance G_{shaded} are called shaded modules. It is assumed that the shading irradiance $G_{\text{shaded}} = 50$ W/m^2 [11].

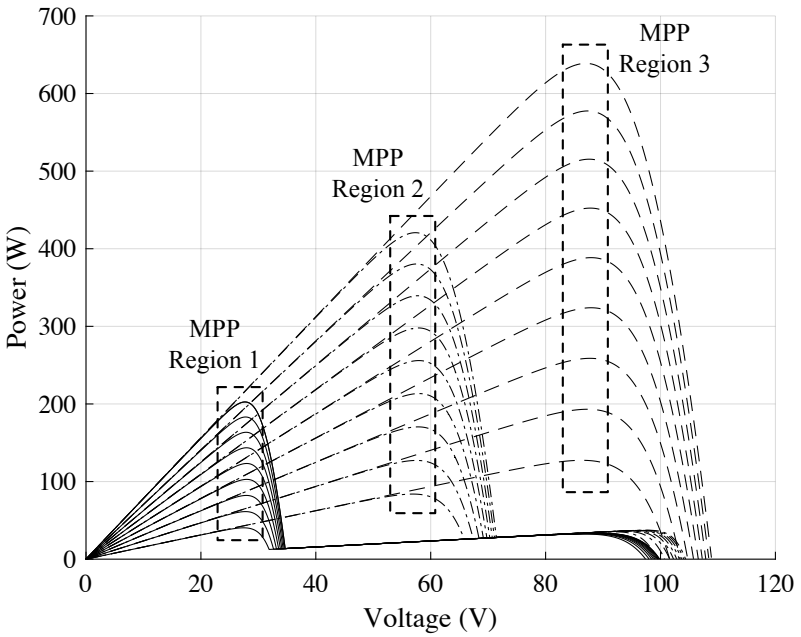

Figure 5.1: P-V curves of a PV string with three modules containing three MPP regions under various shading conditions. (Temperature $T = 25$ °C)

Figure 5.1 shows multiple P-V curves under various shading patterns for a PV string with three PV modules at a temperature of 25 °C. The insolated irradiance is varied from 200 to 1000 W/m^2. The peak power points are apparently distributed in three MPP regions, namely MPP regions 1-3 as shown in Figure 5.1. These MPP regions are approximately the multiples of $0.8 * V_{\mathrm{OC}}$. Such $0.8 * V_{\mathrm{OC}}$ is also the vicinity of V_{MPP} (voltage at MPP) for the individual PV modules.

The 0.8V$_{\mathrm{OC}}$-model-based MPPT method measures the power at these regions iteratively and determines the largest one as the GMPP using different approaches. The most typical ones use the comparing method [39, 55, 56, 60, 63].

5.2.1.2 Shading Information and V_{GMPP}

Figure 5.2 shows the relationships between the voltage at the GMPP, temperature, and the shading information. When the shading rate is zero, which means that there is no shading in the PV string. Under such condition, all the PV modules receive uniform solar irradiance. When the shading rate is not zero, the PV string operates under PSC. Therefore, Figure 5.2 is split into two sub-figures:

1. Figure 5.2(a) is the V_{GMPP} at various temperatures and shading strengths when the shading rate is not zero.

2. Figure 5.2(b) is the V_{GMPP} at various temperatures and solar irradiances when the shading rate is zero.

The three planes in Figure 5.2 are respectively the three different MPP regions in Figure 5.1. Obviously, the shading rate is the key factor to determine the location of the GMPP and the other factors (i.e., the shading strength and the temperature) have limited impact. Meanwhile, the V_{GMPP} is shown to be located at the vicinity of multiples of $0.8 * V_{\mathrm{OC}}$. Therefore, the voltage at the GMPP V_{GMPP} can be estimated by the shading rate combined with the 0.8V$_{\mathrm{OC}}$ model.

5.2.1.3 Duty Cycle Computation Method

In order to rapidly change the operating point to the estimated voltage, the duty cycle computation method from [55] is used. The duty cycle computation method is introduced as follows.

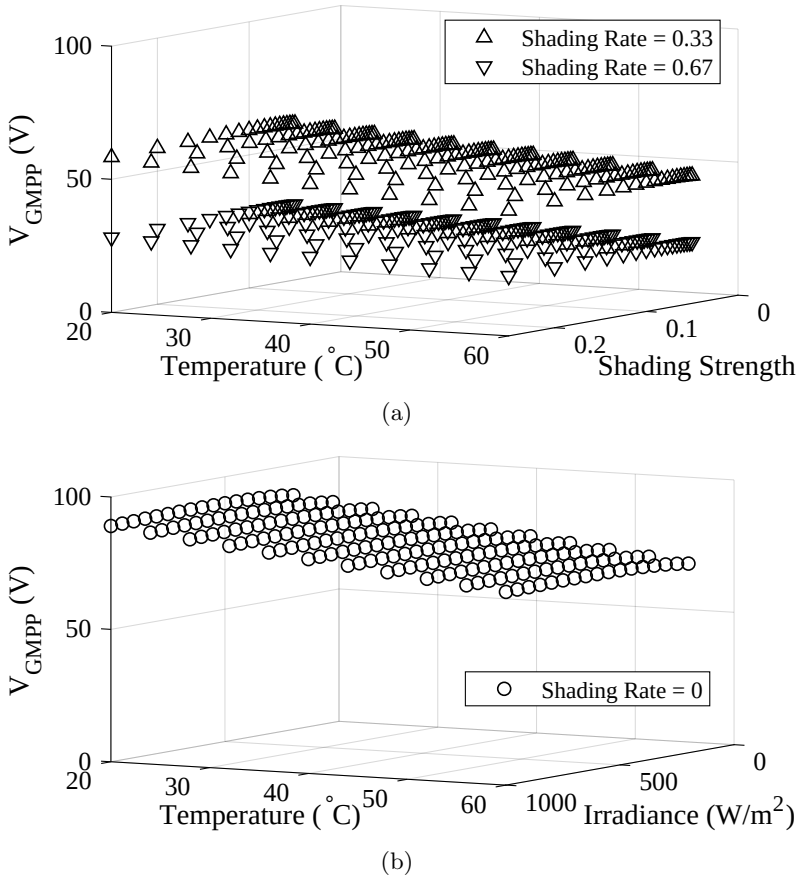

Figure 5.2: Voltage at the GMPP under various temperatures and shading conditions: (a) shading rate $\neq 0$; (b) shading rate $= 0$.

The DC-DC buck-boost converter is selected for tuning the operating point of the PV string, as the DC-DC buck-boost converter has a larger tuning range compared with the buck and boost converters [39]. The relationships between the output and input voltage/current of a DC-DC buck-boost converter are formulated in Equation (5.1) and Equation (5.2).

$$V_{\text{out}} = \frac{D}{1-D} V_{\text{in}}. \tag{5.1}$$

$$I_{\text{out}} = \frac{1-D}{D} I_{\text{in}}, \tag{5.2}$$

where D is the controlling duty cycle of the DC-DC converter. V_{in} and V_{out} (I_{in} and I_{out}) are the input and output voltage (current) respectively. Equation (5.1) can be transformed into Equation (5.3).

$$D = \frac{V_{\text{out}}}{V_{\text{out}} + V_{\text{in}}} = \frac{R_{\text{out}} I_{\text{out}}}{R_{\text{out}} I_{\text{out}} + R_{\text{in}} I_{\text{in}}}, \tag{5.3}$$

where R_{out} and R_{in} are respectively the output and input resistances. The current values can be eliminated by substituting Equation (5.2) into Equation (5.3) as in Equation (5.4).

$$D = \frac{R_{\text{out}}(1-D)/D I_{\text{in}}}{R_{\text{out}}(1-D)/D I_{\text{in}} + R_{\text{in}} I_{\text{in}}} = \frac{R_{\text{out}}(1-D)/D}{R_{\text{out}}(1-D)/D + R_{\text{in}}}. \tag{5.4}$$

Hence, D can be solved as in Equation (5.5)

$$D = \frac{1}{1 + \sqrt{R_{\text{in}}/R_{\text{out}}}}. \tag{5.5}$$

For the DC-DC buck-boost converter in a PV system, the relationship can be obtained by substituting $R_{\text{in}} = V_{\text{PV}}/I_{\text{PV}}$ and $R_{\text{out}} = R_{\text{load}}$ into Equation (5.5) as in Equation (5.6).

$$D = \frac{1}{1 + \sqrt{a}}, a = \frac{V_{\text{PV}}}{I_{\text{PV}}} \frac{1}{R_{\text{load}}}. \tag{5.6}$$

Therefore, the value of the duty cycle depends on the PV characteristics and load resistance. The load in this approach is selected to have a constant resistance. The PV characteristics are mainly influenced by the environment. Figure 5.3 shows the current-voltage (I-V) curve of a PV string. (V_i, I_i) is the initial operating point. The black vertical dash-line is the target voltage V_t. However, the current at the target point is unknown. Therefore, the initial current I_i and the target voltage V_t are substituted into Equation (5.6), and the next operating point of the PV string converges to the point (V_1, I_1). The next duty cycle is obtained by substituting I_1 and V_t into Equation (5.6) again. The upper two crosses in Figure 5.3 are the following two operating points. This process continues until the difference in the current dI is smaller than a threshold value. Then, the operating voltage is close to the target value. According to the research in [55], the threshold value dI_{Th} is set to 0.03 A and this method is capable of significantly reducing the tuning time.

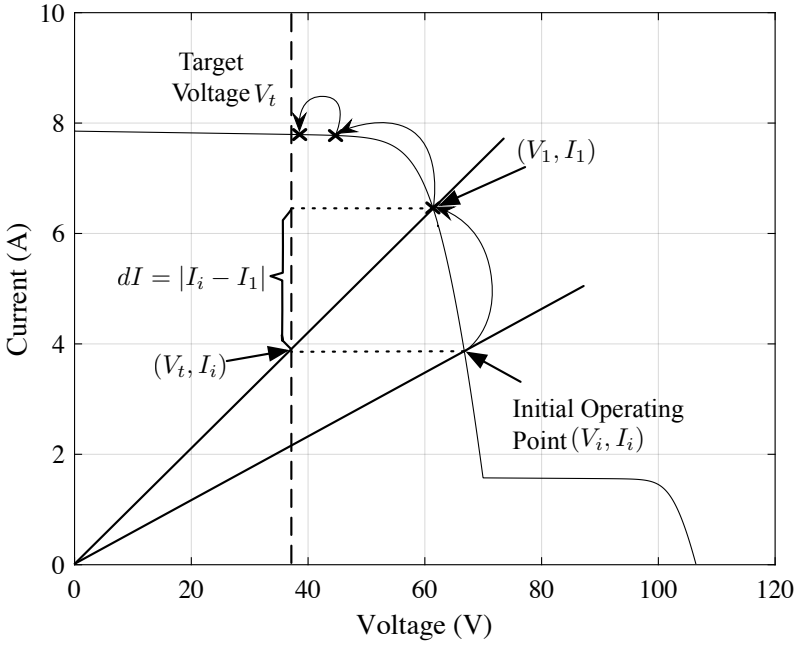

Figure 5.3: I-V curve of a PV string under PSC.

5.2.2 Proposed GMPPT Method

Based on the $0.8V_{OC}$ model, the proposed GMPPT method assumes that the GMPP exists at multiples of $0.8 * V_{OC}$. As shown in Figure 5.2, the key factor to determine the location of the V_{GMPP} is the shading rate χ. Hence, the V_{GMPP} can be approximately calculated using Equation (5.7).

$$V_{GMPP} \approx (1 - \chi) N_{String} * 0.8 * V_{OC}, \tag{5.7}$$

where the shading rate χ is obtained from the shading detection method introduced in Chapter 3.

A block diagram of the hardware implementing the proposed GMPPT method is shown in Figure 5.4. The shading detection module uses a switch module to detect the shading rate of a PV string comprising three PV modules. The microcontroller implementing the GMPPT method controls the duty cycle of the DC-DC converter. The load resistance is constant.

Figure 5.5 shows the flowchart for the proposed GMPPT method. The proposed shad-

ing detection circuit detects the shading rate. Then, the shading rate is substituted into Equation (5.7) to obtain the estimated voltage at the GMPP. The duty cycle computation method for the DC-DC buck-boost converter, introduced in this chapter, is applied to tune the operating point at the V_{GMPP}. When the operating point is near the estimated V_{GMPP}, the conventional IncCond MPPT method (introduced in Section refch2:inccond) is used to track the exact global maximum. The system is continuously detecting the shading rate at a fixed frequency (every $0.5s$). If a change in the shading rate is detected, the proposed method is reset and rolled back to the initial state. The above procedure is also expressed as pseudocode in Algorithm 5.1.

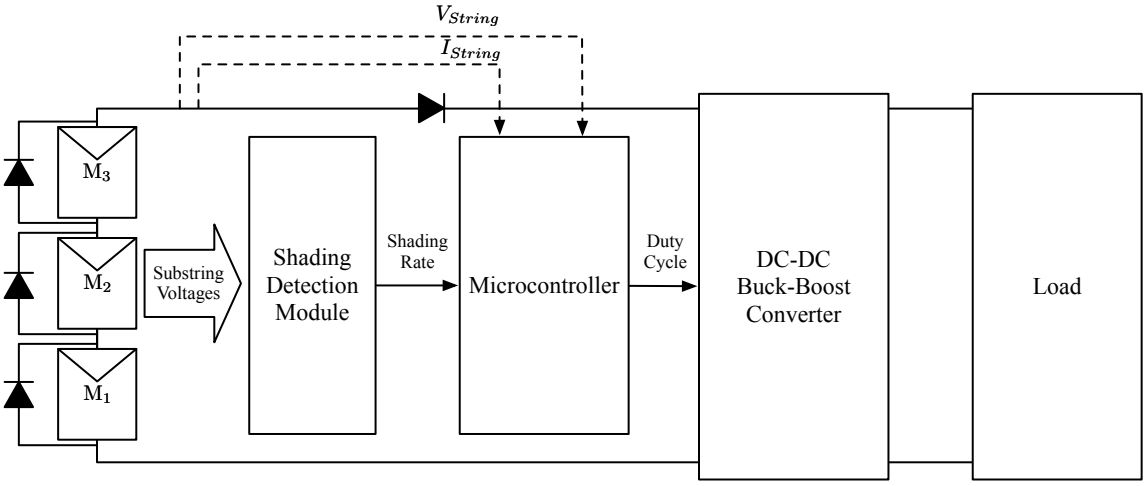

Figure 5.4: Block diagram of the hardware implementing the proposed GMPPT method.

5.2.3 Simulation Results

Simulations were conducted using MATLAB/Simulink 2018a. Figures 5.6 and 5.7 show the simulation results from the classical $0.8\mathrm{V_{OC}}$ GMPPT method and the proposed method respectively.

The PV string used in the simulation comprises three PV modules (one shaded module and two insolated modules). For simplicity, the solar irradiance for the shaded modules was set to 50 $\mathrm{W/m^2}$ and the insolated irradiance was set to 1000 $\mathrm{W/m^2}$. Table 5.1 lists the specifications of the PV modules. For both methods, the tracking algorithms were activated at 0.1 s and the controlling step was 0.01 s. The duty cycle step for the IncCond method was 0.5%.

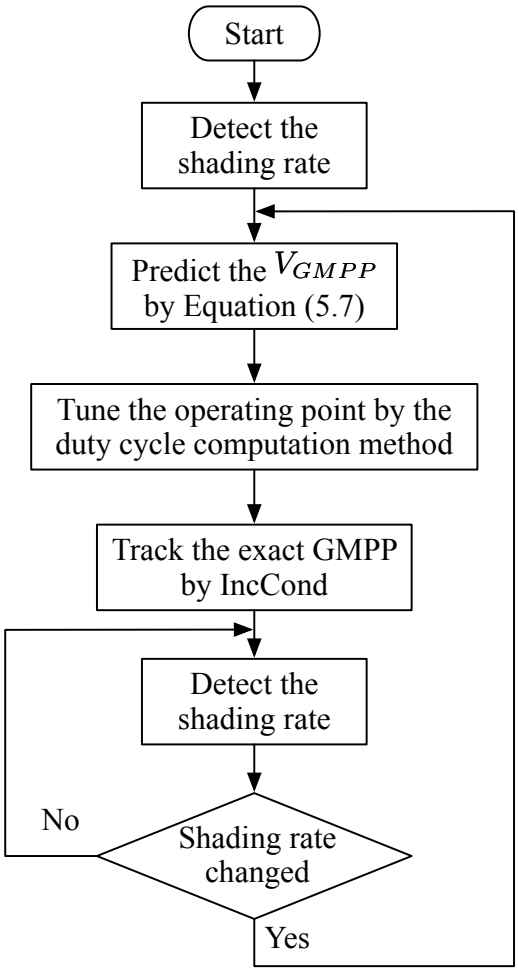

Figure 5.5: Flowchart of the proposed novel $0.8V_{OC}$-model-based GMPPT method.

For the classical $0.8V_{OC}$-model-based method, shown in Figure 5.6, there are three regions with different voltage levels labeled as R1, R2, and R3. These three regions are respectively the MPP regions 1 to 3 in Figure 5.1. The duty cycle computation method introduced in Section 5.2.1.3 was used for searching these three regions. At 0.27 s, the MPPT system finished the scanning of the three regions and determined the GMPP region. Then, the GMPP was tracked at 0.28 s by the IncCond method.

Figure 5.7 shows the simulation results for the proposed method. From 0.1 s to 0.11 s, the shading detection module detected the value of the shading rate χ. Once the shading rate was determined, it was substituted into Equation (5.7) and the estimated voltage at

Algorithm 5.1 The procedure for proposed novel $0.8V_{OC}$-model-based GMPPT method.

1: Detect the shading rate.
2: Predict the V_{GMPP} by Equation (5.7).
3: Tune the operating point to the predicted V_{GMPP}.
4: Track the exact GMPP by IncCond MPPT method.
5: Detect the shading rate.
6: **if** Shading rate has changed **then**
7: **go to** 2.
8: **else**
9: **go to** 5.
10: **end if**

Table 5.1: Specifications of the PV module used in this research under standard test conditions.

Parameters	**Variable**	**Value**	**Unit**
Short-circuit current	I_{SC}	7.84	A
Open-circuit voltage	V_{OC}	36.3	V
Current at MPP	I_{MPP}	7.35	A
Voltage at MPP	V_{MPP}	29	V
Maximum power	P_{MPP}	213.15	W

the GMPP was calculated. The voltage tuning method introduced in Section 5.2.1.3 was used to adjust the current operating point to the estimated one. This process ended at 0.16 s when the global maximum is nearly tracked and switched to the IncCond method. At 0.19 s, the GMPP was tracked.

Both methods could track the GMPP efficiently. The proposed method tracked the GMPP in 0.09 s while the classical $0.8V_{OC}$-model-based method took 0.18 s. The proposed method saved around 50% of the tracking time compared with the classical $0.8V_{OC}$ method. It is worth noting that the oscillations still exist when using IncCond to track the exact location of the GMPP, that is resulted from the conditions to achieve the zero-oscillation in Equation (2.15) are difficult to satisfied even in simulation environments.

Figure 5.8 shows the simulation results for the proposed GMPPT method under changing partial shading conditions. Two shading patterns are involved in the simulation. From

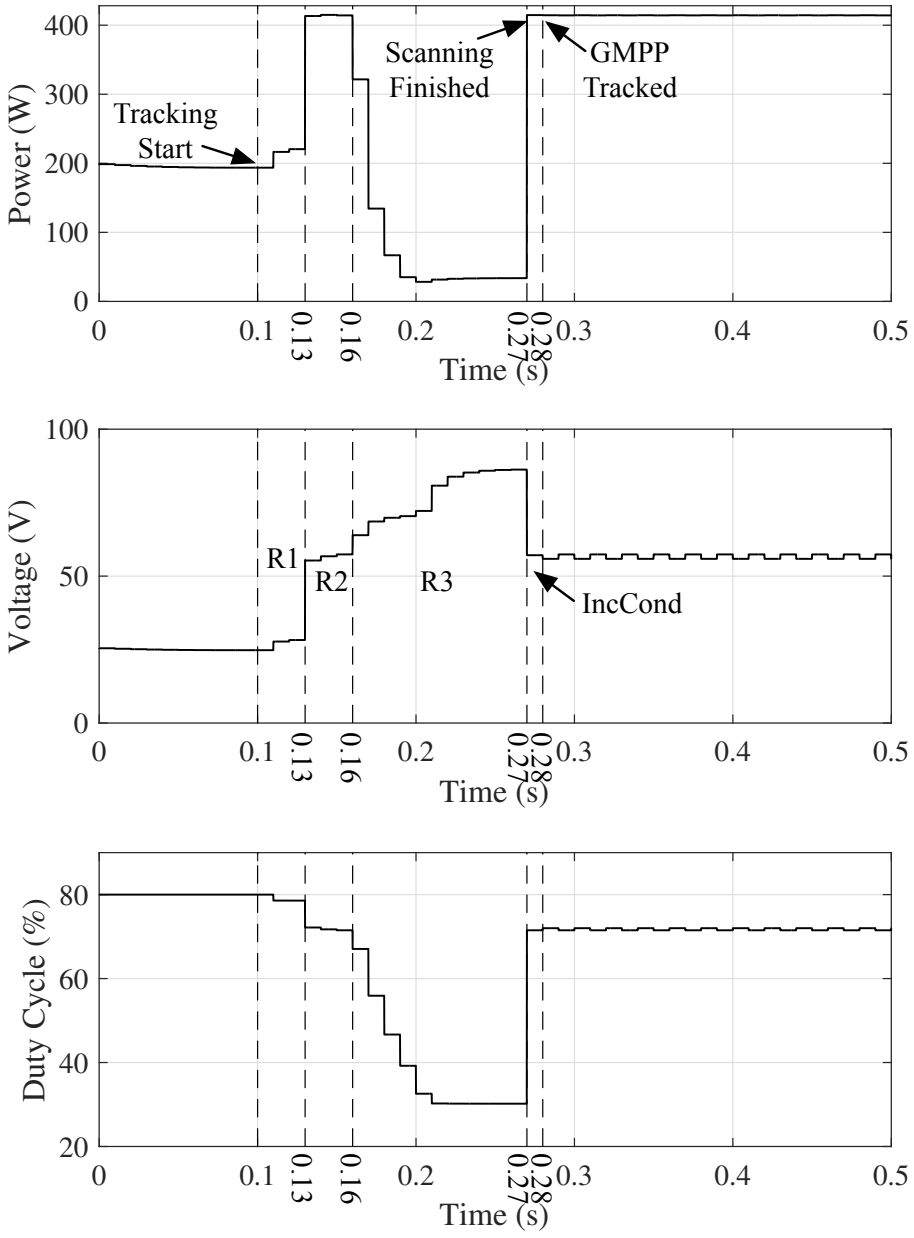

Figure 5.6: Simulation results for the classical $0.8V_{OC}$-model-based method under fixed PSC.

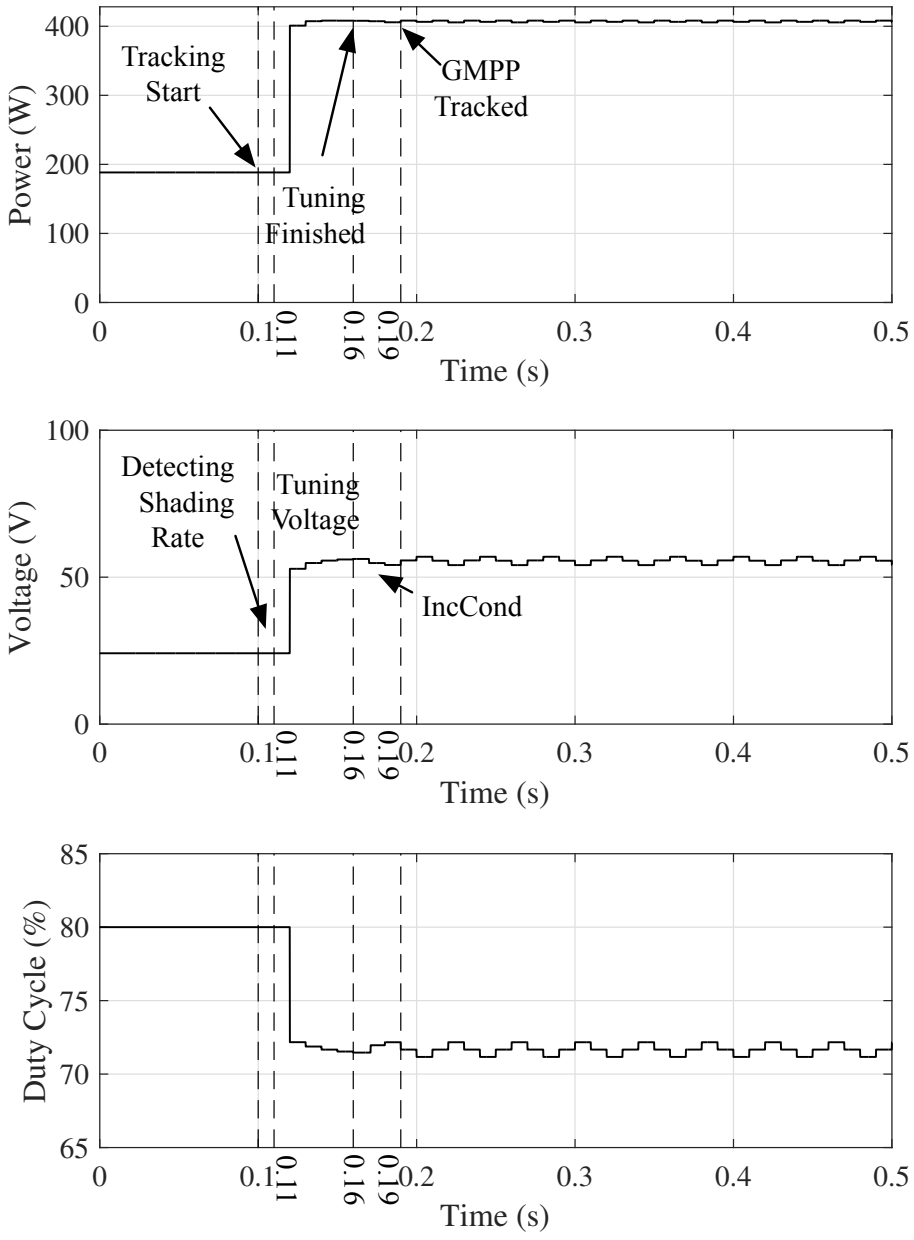

Figure 5.7: Simulation results for the proposed method under fixed PSC.

Table 5.2: Tracking time comparison for the PV strings more than three modules.

N_{String}	N_{Shaded}	**Tracking Time**	
		$0.8V_{OC}$ Model	**Proposed Method**
4	1	0.32 s	0.08 s
	2	0.23 s	0.09 s
5	1	0.41 s	0.08 s
	2	0.32 s	0.09 s
6	1	0.35 s	0.09 s
	2	0.47 s	0.08 s

0 to 0.5 s, the irradiation values for the three PV modules were $\{1000,50,1000\}\text{W/m}^2$ and these were changed to $\{1000,50,50\}\text{W/m}^2$ from 0.5 s to the end. Therefore, at the time of 0.5 s, the value of the shading rate was changed from 0.33 to 0.67. The operating step was 0.01 s. At 0.1 s, the proposed GMPPT method was activated. As can be observed from the results, the proposed GMPPT method is capable of detecting the changes in the shading rate and tracking the GMPP after the shading pattern is changed.

Table 5.2 records the tracking times of the two methods for the PV strings with more than three modules. It is notable that, with the number of the modules in the PV string N_{String} increasing, the tracking time of the classical $0.8V_{\text{OC}}$-model-based method became longer while the proposed method only had a slight fluctuation in the tracking time. The main reason for the unstable tracking time of the classical $0.8V_{\text{OC}}$-model-based method is that the number of scanning steps is uncertain for different shapes of P-V curves. The performance of the proposed method is not influenced by N_{String}. Therefore, the proposed method is more efficient for a long PV string.

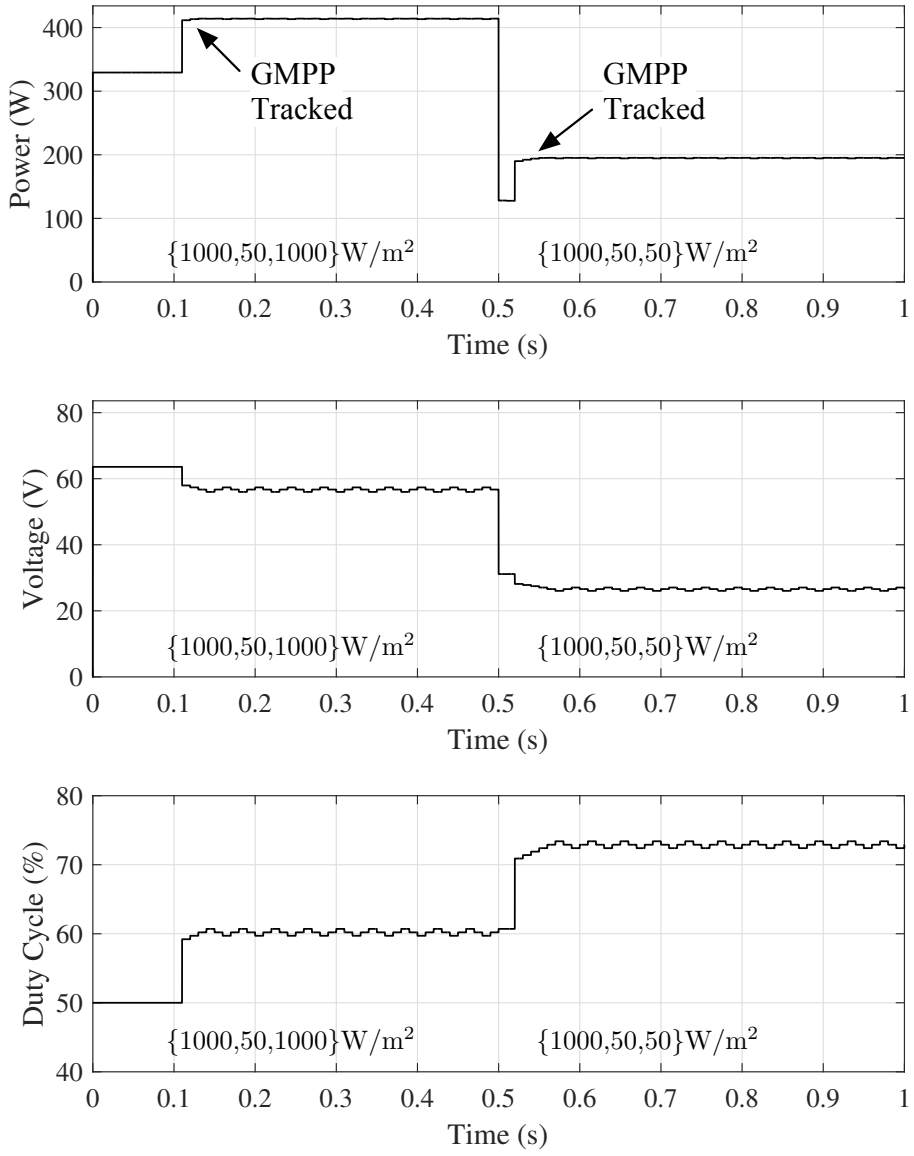

Figure 5.8: Simulation results for the proposed method under changing PSC.

5.3 An Intelligent Tracking Method based on Shading Vector

5.3.1 Shading Vector and Global Maximum Power Point

5.3.1.1 Introduction of the Shading Vector

The shading information is a mathematical indicator to quantitatively evaluate the PSC. The shading rate and shading strength are two typical forms of shading information. According to [11], the definitions for both shading rate and shading strength are based on a strong assumption. Such that the PV string is supposed to be subjected to two different solar irradiation levels. The PV modules that receive the higher irradiance are called insolated modules, and those receiving the lower irradiance are called shaded modules. Thus, these two types of shading information are not compatible with the PSC with more than two irradiation levels. In this chapter, the shading vector is proposed to comprehensively quantify the PSC.

Let γ denote the shading vector, which is defined as the union of the shading strength for the individual modules in the PV string. The shading vector is expressed as in Equation (5.8).

$$\gamma = \bigcup_{i=1}^{N_{\text{String}}} \rho_i, \rho_i = \frac{G_i}{G_{\text{Insolated}}}, \tag{5.8}$$

where ρ_i and G_i are respectively the shading strength and the solar irradiance of the ith PV module. $G_{\text{Insolated}}$ is the irradiance of the insolated or unshaded modules.

Each element in the shading vector represents the shading strength information for the corresponding PV module. The shading vector can also be used to reflect the number of shaded PV modules at each shading level. For example, a PV string with four modules operates under PSC as shown in Figure 5.9(a). The P-V curve with three peaks is shown in Figure 5.9(b). The solar irradiances for the four PV modules are 400, 400, 600, 1000 W/m^2, respectively. Thus, the shading vector under such shading conditions is {0.4, 0.4, 0.6, 1.0} according to the definition. Two elements with the same value 0.4 are in the shading vector, as a result, two PV modules receive the same solar irradiation level. The remaining two PV modules receive different irradiation levels as the elements in the shading vector are not the same. Therefore, multiple identical values in the shading vector indicate that

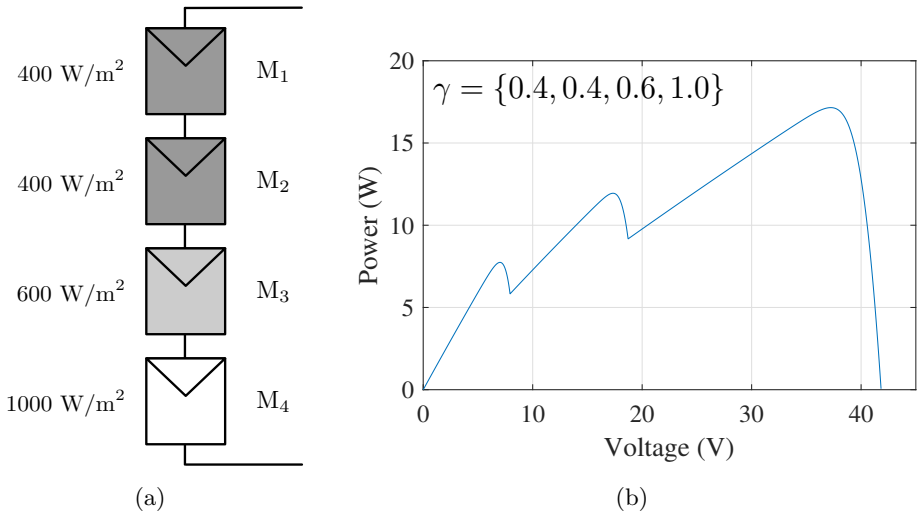

Figure 5.9: An example of using the shading vector: (a) a PV string with four modules; (b) P-V curve of the PV string.

the corresponding PV modules receive the same level of solar irradiance. Since the shading vector is capable of representing the shading rate and the shading strength information, it can be transformed from the shading matrix introduced in Chapter 4, which is the combination of the shading rate and the shading strength information. Compared with the shading matrix, the proposed shading vector here is more compact and simpler. The shading vector is easier to be analyzed as it is in a unidimensional form.

5.3.1.2 Determination of the Global Maximum Power Point

For a single PV module, the Maximum Power Point (MPP) appears at the vicinity of $0.8\times V_{\mathrm{OC,M}}$, where $V_{\mathrm{OC,M}}$ is the open-circuit voltage of a single PV module. For a PV string, based on the $0.8\mathrm{V_{OC}}$ model, the peak regions of the P-V curve are approximately at the multiples of $0.8\times V_{\mathrm{OC,M}}$ and the GMPP is the peak region with the largest power.

The $0.8\mathrm{V_{OC}}$-model-based MPPT method is a typical two-stage GMPPT method. In the first stage, the $0.8\mathrm{V_{OC}}$ model determines the $0.8\mathrm{V_{OC}}$ region with the largest power, as the GMPP region, by iteratively measuring and comparing the power at each $0.8\mathrm{V_{OC}}$ region. In the second stage, a conventional MPPT technique (such as P&O and IncCond) is used to track the accurate GMPP. However, this measuring and comparing process takes a long time to get to the GMPP region, especially for long PV strings. The efficiency of

the $0.8V_{OC}$-model-based MPPT method can be improved by predicting the $0.8V_{OC}$ region with the GMPP from the extracted shading vector.

In order to have a clear illustration of the relationship between the $0.8V_{OC}$ region with the GMPP and the shading vector under various shading conditions, a PV string with three modules is used in the analysis. Figure 5.10 shows the relationship between the $0.8V_{OC}$ region with the GMPP and three elements in the shading vector. Let n_{GMPP} denote the $0.8V_{OC}$ region with the GMPP, three shapes with different colors are used to distinguish the different n_{GMPP} values. Figure 5.10(a) is the three-dimension view of the data distribution. From the definition of the shading vector, at least one element in the shading vector is 1. Thus, all the data are distributed at the surface of a cubic. Figures 5.10(b), 5.10(c) and 5.10(d) are views in three different directions. It is clearly observed that the data with different n_{GMPP} values is distributed in clusters. Therefore, the $0.8V_{OC}$ region with the GMPP n_{GMPP} can be predicted from the shading vector by classification algorithms as shown in Figure 5.11. The inputs of the classifier are the elements in the shading vector. As a result, the size of the input of the classifier is dependent on the number of PV modules in the string. PV strings with different lengths need varied classifiers. The output of the classifier is the $0.8V_{OC}$ region with the GMPP n_{GMPP}. In the proposed GMPPT method, a k-Nearest Neighbors (k-NN) classification algorithm [97] is used to predict the $0.8V_{OC}$ region with the GMPP, that is widely applied in the Internet of Things (IoT) [98], Wireless Sensor Networks (WSN) [99], electric vehicles [100] and many other scenarios.

Assuming that the temperature is evenly distributed for all the PV modules in the PV string, the open-circuit voltage for each module is identical. According to the theory of the $0.8V_{OC}$ model, the GMPP exists at multiples of $0.8\times V_{\mathrm{OC,M}}$. With knowledge of the $0.8V_{OC}$ region with the GMPP n_{GMPP}, the voltage at the GMPP can be estimated by Equation (5.9).

$$V_{\mathrm{GMPP}} \approx 0.8 \times V_{\mathrm{OC,M}} \times n_{\mathrm{GMPP}}, \tag{5.9}$$

where $V_{\mathrm{OC,M}}$ is the open-circuit voltage of a single PV module, which can be estimated from the value under the Standard Test Conditions (STC, 25 °C and 1000 W/m^2) by Equation (5.10) [15].

$$V_{\mathrm{OC,M}} = V_{\mathrm{OC,M,STC}} + K_{\mathrm{V}}\Delta T, \tag{5.10}$$

where K_{V} is the open-circuit voltage temperature coefficient.

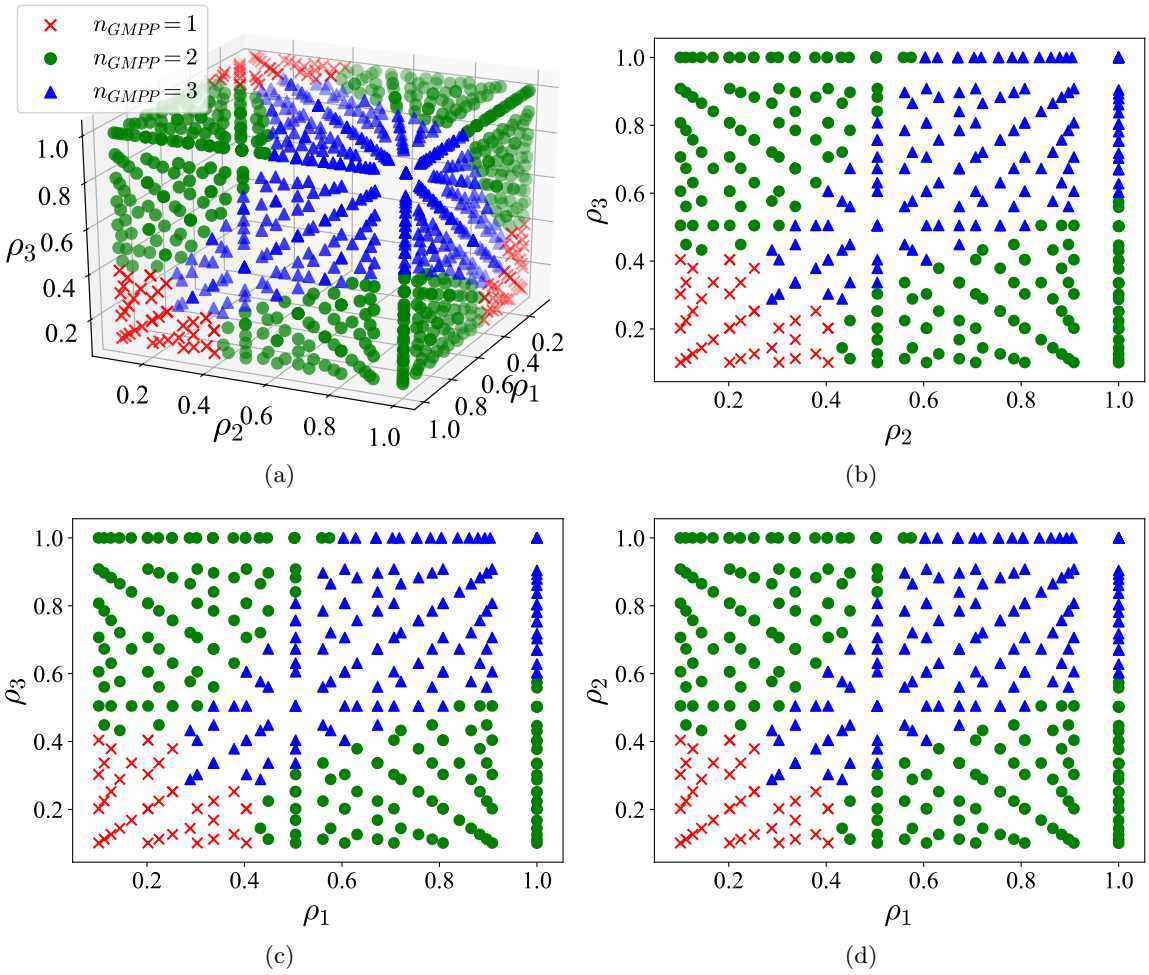

Figure 5.10: The relationship between the n_{GMPP} and the shading vector for a PV string with three modules under various shading conditions: (a) three-dimension view; (b) $\rho_1 = 1$; (c) $\rho_2 = 1$; (d) $\rho_3 = 1$.

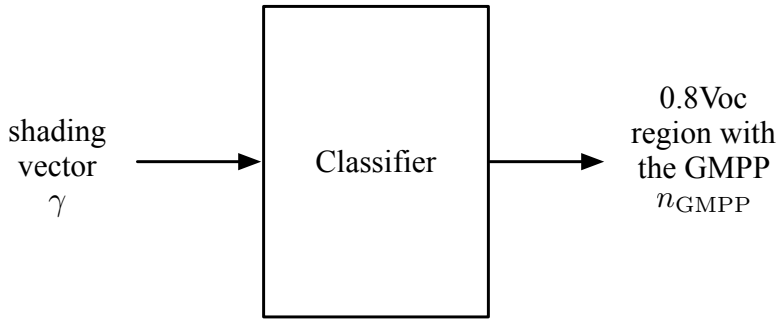

Figure 5.11: The structure of the predictor for the region with the GMPP.

5.3.2 Proposed Global Maximum Power Point Tracking Method

5.3.2.1 Detection of the Shading Vector

The shading vector is critical for predicting the position of the GMPP. The detection of the shading vector is the first step to obtain the $0.8\mathrm{V_{OC}}$ region with the GMPP. Although the shading vector can be trasformed from the shading matrix, a novel detection method is proposed here, which is capable of obtaining the results in one measuring step.

The relationship between the short-circuit current I_{SC} and the solar irradiance G for a single PV module is given in Equation (5.11) [15].

$$I_{\mathrm{SC}} = (I_{\mathrm{SC,STC}} + K_{\mathrm{I}}\Delta T)\frac{G}{G_{\mathrm{STC}}}, \tag{5.11}$$

where $I_{\mathrm{SC,STC}}$ is the short-circuit current at STC; K_{I} is the short-circuit current temperature co-efficient; $\Delta T = T - T_{\mathrm{STC}}$ is the temperature difference between the actual ambient temperature and the reference temperature at STC; G_{STC} is the reference solar irradiance at STC. The value of $I_{\mathrm{SC,STC}}$ and K_{I} can be found in the datasheet of the PV modules. When the temperature is fixed, the value of the short-circuit current I_{SC} is proportional to the value of the solar irradiance G. Thus, the ratio of the solar irradiance can be estimated by measuring the ratio of the short-circuit currents.

Figure 5.12 analyzes the current characteristics of a PV string with three modules. The PV string shown in Figure 5.12(a) operates under PSC. Figures 5.12(b), 5.12(c) and 5.12(d) record the current of the PV modules and the bypass diodes across the whole string voltage range. When the whole PV string is short-circuited, the individual PV module generates the maximum current that can produce under each solar irradiation

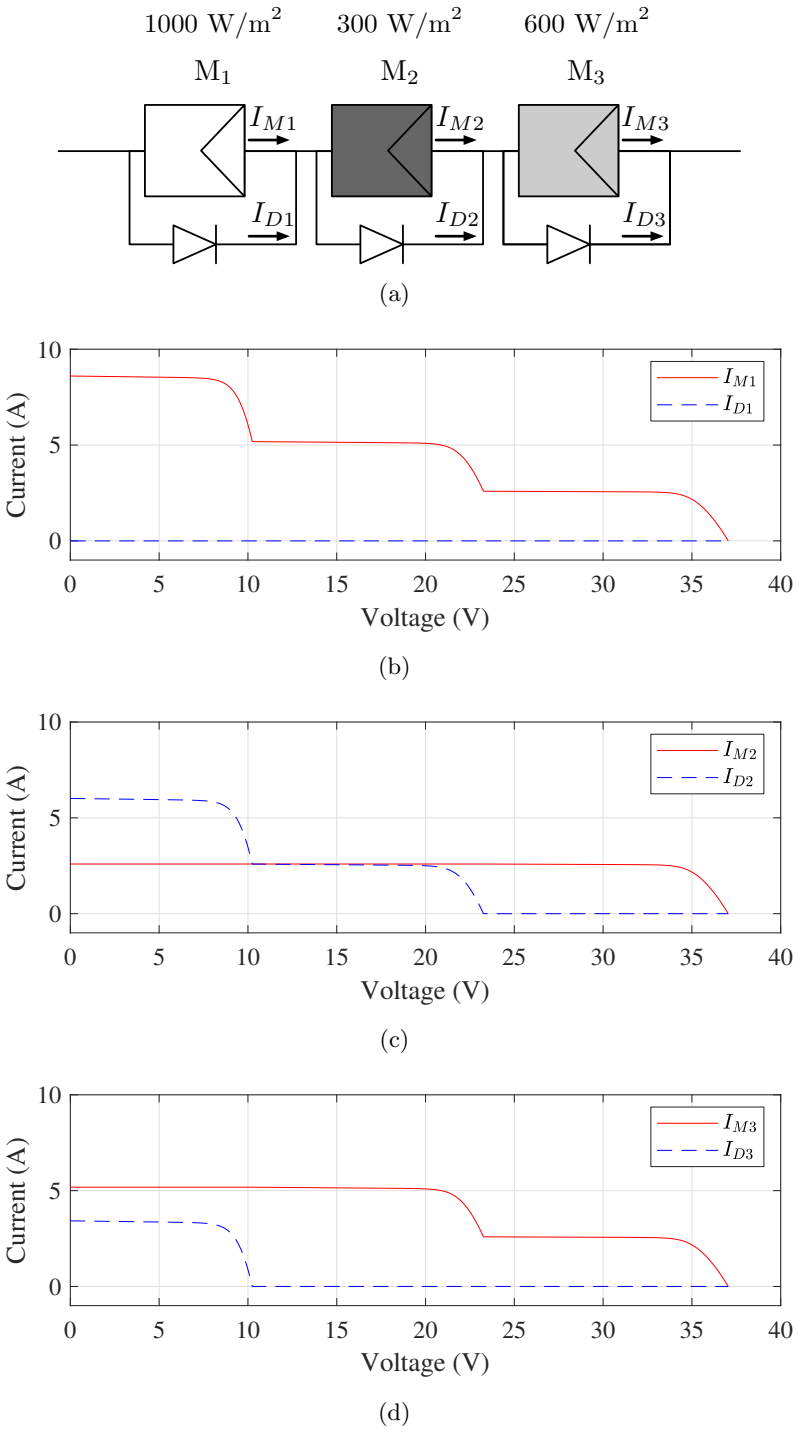

Figure 5.12: Current characteristics of PV modules and bypass diodes in the PV string under PSC: (a) the block diagram; (b) module 1; (c) module 2 and (d) module 3.

condition. The summation of the current from the PV module and its bypass diode is the string current. Therefore, only the short-circuit point of the PV string is needed to measure the short-circuit current for all the PV modules.

According to the current characteristics, the current sensors are used for all the PV modules to detect the shading strength vector. The block diagram of the shading detection circuit for the shading vector is shown in Figure 5.13. The current sensor is connected in series with each PV module to measure the module current. The detection procedure is described in Algorithm 5.2.

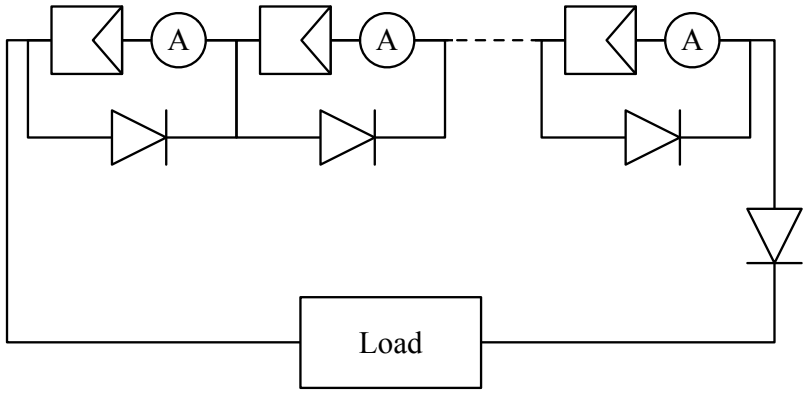

Figure 5.13: Shading detection circuit for the shading vector.

At the start, the current operating status is saved by recording the operating string voltage V_{OP}. To measure the short-circuit current, the PV string is set to operate at the short-circuit point. The currents at the string voltage of $10\% \times V_{\mathrm{OC,M}}$ are collected as the short-circuit currents $\boldsymbol{I_{\mathrm{SC}}}$ $(I_{\mathrm{SC},1}, \ldots, I_{\mathrm{SC},N_{\mathrm{String}}})$ to avoid the PV string from being totally short-circuited. Then, the operating string voltage is adjusted to the saved V_{OP}. The largest current is selected as the short-circuit current of the insolated module $I_{\mathrm{SC,Insolated}}$. Finally, the shading vector is obtained by Equation (5.12).

$$\gamma = \bigcup_{i=1}^{N_{\mathrm{String}}} \frac{I_{\mathrm{SC},i}}{I_{\mathrm{SC,Insolated}}}. \tag{5.12}$$

Algorithm 5.2 The procedure for the shading detection circuit.

Input: the number of PV modules in the PV string N_{String}
Output: the shading vector γ
1: Record the current operating voltage V_{OP}.
2: Adjust the string voltage to $10\% \times V_{\text{OC,M}}$.
3: Collect the value of each current sensor $\boldsymbol{I_{\text{SC}}}$.
4: Adjust the operating voltage to the recorded V_{OP}.
5: $I_{\text{SC,Insolated}} \leftarrow$ the largest current in $\boldsymbol{I_{\text{SC}}}$.
6: Obtain the shading vector by Equation (5.12).

5.3.2.2 Overview of the Proposed Method

Figure 5.14 depicts the block diagram of the proposed GMPPT method. The shading vector is detected by the shading detection circuit integrated into the PV string. The ambient temperature is collected by the thermometer to adjust the module open-circuit voltage by Equation (5.10). The microcontroller obtains the detected shading vector and gets the predictions of the n_{GMPP} from the k-NN. The operating voltage of the PV string is adjusted to the estimated V_{GMPP} from Equation (5.9) by controlling the DC-DC converter.

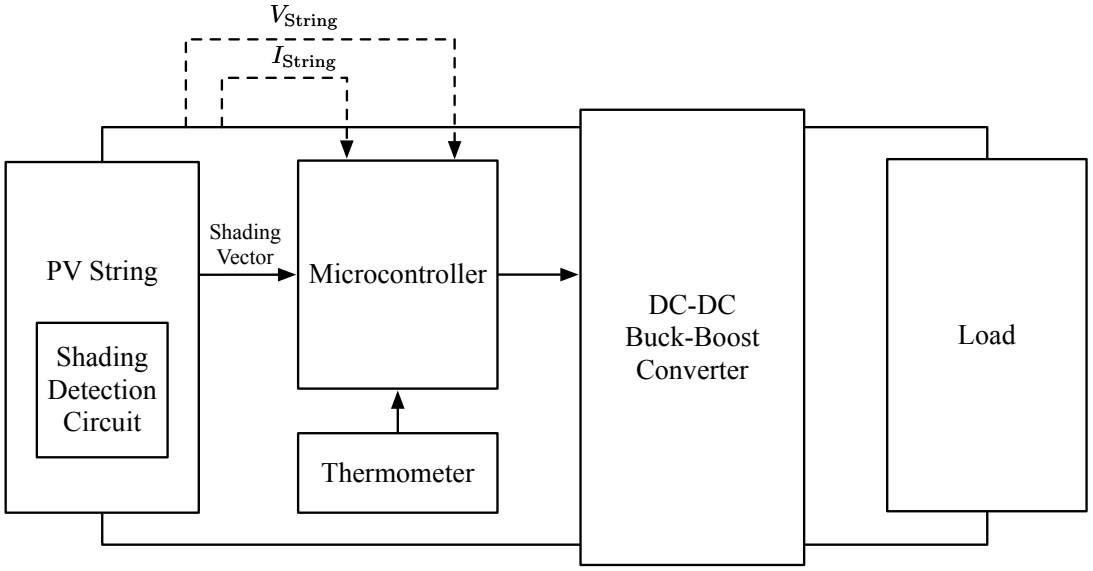

Figure 5.14: Block diagram of the proposed GMPPT method.

Algorithm 5.3 The procedure for proposed enhanced GMPPT method based on the shading vector.

1: Detect the shading vector.
2: Predict n_{GMPP} from the shading vector via k-NN.
3: Collect the ambient temperature.
4: Predict the V_{GMPP} by Equation (5.9).
5: Adjust the operating point to the predicted V_{GMPP}.
6: Track the exact GMPP by IncCond MPPT method.
7: Detect ΔP between two samplings.
8: **if** $\Delta P > 5\% \times P_{\mathrm{STC}}$ **then**
9: **go to** 3.
10: **else**
11: **go to** 6.
12: **end if**

The pseudocode of the proposed enhanced GMPPT method based on the shading vector is given in Algorithm 5.3. The flowchart of the proposed GMPPT method is shown in Figure 5.15. Firstly, the $0.8\mathrm{V_{OC}}$ region with the GMPP n_{GMPP} is predicted by the k-NN classification algorithm from the detected shading vector. The ambient temperature is collected and the voltage at the GMPP V_{GMPP} is estimated by Equation (5.9). After tuning the operating voltage to the estimated V_{GMPP}, the traditional MPPT scheme IncCond is finally used to track the exact GMPP. The power difference ΔP between two adjacent samples is detected continuously at a fixed frequency (depends on the step of IncCond). The shading pattern is assumed as changed when the power difference ΔP is larger than $5\% \times P_{\mathrm{STC}}$. At the same time, the proposed tracking method is rolled back to the initial state and a new V_{GMPP} is predicted.

5.3.3 Results and Discussions

5.3.3.1 Simulation Results

Three datasets for PV strings with 3, 4, and 5 modules under various shading patterns were generated in MATLAB/Simulink 2019b. According to the structure shown in Figure 5.11, the input of the classifier is the shading vector, and the output is the n_{GMPP}. All the combinations of the shading scenarios are simulated in the Simulink environments with

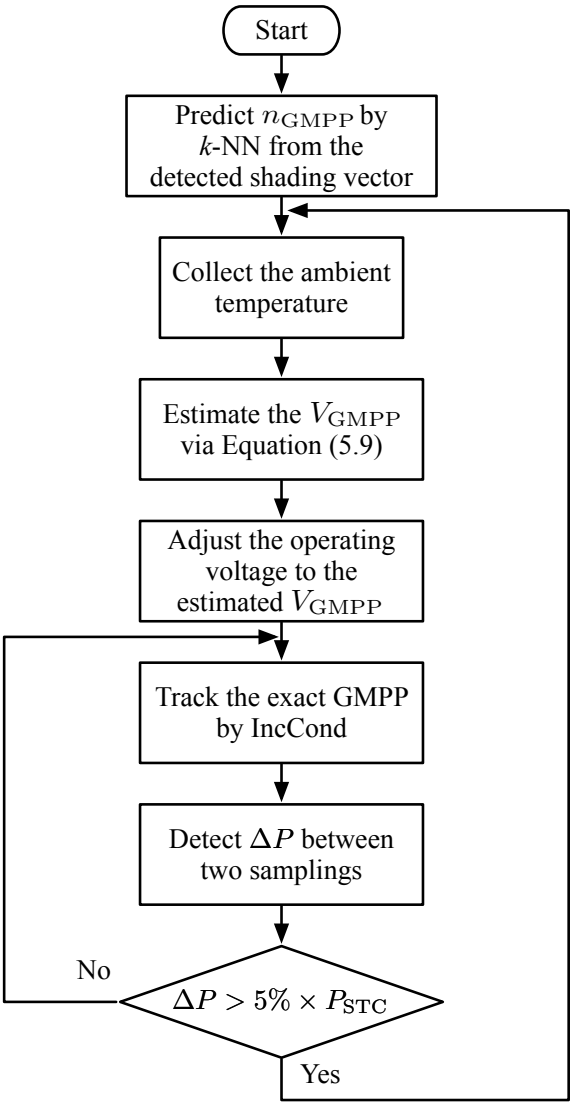

Figure 5.15: Flowchart of the proposed enhanced GMPPT method based on the shading vector.

the solar irradiance from 100 to 1000 W/m^2, every 100 W/m^2. The inputs are collected from the calculation results based on the solar irradiance. The output is the value from 1 to N_{String}, which is the index number of the GMPP region extracted from the simulated P-V characteristics. The specification of the PV module used is listed in Table 5.3. Figures 5.16, 5.17, and 5.18 show the distribution of the voltage at the GMPP for PV strings with a length of three, four, and five, respectively. The green horizontal dash-lines are the voltage at multiples of 0.8V_{OC}, which are the potential position of the predicted V_{GMPP}. It is observed that the measured V_{GMPP} values are distributed close to the multiples of 0.8V_{OC} at the middle voltage region, while there are some errors at the two edges. With the help of the traditional IncCond MPPT method, the actual GMPP can be tracked from the predicted V_{GMPP} within a few steps.

To verify the prediction performance of the k-NN classification algorithm in the proposed GMPPT method, four popular classification algorithms including Logistic Regression (LR), Gaussian Naive Bayes (GNB), Artificial Neural Network (ANN), and Support Vector Machine (SVM) were introduced into the comparison study. The classification tools from Scikit-learn [101] were used to assess the five algorithms on the generated datasets. The comparison results, as shown in Table 5.4, are the average accuracy from the three classification algorithms based on 100 times of 10-fold cross-validation.

Table 5.3: Specifications of the PV module used in this research under standard test conditions.

Parameters	**Variable**	**Value**	**Unit**
Short-circuit current	I_{SC}	1.23	A
Open-circuit voltage	V_{OC}	10.71	V
Current at MPP	I_{MPP}	1.12	A
Voltage at MPP	V_{MPP}	9.00	V
Maximum power	P_{MPP}	10.00	W
Temperature co-effcient of I_{SC}	K_{I}	0.062	A/°C
Temperature co-effcient of V_{OC}	K_{V}	-0.080	V/°C

The sizes of the three datasets were 1,000, 10,000, and 100,000 respectively. The increment in the size of the dataset had a huge impact on the average accuracy for the classification algorithms except for the k-NN. The average accuracy values for LR, GNB,

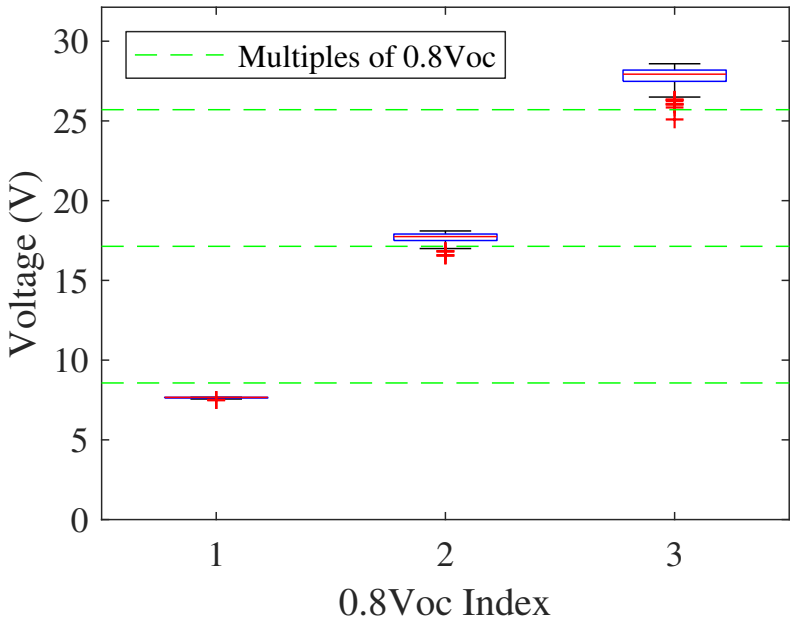

Figure 5.16: The distribution of the voltage at the GMPP under various shading conditions for PV strings with 3 modules.

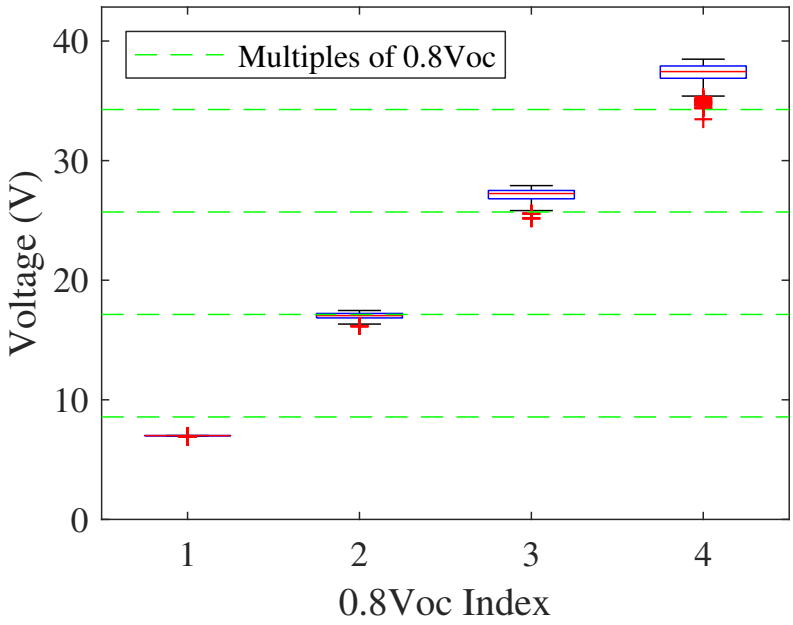

Figure 5.17: The distribution of the voltage at the GMPP under various shading conditions for PV strings with 4 modules.

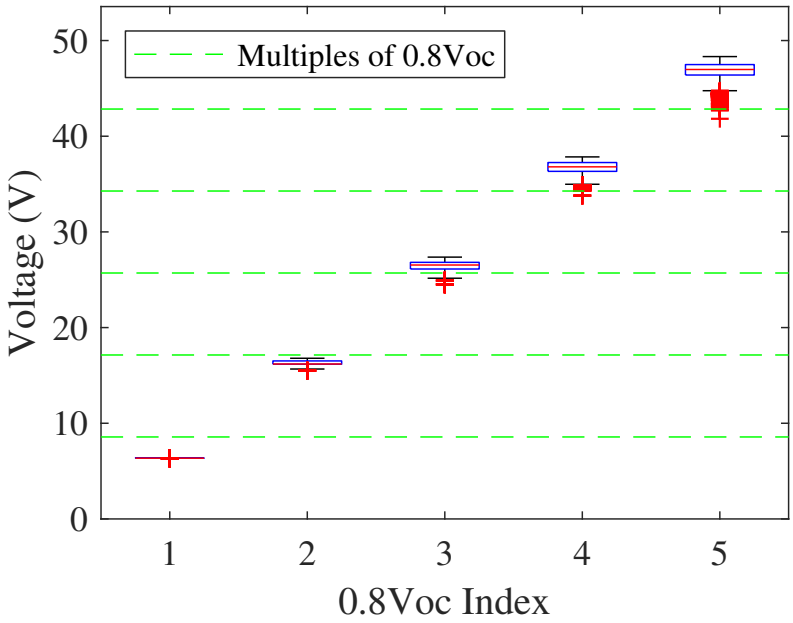

Figure 5.18: The distribution of the voltage at the GMPP under various shading conditions for PV strings with 5 modules.

Table 5.4: Average classification accuracy from different classification algorithms based on 100 times of 10-fold cross-validation.

N_{String} (Size of dataset)	3 (10^3)	4 (10^4)	5 (10^5)
k-Nearest Neighbors (k=20)	97.00%	96.05%	95.14%
Logistic Regression	71.57%	54.23%	44.52%
Gaussian Naive Bayes	70.76%	59.78%	50.39%
Artificial Neural Network	62.39%	56.10%	46.70%
Support Vector Machine	79.16%	68.40%	60.42%

ANN, and SVM became lower with the increasing size of the dataset. However, the average accuracy for the k-NN classifier was above 95% for all three datasets in the comparison test. Thus, the comparison study has shown that the k-NN algorithm has a better performance in classifying the $0.8V_{OC}$ region with the GMPP.

Figure 5.19 visualizes the classification results for PV strings with three modules. Different colors are used to distinguish different prediction labels. The solid circles are the correct predictions, while the crosses are the incorrect predictions. It can be found from the distribution results that the incorrect predictions are located at the intersections between different classes, where the power between two MPP regions is close to each other.

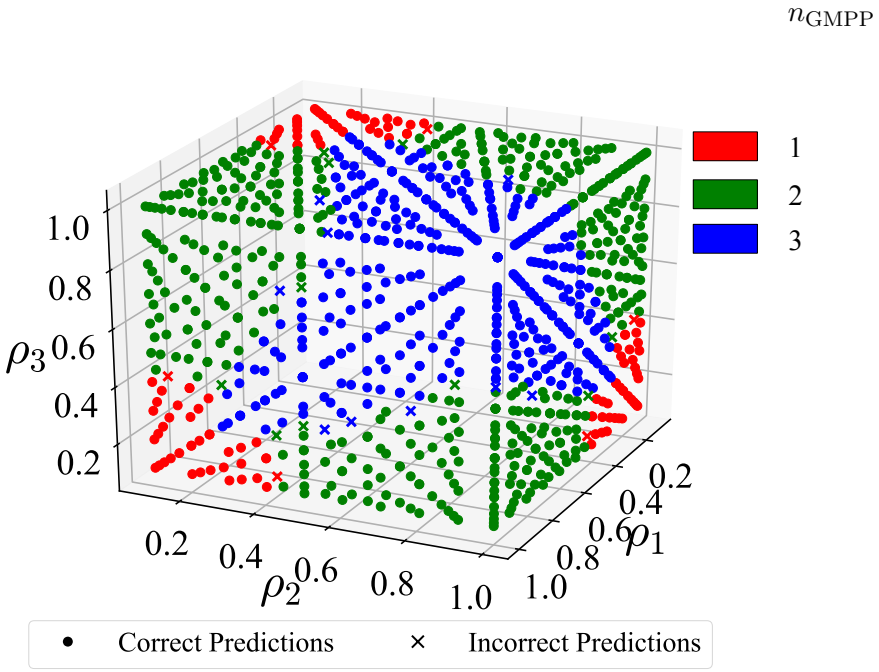

Figure 5.19: Visualization for the classification results ($N_{String} = 3$, $k = 20$).

The performance of the proposed GMPPT method was compared with the traditional $0.8V_{OC}$-model-based method, the Full Scanning (FS) method in [54] and the PSO-based method in [45]. The simulation was implemented with a PV string with four modules under three different shading patterns. The specification of the used PV module is the same and listed in Table 5.3. The parameter setting of PSO-based method was referred to [45], where the inertia weight $\omega = 0.4$; acceleration coefficients $c_1 = 1.2$ and $c_2 = 1.6$. The simulated

tracking results are shown in Figures 5.20, 5.21 and 5.22, where Figures 5.20(a), 5.21(a) and 5.22(a) depict the PV characteristics for the three shading patterns. The power at multiples of $0.8\times V_{\mathrm{OC,M}}$ (black vertical dash-lines in P-V curves) are labeled as P_1, P_2, P_3 and P_4. The corresponding comparison results between four GMPPT methods are shown in Figures 5.20(b), 5.21(b) and 5.22(b).

All the tested GMPPT methods were activated at 1 s and the controlling step was 0.1 s. The voltage scanning step for the full scanning method was set to 2 V. When starting tracking, the proposed GMPPT method detected the shading vector by adjusting the string voltage to the measuring point. The traditional $0.8\mathrm{V_{OC}}$-model-based method iteratively measured the power values at multiples of the $0.8\times V_{\mathrm{OC,M}}$ point. For all three shading patterns, the proposed method finished detecting the shading vector and obtained the predictions by one step, while the traditional $0.8\mathrm{V_{OC}}$-model-based method finished comparing after 4 steps. Based on the current simulation setup, the proposed method reduced the tracking step by 75% compared with the traditional $0.8\mathrm{V_{OC}}$-model-based method. The scanning time of the FS method was highly dependent on the voltage scanning step. Under the present voltage scanning step of 2 V, it took 2.1 s for the FS method to finish the voltage scanning for all three shading patterns. Such a scanning time was much longer than the time for reaching the GMPP by the proposed method. Moreover, since the voltage scanning step was quite large, under the shading pattern 1 and 2, the final tracked powers of the FS method were lower than the real GMPPs. Furthermore, the performance of the traditional $0.8\mathrm{V_{OC}}$-model-based method was dependent on the string length. It took more steps to get the $0.8\mathrm{V_{OC}}$ region with the GMPP for the traditional $0.8\mathrm{V_{OC}}$-model-based method when applied to a longer PV string. The performance of the proposed GMPPT method was not affected by the string length since the detection of the shading vector was executed in parallel.

Under shading patterns 2 and 3, the PSO-based method failed to track the GMPP and was trapped in the local peaks. It usually took around 0.8 s for the PSO-based method to reach a solution with small oscillations. Although the tracking speed of the PSO-based method was sometimes faster than the proposed method, it could not guarantee that the GMPP can always be tracked.

As can be seen from the P-V curves, the peak power points not always existed at the multiples of $0.8\times V_{\mathrm{OC,M}}$. In shading pattern 3, the power at the second $0.8\mathrm{V_{OC}}$ point P_2 (LMPP) was larger than the third one P_3 (GMPP). As a result, the traditional $0.8\mathrm{V_{OC}}$-model-based method did not track the global maximum for shading pattern 3. This prob-

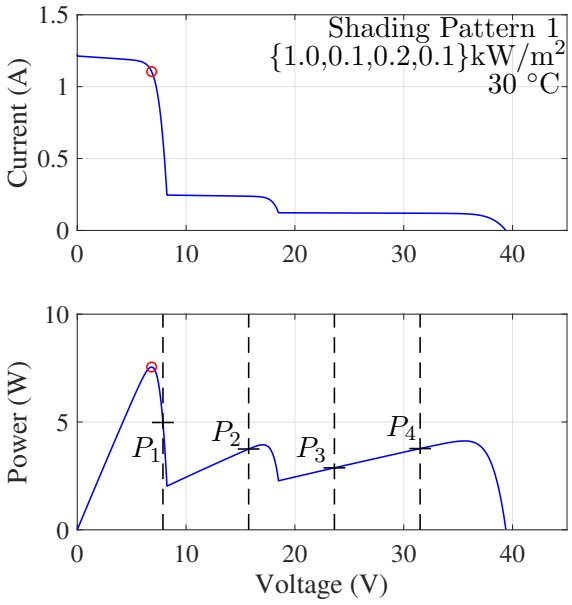

(a)

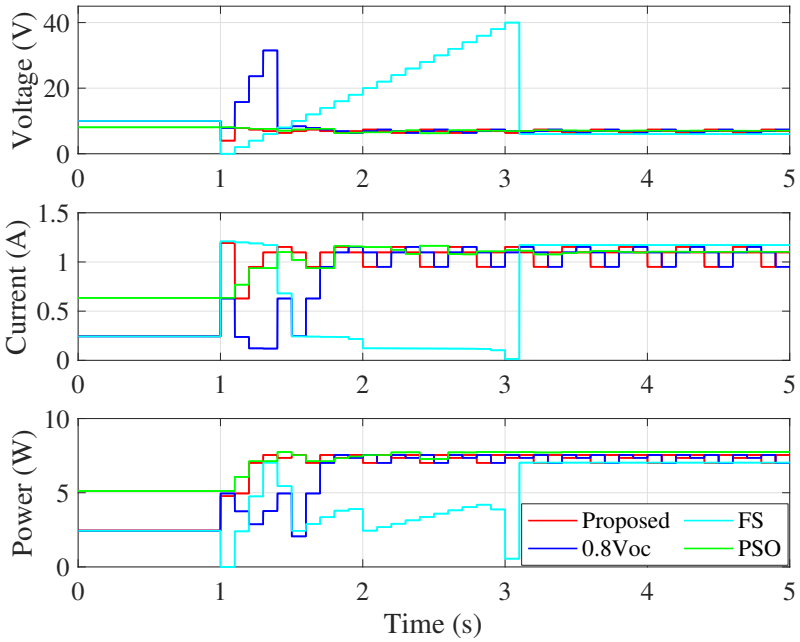

(b)

Figure 5.20: Simulated tracking results for a PV string with four modules under fixed shading patterns 1: (a) PV characteristics and (b) tracking results.

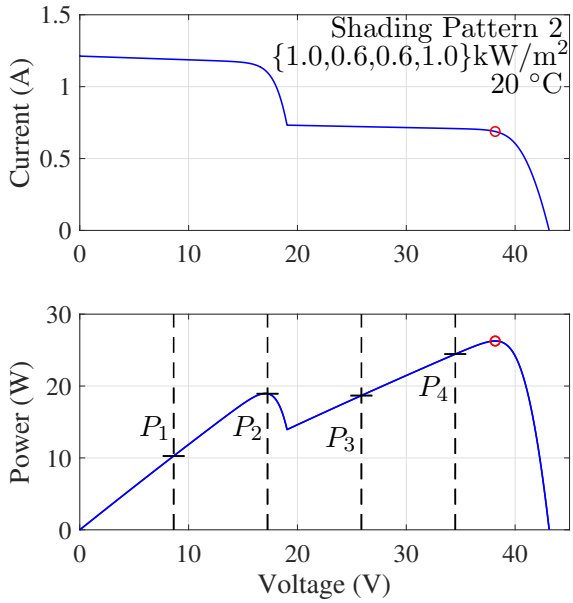

(a)

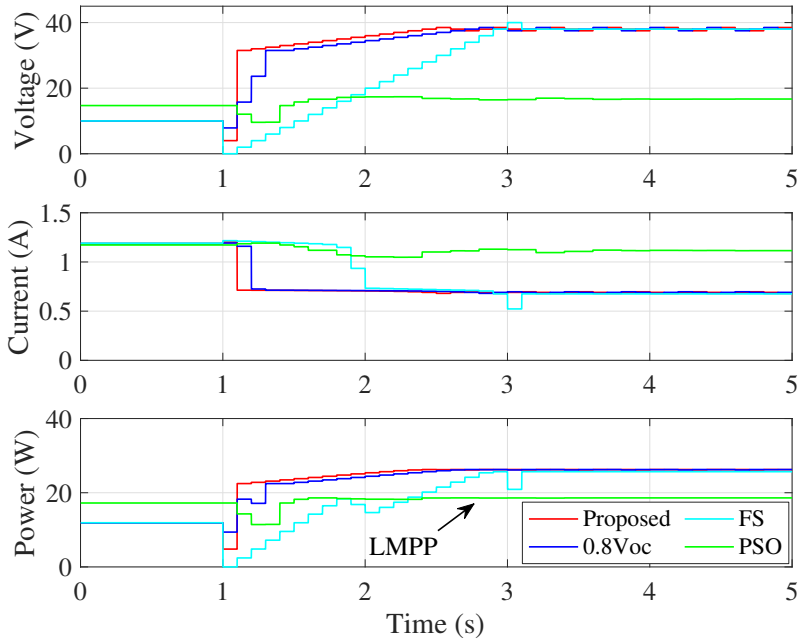

(b)

Figure 5.21: Simulated tracking results for a PV string with four modules under fixed shading patterns 2: (a) PV characteristics and (b) tracking results.

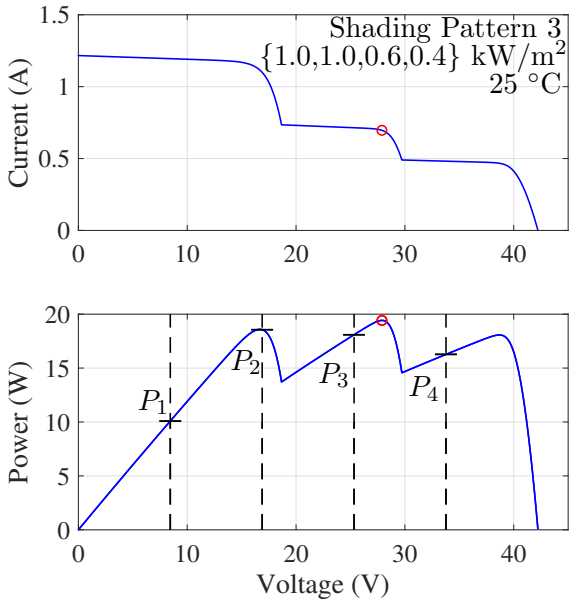

(a)

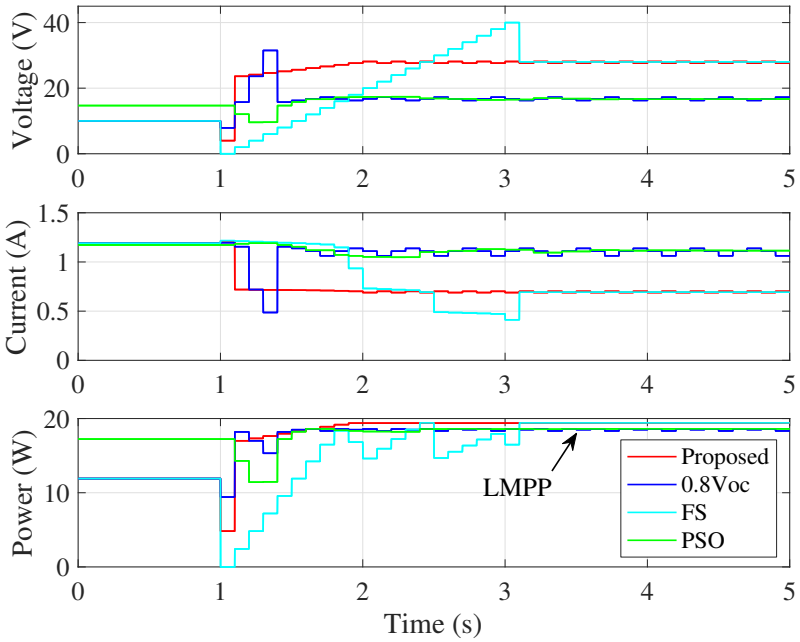

(b)

Figure 5.22: Simulated tracking results for a PV string with four modules under fixed shading patterns 3: (a) PV characteristics and (b) tracking results.

lem did not influence the prediction of the proposed method as the trained dataset had the correct $0.8V_{OC}$ region with the GMPP.

5.3.3.2 Experimental Results

A PV string with four PV modules was used to validate the effectiveness of the proposed GMPPT method. The setup of the hardware implementation is shown in Figure 5.23. The four PV modules have the same specification as the PV module used in the simulation. In order to make the PV string operate under stable partial shading conditions, some floodlights with Halogen lamps were used to emulate the sunlight in an indoor environment. The ambient temperature was captured by the thermometer (DS18B20) attached at the rear of the PV module. The sensor module (JSY-MK-218) was used to measure the string voltage, string current, and current of each PV module. The microcontroller (UDOO NEO) implemented the shading detection and the proposed GMPPT algorithms. The oscilloscope (GW Instek GDS-2202A) was used to record the tracking results using voltage and current probes. The operating point of the PV string was adjusted by a DC-DC buck-boost converter (ANHE BB4805S) and an electronic load (ITECH IT8512A+) with fixed resistance.

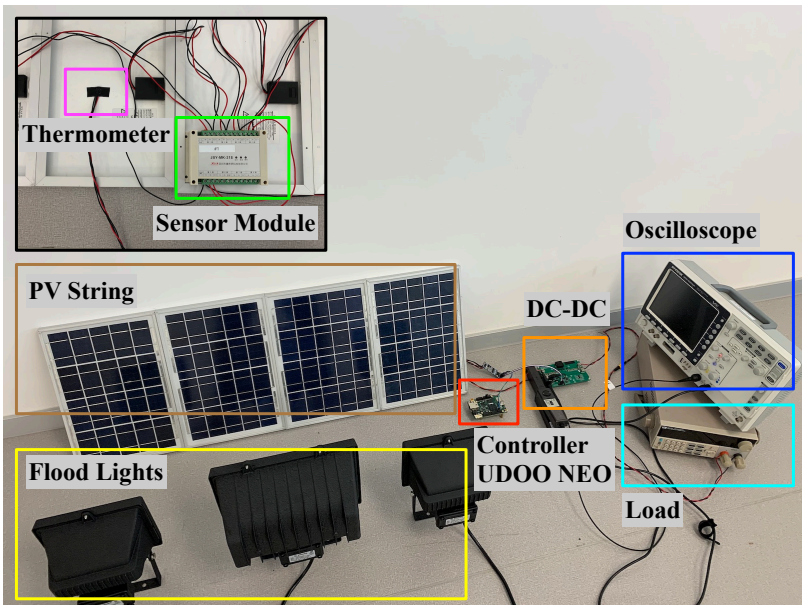

Figure 5.23: Hardware setup of the experimental implementation.

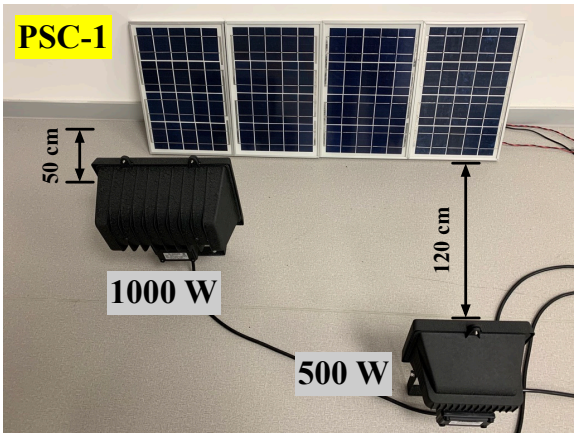

(a)

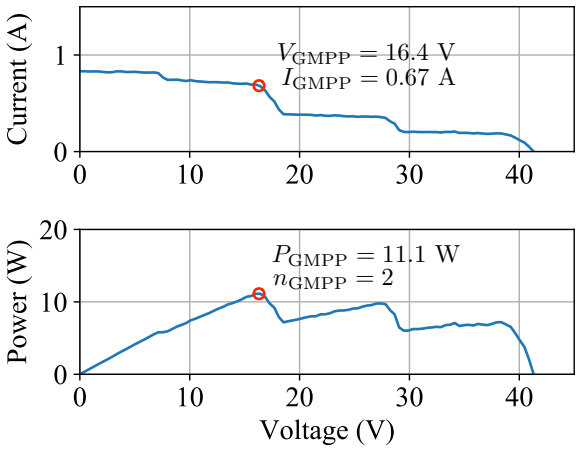

(b)

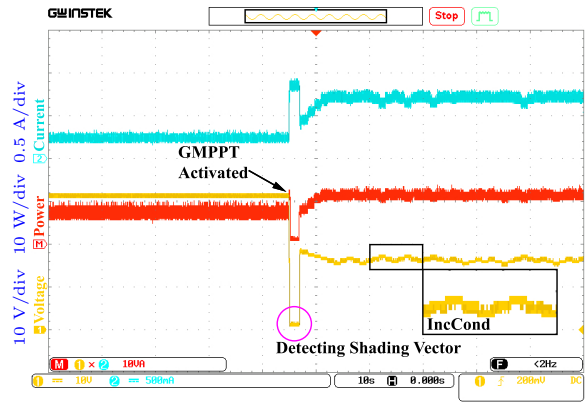

(c)

Figure 5.24: Experimental results of the proposed GMPPT method under fixed PSC-1. (a) light position, (b) scanned PV characteristic curves and (c) tracking results.

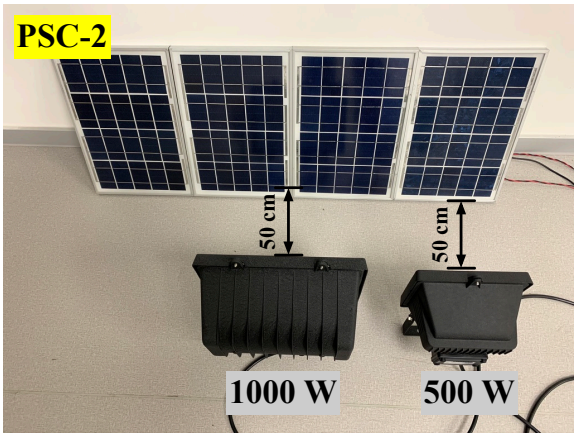

(a)

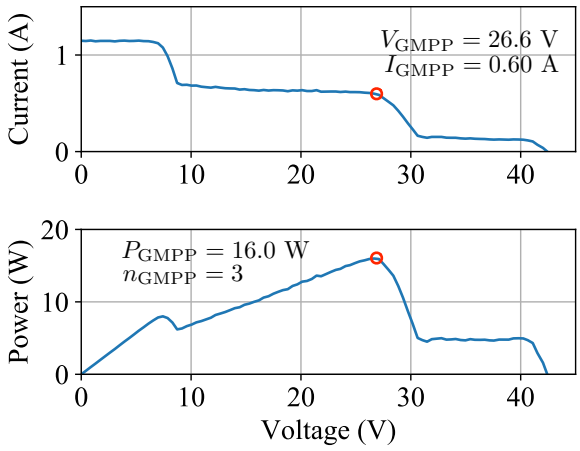

(b)

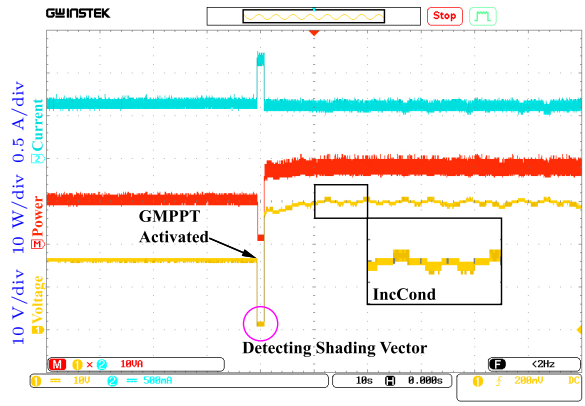

(c)

Figure 5.25: Experimental results of the proposed GMPPT method under fixed PSC-2. (a) light position, (b) scanned PV characteristic curves and (c) tracking results.

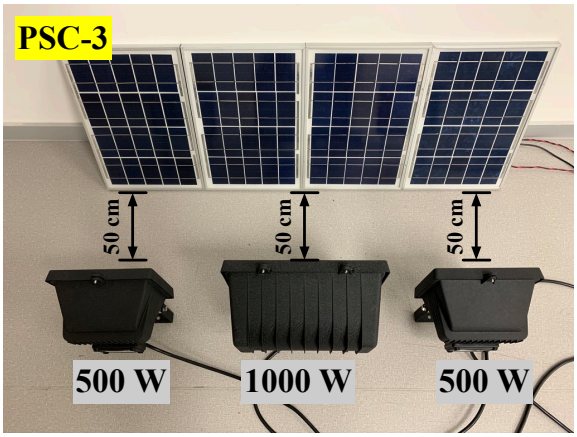

(a)

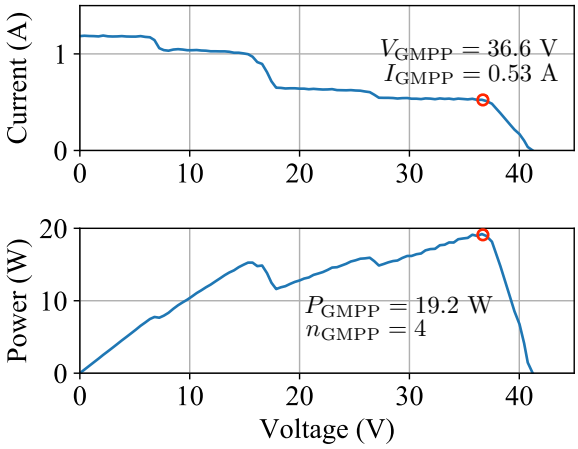

(b)

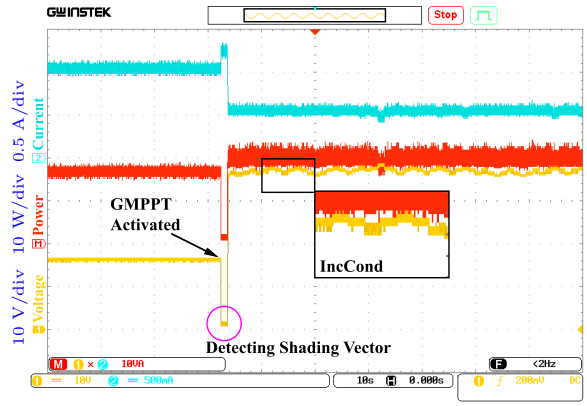

(c)

Figure 5.26: Experimental results of the proposed GMPPT method under fixed PSC-3. (a) light position, (b) scanned PV characteristic curves and (c) tracking results.

The experimental validations were split into two case studies (fixed PSC and changing shading patterns) to show the tracking performance of the proposed GMPPT method under the different shading scenarios.

Case Study 1: Fixed Shading Conditions Three partial shading conditions were emulated in this case study. The ambient temperature was around 25 °C in the indoor environment. The positions of the floodlights and the PV modules are as shown in Figures 5.24(a), 5.25(a) and 5.26(a). The power of each floodlight and the distances between the lights and the PV modules are labeled on the figures.

For each shading pattern, the currents and voltages were measured by scanning the string voltage from 0 V to the string open-circuit voltage in order to acquire the I-V characteristics. The power information was calculated from the measured current and voltage data. The I-V and P-V characteristics under each PSC were drawn in MATLAB as shown in Figures 5.24(b), 5.25(b) and 5.26(b). The GMPPs are marked by the red circles on the I-V curves and P-V curves. Under three PSCs, the GMPPs are respectively distributed at the $0.8V_{OC}$ regions 2, 3, and 4. The corresponding voltage and current values at the GMPP are listed near the GMPP on each I-V curve.

Figures 5.24(c), 5.25(c) and 5.26(c) are the tracking results captured by the oscilloscope. The string voltage and current are recorded as the yellow and blue curves. The red curve is the string power generated by a function of the oscilloscope. When the tracking algorithm was activated, it can be observed that the string voltage was tuned to a lower value to detect the shading vector. For all three PSCs, the $0.8V_{OC}$ region with the GMPP was correctly predicted and the operating point was adjusted to the predicted value after finishing the shading detection process. Then, the traditional MPPT method IncCond was used to track the exact GMPP.

Case Study 2: Changing Shading Conditions When using the IncCond method to track the exact GMPP, the proposed GMPPT method continuously detected the power difference between two data samplings in case that there would have a sudden change in the shading pattern. In this test, the shading pattern was suddenly changed when the system operated at a steady state to verify the effectiveness of the proposed GMPPT method under changing shading conditions. The string power at STC P_{STC} for the current setup was 40 W, and as a result, the threshold was set to $5\% \times P_{\mathrm{STC}} = 2$ W.

Figure 5.27 shows the tracking results under changing shading conditions. PSC-2 and

PSC-3 used in the test under fixed shading conditions were involved in this experiment. The shading pattern was initially set to PSC-3, the proposed GMPPT method successfully tracked the GMPP under PSC-3 after the method was activated. When the string power was optimized by the IncCond, the shading pattern was suddenly changed to PSC-2. As the detected power difference ΔP was greater than 2 W, the shading detection algorithm was activated again to update the shading vector. The new prediction was generated based on the updated shading vector.

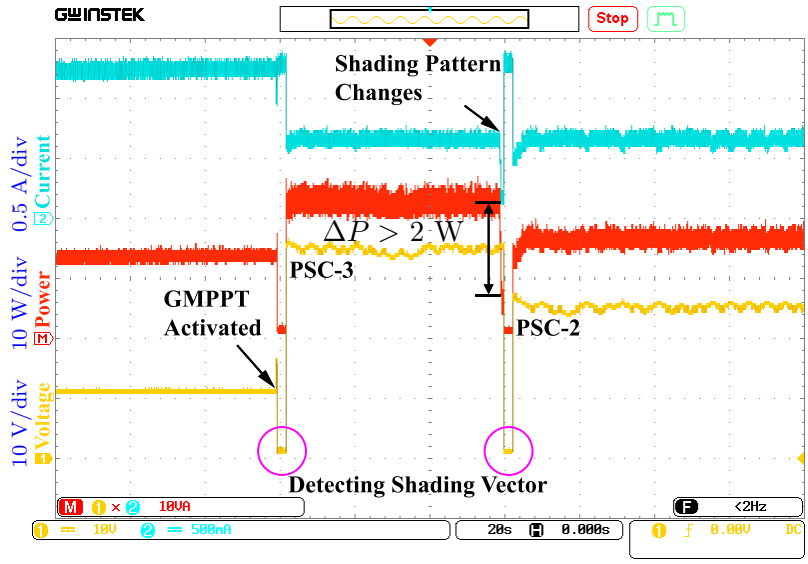

Figure 5.27: Tracking results of the proposed method under changing partial shading conditions (changing from PSC-3 to PSC-2).

Under both shading patterns, the locations of the GMPP were correctly predicted by the proposed GMPPT method. The proposed GMPPT method is capable of tracking the GMPP under rapidly changing partial shading conditions.

5.4 Summary

This chapter has presented two enhanced $0.8V_{OC}$-model-based GMPPT methods. The first one estimates the GMPP locus from the detected shading rate through a mathematical relation model. The second method introduces a shading vector to characterize the complex

shading scenarios. In such method, the GMPP location is obtained from the shading vector using the k-NN algorithm. Simulations and experimental results have validated the improved performance of the proposed MPPT methods. The first GMPPT method based on the shading rate detection saved around 50% of the tracking time for a PV string with three modules when comparing with the classical $0.8V_{OC}$-model-based method. The second GMPPT method based on the shading vector detection had an accuracy of around 96% when predicting the GMPP region using k-NN. Compared with the other GMPPT methods including $0.8V_{OC}$-model-based, FS, and PSO-based methods, the second GMPPT method reduced the tracking step by at lease 75% for a PV string with four modules.

Chapter 6

Conclusions and Future Work

In this thesis, the problems of the partial shading perception and Global Maximum Power Point Tracking (GMPPT) under Partial Shading Conditions (PSC) have been investigated for the Photovoltaic (PV) systems. To solve the two problems, several shading detection methods and GMPPT methods have been proposed as follows:

1. In Chapter 3, an automatic shading detection system was proposed to estimate the shading information. The main features of the proposed method are the utilization of a reduced number of sensors, a simple switching control strategy, and a high detection rate. The feasibility and effectiveness of the proposed shading detecting system were verified through hardware experiments.

2. In Chapter 4, a shading matrix was proposed to describe the shading rate and shading strength information. The proposed shading matrix would provide Maximum Power Point Tracking (MPPT) controllers with the essential environmental information to improve the Global Maximum Power Point (GMPP) tracking performance. Furthermore, a Modified Tabu Search (MTS)-based identification method was proposed to estimate the shading matrix. The proposed modified method involves a preselection process of updating the Tabu list to optimize the searching efficiency. The accuracy and efficiency of the proposed analytical estimation expression were verified through simulations and experiments. By comparing with Binary Search (BS), Golden-section Search (GS), and Tabu Search (TS) algorithms, the proposed MTS algorithm can be applied to perceive the shading information at least 18.75% faster.

3. Section 5.2 proposed a novel $0.8V_{OC}$-model-based GMPPT method based on the shading rate detection method in Chapter 3. A mathematical relationship between the shading rate and GMPP location was presented and the GMPP can be estimated by the shading detection results. Simulation results proved the proposed GMPPT method saved around 50% of the tracking time for a PV string with three modules when comparing with the classical $0.8V_{OC}$-model-based method.

4. In Section 5.3, a shading vector was proposed to characterize the complex PSC. The shading vector improves the performance of the traditional shading information and is capable of describing complex shading conditions. Based on the electrical characteristics of the PV string, a shading detection circuit was proposed to estimate the shading vector.

5. Section 5.3 also introduced an enhanced GMPPT method based on the detection of the shading vector. The proposed GMPPT method estimates the $0.8V_{OC}$ region with the GMPP directly from the measured shading vector by the k-Nearest Neighbors (k-NN) approach and saves the time consumed in the comparison process used in the conventional method. Based on the simulation and experimental results, such GMPPT method had an accuracy of around 96% when predicting the GMPP region using k-NN. Compared with the other GMPPT methods including $0.8V_{OC}$-model-based, FS, and PSO-based methods, the proposed GMPPT method reduced the tracking step by at lease 75% for a PV string with four modules.

With the help of the identification of PSC, the efficiency of the proposed GMPPT techniques has been largely improved when comparing to the traditional MPPT methods. Although the proposed shading identification and detection methods, and the GMPPT methods have achieved promising results with respect to the investigated research problems, there are still some directions that can be further investigated as follows:

1. The shading matrix proposed in Chapter 4 would be applied into the MPPT techniques to help PV systems optimize the power efficiency.

2. The mathematical modeling for the PV string under PSC is a challenging topic recently. Based on the shading identification and detection methods proposed in this thesis, an extended research area could be developing an accurate model for the electrical characteristics of PV string.

3. Part of the proposed MPPT methods in this thesis requires the measurement of the string short-circuit current. When measuring the short-circuit current, the power of the PV system is zero. This will lead to power loss. To avoid this problem, further research could be developing the methods without measuring the power loss points (i.e. short-circuit and open-circuit points).

4. The PV systems used in this thesis are mainly tested based on a DC-DC converter connected with a constant load. In practice, charging the DC batteries and connecting to the grid-connected inverters are more useful for industry fields. These can be investigated in future work.

References

[1] S. Mekhilef, R. Saidur, and A. Safari. A review on solar energy use in industries. *Renewable and Sustainable Energy Reviews*, 15(4):1777 – 1790, 2011.

[2] J. Ma, H. Jiang, K. Huang, Z. Bi, and K. L. Man. Novel field-support vector regression-based soft sensor for accurate estimation of solar irradiance. *IEEE Transactions on Circuits and Systems I: Regular Papers*, 64(12):3183–3191, Dec 2017.

[3] P. Samantaray and S. Sasmita. Performance of solar photovoltaic module under partial shading conditions. In *2016 10th International Conference on Intelligent Systems and Control (ISCO)*, pages 1–4, Jan 2016.

[4] K. Kato and H. Koizumi. A study on effect of blocking and bypass diodes on partial shaded PV string with compensating circuit using voltage equalizer. In *2015 IEEE International Symposium on Circuits and Systems (ISCAS)*, pages 241–244, May 2015.

[5] N. Femia, G. Petrone, G. Spagnuolo, and M. Vitelli. Optimization of perturb and observe maximum power point tracking method. *IEEE Transactions on Power Electronics*, 20(4):963–973, July 2005.

[6] S. Jianping and L. Xiaozheng. A new Mppt control strategy: Study of auto-adapted step size incremental conductance method based on segmented numerical approximation. In *2011 International Conference on Mechatronic Science, Electric Engineering and Computer (MEC)*, pages 239–242, Aug 2011.

[7] H. Renaudineau, F. Donatantonio, J. Fontchastagner, G. Petrone, G. Spagnuolo, J. Martin, and S. Pierfederici. A PSO-based global MPPT technique for distributed

PV power generation. *IEEE Transactions on Industrial Electronics*, 62(2):1047–1058, 2015.

[8] S. Hadji, J. Gaubert, and F. Krim. Experimental analysis of genetic algorithms based MPPT for PV systems. In *2014 International Renewable and Sustainable Energy Conference (IRSEC)*, pages 7–12, Oct 2014.

[9] S. Bifaretti, V. Iacovone, L. Cin‡, and E. Buffone. Global MPPT method for partially shaded photovoltaic modules. In *2012 IEEE Energy Conversion Congress and Exposition (ECCE)*, pages 4768–4775, Sept 2012.

[10] M. Y. Javed, M. M. Gulzar, S. T. H. Rizvi, and A. Arif. A hybrid technique to harvest maximum power from PV systems under partial shading conditions. In *2016 International Conference on Emerging Technologies (ICET)*, pages 1–5, Oct 2016.

[11] J. Ma, X. Pan, K. L. Man, X. Li, H. Wen, and T. On Ting. Detection and assessment of partial shading scenarios on photovoltaic strings. *IEEE Transactions on Industry Applications*, 54(6):6279–6289, Nov 2018.

[12] F. Salem and M. A. Awadallah. Detection and assessment of partial shading in photovoltaic arrays. *Journal of Electrical Systems and Information Technology*, 3(1):23–32, May 2016.

[13] M. Kermadi, V. J. Chin, S. Mekhilef, and Z. Salam. A fast and accurate generalized analytical approach for PV arrays modeling under partial shading conditions. *Solar Energy*, 208:753–765, 2020.

[14] Y.-H. Ji, J.-G. Kim, S. Park, J.-H. Kim, and C.-Y. Won. C-language based PV array simulation technique considering effects of partial shading. In *2009 IEEE International Conference on Industrial Technology*, pages 1–6, Gippsland, VIC, Australia, Feb 2009.

[15] M. G. Villalva, J. R. Gazoli, and E. R. Filho. Comprehensive approach to modeling and simulation of photovoltaic arrays. *IEEE Transactions on Power Electronics*, 24(5):1198–1208, 2009.

[16] J. Ma, Z. Bi, T. O. Ting, S. Hao, and W. Hao. Comparative performance on photovoltaic model parameter identification via bio-inspired algorithms. *Solar Energy*, 132:606 – 616, 2016.

[17] J.-C. Wang, Y.-L. Su, J.-C. Shieh, and J.-A. Jiang. High-accuracy maximum power point estimation for photovoltaic arrays. *Solar Energy Materials and Solar Cells*, 95(3):843 – 851, 2011.

[18] S. Sarikh, M. Raoufi, A. Bennouna, A. Benlarabi, and B. Ikken. Fault diagnosis in a photovoltaic system through I-V characteristics analysis. In *2018 9th International Renewable Energy Congress (IREC)*, pages 1–6, 2018.

[19] S. S. Kumar and A. I. Selvakumar. Detection of the faults in the photovoltaic array under normal and partial shading conditions. In *2017 Innovations in Power and Advanced Computing Technologies (i-PACT)*, pages 1–5, 2017.

[20] Q. Zhao, S. Shao, L. Lu, X. Liu, and H. Zhu. A new PV array fault diagnosis method using fuzzy c-mean clustering and fuzzy membership algorithm. *Energies*, 11(1), 2018.

[21] J. Huang, R. Wai, and W. Gao. Newly-designed fault diagnostic method for solar photovoltaic generation system based on IV-curve measurement. *IEEE Access*, 7:70919–70932, 2019.

[22] S. Fadhel, C. Delpha, D. Diallo, I. Bahri, A. Migan, M. Trabelsi, and M.F. Mimouni. PV shading fault detection and classification based on I-V curve using principal component analysis: Application to isolated PV system. *Solar Energy*, 179:1 – 10, 2019.

[23] A. K. Tripathi, M. Aruna, and Ch. S. N. Murthy. Performance of a PV panel under different shading strengths. *International Journal of Ambient Energy*, 40(3):248–253, 2019.

[24] J. Ma, Z. Bi, K. L. Man, H. Liang, and J. S. Smith. Predicting the global maximum power point locus using shading information. In *2019 IEEE International Conference on Environment and Electrical Engineering and 2019 IEEE Industrial and Commercial Power Systems Europe (EEEIC / I CPS Europe)*, pages 1–5, 2019.

[25] Z. Bi, J. Ma, K. L. Man, J. S. Smith, Y. Yue, and H. Wen. Global MPPT method for photovoltaic systems operating under partial shading conditions using the 0.8voc

model. In *2019 IEEE International Conference on Environment and Electrical Engineering and 2019 IEEE Industrial and Commercial Power Systems Europe (EEEIC / I CPS Europe)*, pages 1–6, 2019.

[26] J. Ma, Z. Bi, K. L. Man, Y. Yue, and J. S. Smith. Automatic shading detection system for photovoltaic strings. In *2018 International SoC Design Conference (ISOCC)*, pages 176–177, 2018.

[27] F. Zhang, J. Li, C. Feng, and Y. Wu. In-depth investigation of effects of partial shading on PV array characteristics. In *2012 Power Engineering and Automation Conference*, pages 1–4, 2012.

[28] M. Davarifar, A. Rabhi, A. Hajjaji, E. Kamal, and Z. Daneshifar. Partial shading fault diagnosis in PV system with discrete wavelet transform (DWT). In *2014 International Conference on Renewable Energy Research and Application (ICRERA)*, pages 810–814, 2014.

[29] L. Davies, R. Thornton, P. Hudson, and B. Ray. Automatic detection and characterization of partial shading in PV system. In *2018 IEEE 7th World Conference on Photovoltaic Energy Conversion (WCPEC) (A Joint Conference of 45th IEEE PVSC, 28th PVSEC 34th EU PVSEC)*, pages 1185–1187, 2018.

[30] P. Lei, Y. Li, and J. E. Seem. Sequential esc-based global MPPT control for photovoltaic array with variable shading. *IEEE Transactions on Sustainable Energy*, 2(3):348–358, 2011.

[31] J. M. Riquelme-Dominguez and S. Martinez. Comparison of different photovoltaic perturb and observe algorithms for drift avoidance in fluctuating irradiance conditions. In *2020 IEEE International Conference on Environment and Electrical Engineering and 2020 IEEE Industrial and Commercial Power Systems Europe (EEEIC / I CPS Europe)*, pages 1–5, 2020.

[32] M. A. Elgendy, B. Zahawi, and D. J. Atkinson. Assessment of the incremental conductance maximum power point tracking algorithm. *IEEE Transactions on Sustainable Energy*, 4(1):108–117, 2013.

[33] J. Ahmad. A fractional open circuit voltage based maximum power point tracker for

photovoltaic arrays. In *2010 2nd International Conference on Software Technology and Engineering*, volume 1, pages V1–247–V1–250, 2010.

[34] I. Owusu-Nyarko, M. A. Elgenedy, and K. Ahmed. Combined temprature and irradiation effects on the open circuit voltage and short circuit current constants for enhancing their related pv-mppt algorithms. In *2019 IEEE Conference on Power Electronics and Renewable Energy (CPERE)*, pages 343–348, 2019.

[35] M. M. Shebani, T. Iqbal, and J. E. Quaicoe. Comparing bisection numerical algorithm with fractional short circuit current and open circuit voltage methods for MPPT photovoltaic systems. In *2016 IEEE Electrical Power and Energy Conference (EPEC)*, pages 1–5, 2016.

[36] H. A. Sher, A. F. Murtaza, A. Noman, K. E. Addoweesh, and M. Chiaberge. An intelligent control strategy of fractional short circuit current maximum power point tracking technique for photovoltaic applications. *Journal of Renewable and Sustainable Energy*, 7(1):013114, 2015.

[37] M. Drif, P.J. Pérez, J. Aguilera, and J.D. Aguilar. A new estimation method of irradiance on a partially shaded PV generator in grid-connected photovoltaic systems. *Renewable Energy*, 33(9):2048–2056, September 2008.

[38] J. C. Teo, Rodney H. G. Tan, V. H. Mok, Vigna K. Ramachandaramurthy, and ChiaKwang Tan. Impact of partial shading on the P-V characteristics and the maximum power of a photovoltaic string. *Energies*, 11(7):1–22, July 2018.

[39] M. E. Başoğlu. An improved 0.8 Voc model based GMPPT technique for module level photovoltaic power optimizers. *IEEE Transactions on Industry Applications*, 55(2):1913–1921, March 2019.

[40] X. Li, H. Wen, Y. Hu, L. Jiang, and W. Xiao. Modified beta algorithm for GMPPT and partial shading detection in photovoltaic systems. *IEEE Transactions on Power Electronics*, 33(3):2172–2186, 2018.

[41] A. A. Saferi, J. Selvaraj, and N. A. Rahim. Fast two stage MPPT method using power estimation technique for partially shaded condition. In *4th IET Clean Energy and Technology Conference (CEAT 2016)*, Kuala Lumpur, Malaysia, November 2016.

[42] L. Bouselham, M. Hajji, B. Hajji, and H. Bouali. A new MPPT-based ANN for photovoltaic system under partial shading conditions. *Energy Procedia*, 111:924 – 933, 2017. 8th International Conference on Sustainability in Energy and Buildings, SEB-16, 11-13 September 2016, Turin, Italy.

[43] K. Y. Yap, C. R. Sarimuthu, and J. M. Y. Lim. Artificial intelligence based MPPT techniques for solar power system: A review. *Journal of Modern Power Systems and Clean Energy*, 8(6):1043–1059, 2020.

[44] R. Divyasharon, R. Narmatha Banu, and D. Devaraj. Artificial neural network based MPPT with cuk converter topology for PV systems under varying climatic conditions. In *2019 IEEE International Conference on Intelligent Techniques in Control, Optimization and Signal Processing (INCOS)*, pages 1–6, 2019.

[45] K. Ishaque, Z. Salam, M. Amjad, and S. Mekhilef. An improved particle swarm optimization (PSO)–based MPPT for PV with reduced steady-state oscillation. *IEEE Transactions on Power Electronics*, 27(8):3627–3638, 2012.

[46] K. Ishaque and Z. Salam. A deterministic particle swarm optimization maximum power point tracker for photovoltaic system under partial shading condition. *IEEE Transactions on Industrial Electronics*, 60(8):3195–3206, 2013.

[47] C.-Y. Won, D.-H. Kim, S.-C. Kim, W.-S. Kim, and H.-S. Kim. A new maximum power point tracker of photovoltaic arrays using fuzzy controller. In *Proceedings of 1994 Power Electronics Specialist Conference - PESC'94*, volume 1, pages 396–403 vol.1, 1994.

[48] M. Dabboussi, A. Hmidet, and O. Boubaker. An efficient fuzzy logic MPPT control approach for solar PV system: A comparative analysis with the conventional perturb and observe technique. In *2020 6th IEEE International Energy Conference (ENERGYCon)*, pages 366–371, 2020.

[49] B. N. Alajmi, K. H. Ahmed, S. J. Finney, and B. W. Williams. A maximum power point tracking technique for partially shaded photovoltaic systems in microgrids. *IEEE Transactions on Industrial Electronics*, 60(4):1596–1606, 2013.

[50] D. Haji and N. Genc. Fuzzy and P&O based MPPT controllers under different

conditions. In *2018 7th International Conference on Renewable Energy Research and Applications (ICRERA)*, pages 649–655, 2018.

[51] T. L. Nguyen and K. Low. A global maximum power point tracking scheme employing DIRECT search algorithm for photovoltaic systems. *IEEE Transactions on Industrial Electronics*, 57(10):3456–3467, Oct 2010.

[52] N. A. Ahmed and M. Miyatake. A novel maximum power point tracking for photovoltaic applications under partially shaded insolation conditions. *Electric Power Systems Research*, 78(5):777–784, May 2008.

[53] G. Carannante, C. Fraddanno, M. Pagano, and L. Piegari. Experimental performance of MPPT algorithm for photovoltaic sources subject to inhomogeneous insolation. *IEEE Transactions on Industrial Electronics*, 56(11):4374–4380, Nov 2009.

[54] E. Koutroulis and F. Blaabjerg. A new technique for tracking the global maximum power point of PV arrays operating under partial-shading conditions. *IEEE Journal of Photovoltaics*, 2(2):184–190, April 2012.

[55] K. S. Tey and S. Mekhilef. Modified incremental conductance algorithm for photovoltaic system under partial shading conditions and load variation. *IEEE Transactions on Industrial Electronics*, 61(10):5384–5392, Oct 2014.

[56] H. Patel and V. Agarwal. Maximum power point tracking scheme for PV systems operating under partially shaded conditions. *IEEE Transactions on Industrial Electronics*, 55(4):1689–1698, 2008.

[57] A. Kouchaki, H. Iman-Eini, and B. Asaei. A new maximum power point tracking strategy for PV arrays under uniform and non-uniform insolation conditions. *Solar Energy*, 91:221 – 232, 2013.

[58] M. E. Başoğlu and B. Çakir. Experimental evaluations of global maximum power point tracking approaches in partial shading conditions. In *2017 IEEE International Conference on Environment and Electrical Engineering and 2017 IEEE Industrial and Commercial Power Systems Europe (EEEIC / I CPS Europe)*, pages 1–5, 2017.

[59] M. E. Başoğlu and B. Çakir. Hybrid global maximum power point tracking approach for photovoltaic power optimisers. *IET Renewable Power Generation*, 12:875–882, 2018.

[60] K. Chen, S. Tian, Y. Cheng, and L. Bai. An improved MPPT controller for photovoltaic system under partial shading condition. *IEEE Transactions on Sustainable Energy*, 5(3):978–985, 2014.

[61] M. E. Başoğlu. A fast GMPPT algorithm based on PV characteristic for partial shading conditions. *Electronics*, 8(10), 2019.

[62] M. E. Başoğlu. An enhanced scanning-based MPPT approach for DMPPT systems. *International Journal of Electronics*, 105(12):2066–2081, 2018.

[63] Y. Wang, Y. Li, and X. Ruan. High-accuracy and fast-speed MPPT methods for PV string under partially shaded conditions. *IEEE Transactions on Industrial Electronics*, 63(1):235–245, Jan 2016.

[64] M. Aquib, S. Jain, and V. Agarwal. A time-based global maximum power point tracking technique for PV system. *IEEE Transactions on Power Electronics*, 35(1):393–402, 2020.

[65] S. Titri, C. Larbes, K. Y. Toumi, and K. Benatchba. A new MPPT controller based on the ant colony optimization algorithm for photovoltaic systems under partial shading conditions. *Applied Soft Computing*, 58:465 – 479, 2017.

[66] D. Fares, M. Fathi, I. Shams, and S. Mekhilef. A novel global MPPT technique based on squirrel search algorithm for PV module under partial shading conditions. *Energy Conversion and Management*, 230:113773, 2021.

[67] I. Shams, S. Mekhilef, and K. S. Tey. Maximum power point tracking using modified butterfly optimization algorithm for partial shading, uniform shading, and fast varying load conditions. *IEEE Transactions on Power Electronics*, 36(5):5569–5581, 2021.

[68] C. Y. Liao, R. K. Subroto, I. S. Millah, K. L. Lian, and W. Huang. An improved bat algorithm for more efficient and faster maximum power point tracking for a photovoltaic system under partial shading conditions. *IEEE Access*, 8:96378–96390, 2020.

[69] S. Lyden, H. Galligan, and M. E. Haque. A hybrid simulated annealing and perturb and observe maximum power point tracking method. *IEEE Systems Journal*, pages 1–9, 2020.

[70] Z. Zhao, R. Cheng, B. Yan, J. Zhang, Z. Zhang, M. Zhang, and L. L. Lai. A dynamic particles MPPT method for photovoltaic systems under partial shading conditions. *Energy Conversion and Management*, 220:113070, 2020.

[71] G. Li and Z. Yu. The double chaotic particle swarm optimization with the performance avoiding local optimum. In *2015 International Conference on Estimation, Detection and Information Fusion (ICEDIF)*, pages 424–427, 2015.

[72] L. Xu, R. Cheng, Z. Xia, and Z. Shen. Improved particle swarm optimization (PSO)-based MPPT method for PV string under partially shading and uniform irradiance condition. In *2020 Asia Energy and Electrical Engineering Symposium (AEEES)*, pages 771–775, 2020.

[73] S. M. Mirhassani, M. Razzazan, and A. Ramezani. An improved PSO based MPPT approach to cope with partially shaded condition. In *2014 22nd Iranian Conference on Electrical Engineering (ICEE)*, pages 550–555, 2014.

[74] H. Li, D. Yang, W. Su, J. Lü, and X. Yu. An overall distribution particle swarm optimization MPPT algorithm for photovoltaic system under partial shading. *IEEE Transactions on Industrial Electronics*, 66(1):265–275, 2019.

[75] M. A. Abdullah, T. Al-Hadhrami, C. W. Tan, and A. H. Yatim. Towards green energy for smart cities: Particle swarm optimization based MPPT approach. *IEEE Access*, 6:58427–58438, 2018.

[76] C. Charin, D. Ishak, M. A. A. Mohd Zainuri, B. Ismail, and M. K. Mohd Jamil. A hybrid of bio-inspired algorithm based on levy flight and particle swarm optimizations for photovoltaic system under partial shading conditions. *Solar Energy*, 217:1–14, 2021.

[77] H. Heydari-doostabad, R. Keypour, M. R. Khalghani, and M. H. Khooban. A new approach in MPPT for photovoltaic array based on extremum seeking control under uniform and non-uniform irradiances. *Solar Energy*, 94:28 – 36, 2013.

[78] J. Storey, P. R. Wilson, and D. Bagnall. The optimized-string dynamic photovoltaic array. *IEEE Transactions on Power Electronics*, 29(4):1768–1776, April 2014.

[79] B. S. Ali, N. Benalia, and N. Z. Nora. Effect of partial shading on the PV system performances. In *2018 6th International Conference on Control Engineering Information Technology (CEIT)*, pages 1–4, 2018.

[80] H. Zheng, S. Li, R. Challoo, and J. Proano. Shading and bypass diode impacts to energy extraction of PV arrays under different converter configurations. *Renewable Energy*, 68:58 – 66, 2014.

[81] J. Ma, T. Zhang, Y. Shi, X. Li, and H. Wen. Shading pattern detection using electrical characteristics of photovoltaic strings. In *2016 IEEE International Conference on Power Electronics, Drives and Energy Systems (PEDES)*, pages 1–4, Dec 2016.

[82] S. Silvestre, A. Chouder, and E. Karatepe. Automatic fault detection in grid connected PV systems. *Solar Energy*, 94:119 – 127, 2013.

[83] A. Mäki and S. Valkealahti. Power losses in long string and parallel-connected short strings of series-connected silicon-based photovoltaic modules due to partial shading conditions. *IEEE Transactions on Energy Conversion*, 27(1):173–183, 2012.

[84] A. E. Brooks, D. Cormode, A. D. Cronin, and E. Kam-Lum. PV system power loss and module damage due to partial shade and bypass diode failure depend on cell behavior in reverse bias. In *2015 IEEE 42nd Photovoltaic Specialist Conference (PVSC)*, pages 1–6, 2015.

[85] Z. Alqaisi and Y. Mahmoud. Comprehensive study of partially shaded PV modules with overlapping diodes. *IEEE Access*, 7:172665–172675, 2019.

[86] K. Hu, S. Cao, W. Li, and F. Zhu. An improved particle swarm optimization algorithm suitable for photovoltaic power tracking under partial shading conditions. *IEEE Access*, 7:143217–143232, 2019.

[87] Fred Glover. Tabu search: A tutorial. *Interfaces*, 20(4):74–94, 1990.

[88] Fred Glover and Eric Taillard. A user's guide to Tabu search. *Annals of Operations Research*, 41(1):1–28, 1993.

[89] J. C. Teo, R. H. G. Tan, V. H. Mok, V. K. Ramachandaramurthy, and C. Tan. Impact of partial shading on the P-V characteristics and the maximum power of a photovoltaic string. *Energies*, 11(7), 2018.

[90] J. C. Teo, Rodney H. G. Tan, V. H. Mok, V. K. Ramachandaramurthy, and C. Tan. Impact of bypass diode forward voltage on maximum power of a photovoltaic system under partial shading conditions. *Energy*, 191:116491, 2020.

[91] X. Zhang, D. Gamage, B. Wang, and A. Ukil. Hybrid maximum power point tracking method based on iterative learning control and perturb observe method. *IEEE Transactions on Sustainable Energy*, 12(1):659–670, 2021.

[92] M. Kermadi, Z. Salam, J. Ahmed, and E. M. Berkouk. A high-performance global maximum power point tracker of PV system for rapidly changing partial shading conditions. *IEEE Transactions on Industrial Electronics*, 68(3):2236–2245, 2021.

[93] Y. Zhu, H. Wen, G. Chu, Y. Hu, X. Li, and J. Ma. High-performance photovoltaic constant power generation control with rapid maximum power point estimation. *IEEE Transactions on Industry Applications*, 57(1):714–729, 2021.

[94] S. Xu, Y. Gao, G. Zhou, and G. Mao. A global maximum power point tracking algorithm for photovoltaic systems under partially shaded conditions using modified maximum power trapezium method. *IEEE Transactions on Industrial Electronics*, 68(1):370–380, 2021.

[95] A. Sen, S. Pradhan, and A. Kumar. A novel curve scanning based maximum power point tracking algorithm under partial shading conditions. In *2020 IEEE First International Conference on Smart Technologies for Power, Energy and Control (STPEC)*, pages 1–6, 2020.

[96] K. Sundareswaran, S. Peddapati, and S. Palani. MPPT of PV systems under partial shaded conditions through a colony of flashing fireflies. *IEEE Transactions on Energy Conversion*, 29(2):463–472, 2014.

[97] N. S. Altman. An introduction to kernel and nearest-neighbor nonparametric regression. *The American Statistician*, 46(3):175–185, 1992.

[98] M. I. AlHajri, N. T. Ali, and R. M. Shubair. Classification of indoor environments for iot applications: A machine learning approach. *IEEE Antennas and Wireless Propagation Letters*, 17(12):2164–2168, 2018.

[99] M. Xie, J. Hu, S. Han, and H. Chen. Scalable hypergrid k-NN-based online anomaly detection in wireless sensor networks. *IEEE Transactions on Parallel and Distributed Systems*, 24(8):1661–1670, 2013.

[100] Y. Hu, L. Yang, B. Yan, T. Yan, and P. Ma. An online rolling optimal control strategy for commuter hybrid electric vehicles based on driving condition learning and prediction. *IEEE Transactions on Vehicular Technology*, 65(6):4312–4327, 2016.

[101] F. Pedregosa, G. Varoquaux, A. Gramfort, V. Michel, B. Thirion, O. Grisel, M. Blondel, P. Prettenhofer, R. Weiss, V. Dubourg, J. Vanderplas, A. Passos, D. Cournapeau, M. Brucher, M. Perrot, and E. Duchesnay. Scikit-learn: Machine learning in Python. *Journal of Machine Learning Research*, 12:2825–2830, 2011.